From early Miocene to present:
Reconstruction of the
deep Thermohaline Circulation
at the Eirik Drift

DISSERTATION

zur Erlangung des Grades Dr. rer. nat.

vorgelegt dem Fachbereich Geowissenschaften

der Universität Bremen im Dezember 2013

von Antje Müller-Michaelis

Universität Bremen

ALFRED-WEGENER-INSTITUT
HELMHOLTZ-ZENTRUM FÜR POLAR-
UND MEERESFORSCHUNG

Erstgutachter: Prof. Dr. Rüdiger Stein
Zweitgutachterin: Prof. Dr. Katrin Huhn

Datum des Kolloquiums: 26. Februar 2014

Name: Antje Müller-Michaelis

Anschrift: Am Leher Tor 13, 27568 Bremerhaven

ERKLÄRUNG

Hiermit versichere ich, dass ich

1. die Arbeit ohne unerlaubte fremde Hilfe angefertigt habe

2. keine anderen als die von mir angegebenen Quellen und Hilfsmittel benutzt habe

3. die den benutzten Werken wörtlich oder inhaltlich entnommenen Stellen als solche kenntlich gemacht habe

---

Bremerhaven, den   Antje Müller-Michaelis

Contents

Summary

The Thermohaline Circulation (THC) distributes heat and freshwater around the global oceans, interacts with the atmosphere, and therefore is closely connected to the global climate. The deep branch of the North Atlantic THC mainly consists of deep-water formed by atmospheric cooling in the Nordic Seas, which overflows the Greenland-Scotland Ridge into the North Atlantic. The Eirik Drift south of Greenland is located closely downstream of the North Atlantic deep-water formation region and has been shaped by the Western Boundary Undercurrent (WBUC), which constitutes the main part of the deep North Atlantic THC. The sedimentary record of the Eirik Drift documents changes of the WBUC activity, which can be related to climate changes. The analysis of the sedimentary structure in combination with geological information from scientific drilling leads to a revised seismostratigraphic concept at the Eirik Drift and reveals particularly that the Eirik Drift has been influenced by the WBUC already since the early Miocene (~19 Ma). A more detailed structural analysis of the depocenter locations and their redistribution results in a temporal reconstruction of the deep paleocirculation at the Eirik Drift. The observed changes of pathways and intensity of the WBUC at the Eirik Drift were linked to the development of the Greenland-Scotland Ridge and climate changes. The onset of drift building at the Eirk Drift followed the formation of the Faroe Conduit in early Miocene, which allowed northern sourced deep-water to overflow the eastern part of the Greenland-Scotland Ridge. A separation of the WBUC at the Eirik Drift into two branches occurred contemporaneously with the onset of deep-water overflow at the Denmark Strait, the western part of the Greenland-Scotland Ridge (~7 Ma). At the Eirik Drift, strong WBUC activity is inferred to occur during warm climates and at the beginning of cooling phases, while cooling phases with enhanced ice extent are characterized by weak WBUC activity. Based on a combination of these observations with interpretations from other North Atlantic sediment drifts, a paleo flow path reconstruction for the northern North Atlantic is proposed. It is suggested that the deep-water formation regions and the main deep-water pathway shifted to the south during cold phases with enhanced ice-extent, i.e. Northern Hemisphere Glaciation. This implies that during these cool phases solely weak branches of the deep-water circulation overflowed the Eirik Drift and that the main North Atlantic deep-water route affected the Eirik Drift just during warm phases.

Moreover, by applying the seismic oceanography method the present pathway and structure of the upper WBUC core at the Eirik Drift is imaged. For the first time, this method is successfully applied in water depth > 1500 m. The study confirms not only the improvement of oceanographic research by use of the seismic oceanography method but also supports the interpretation of the analysis of the sedimentary structure at the Eirik Drift.

Zusammenfassung

Die Thermohaline Zirkulation transportiert Wärme und Frischwasser durch die Ozeane und interagiert mit der Atmosphäre. Deshalb ist die Thermohaline Zirkulation eng mit dem globalen Klima verbunden. Der tiefe Teil der nordatlantischen Thermohalinen Zirkulation besteht hauptsächlich aus Tiefenwasser, das in der Grönland/Norwegen See gebildet wird und über den Grönland-Schottland Rücken in den Nord Atlantik fließt. Die Eirik Drift südlich von Grönland wird vom Western Boundary Undercurrent (WBUC) geformt, der den Hauptteil der tiefen nordatlantischen Thermohalinen Zirkulation darstellt. Die Sedimentstruktur der Eirik Drift dokumentiert somit Veränderungen im WBUC, welche in Bezug zu unterschiedlichen klimatischen Bedingungen gesetzt werden können. Die Untersuchung der Sedimentstrukturen in Verbindung mit geologischen Informationen aus Bohrungen führt zu einem verbesserten seismostratigraphischen Modell an der Eirik Drift und macht vor allem deutlich, daß die Eirik Drift bereits seit dem frühen Miozän (~19 Ma) von dem WBUC beeinflußt wird. Eine zeitliche Rekonstruktion der tiefen Paläoströmungen an der Eirik Drift konnte durch die detailliertere Analyse der Lage und Umverteilung von Depotzentren abgeleitet werden. Die Änderungen der Strömungswege und Strömungsintensität des WBUC an der Eirik Drift kann mit der Entwicklungsgeschichte des Grönland-Schottland Rückens und Änderungen der klimatischen Bedingungen in Verbindung gebracht werden. Der Aufbau der Eirik Drift folgte der Formation des Faroe Conduits im frühen Miozän, welches den Ersten Tiefenwasseraustausch über diesen östlichen Teil des Grönland-Schottland Rückens zuließ. Die Teilung des WBUCs in zwei Strömungsarme an der Eirik Drift erfolgte zeitgleich mit dem ersten Tiefenwasser-Überlauf an der Dänemark Straße (~7 Ma), dem westlichen Teil des Grönland-Schottland Rückens. Ein starker Einfluß von Tiefenströmungen an der Eirik Drift wird für warme Klimaphasen und am Anfang von Kaltphasen deutlich. In Kaltphasen mit erhöhter Eisausdehnung hingegen sind nur schwache Tiefenströmungen an der Eirik Drift dokumentiert. Basierend auf einer Verbindung dieser Beobachtungen mit Ergebnissen von anderen Driftkörpern des Nord Atlantiks wurde eine Rekonstruktion der Tiefenwasserbildungsgebiete und Tiefenwasserströmung im nördlichen Nord Atlantik erstellt. Die Tiefenwasserbildungsgebiete haben sich ebenso wie die Haupttiefenströmung in kalten Phasen mit zunehmender Vereisung der Nordhemisphäre gen Süden verlagert. Dies bedeutet, daß in solchen Kaltphasen nur schwache Ausläufer der Tiefenströmung über die Eirik Drift geflossen sind und die Eirik Drift nur in Warmphasen im Hauptflußweg des Tiefenwassers lag.

Zusätzlich konnten mit der seismischen Ozeanographie Methode der aktuelle Strömungsweg und die Struktur des oberen Kerns des WBUC abgebildet werden. Damit wurde diese Methode zum ersten Mal erfolgreich in Wassertiefen > 1500 m angewendet. Die Untersuchung hat nicht nur gezeigt, daß seismische Ozeanographie eine hilfreiche Ergänzung für ozeanographische Untersuchungen darstellt, sondern bestätigt auch die Interpretation von den Sedimentstrukturen der Eirik Drift.

1 Introduction and Motivation

The global climate is intrinsically tied to the global ocean circulation as the surface ocean stores and transports heat and freshwater and exchanges it with the atmosphere. The global Thermohaline Circulation (THC; Fig. 1.1) is a main conveyor for the global heat transfer. Warm and saline surface water is distributed towards high latitudes in the upper branch of the THC and cools down due to heat exchange with the atmosphere and surrounding water (Fig. 1.1; Kuhlbrodt *et al.*, 2007; Schmitz, 1996; Van Aken, 2007). Therefore, the surface water becomes denser, due to the lower temperature and higher salt content. This results in downwelling of the denser water, which pulls warm surface water towards high latitudes. The formation of the deep-water masses in high latitudes is the main driving process for the THC and connects the surface flow with the reversed deep flow of dense deep-water (Dickson and Brown, 1994; Kuhlbrodt *et al.*, 2007; Schmitz, 1996; Van Aken, 2007). There are only three known regions of deep-water production: The Nordic Seas along with the Labrador Sea on the Northern Hemisphere and on the Southern Hemisphere the Ross Sea and the Weddell Sea (Fig. 1.1; Kuhlbrodt *et al.*, 2007; Van Aken, 2007). Cooling of the surface branch of the THC in high latitudes is a pre-condition for deep-water formation and thus the THC system is sensitive to climate changes (Quadfasel and Käse, 2007; Van Aken, 2007). Understanding of the present THC system and the changes it underwent during changing climatic conditions will provide important information for the improvement of future climate models.
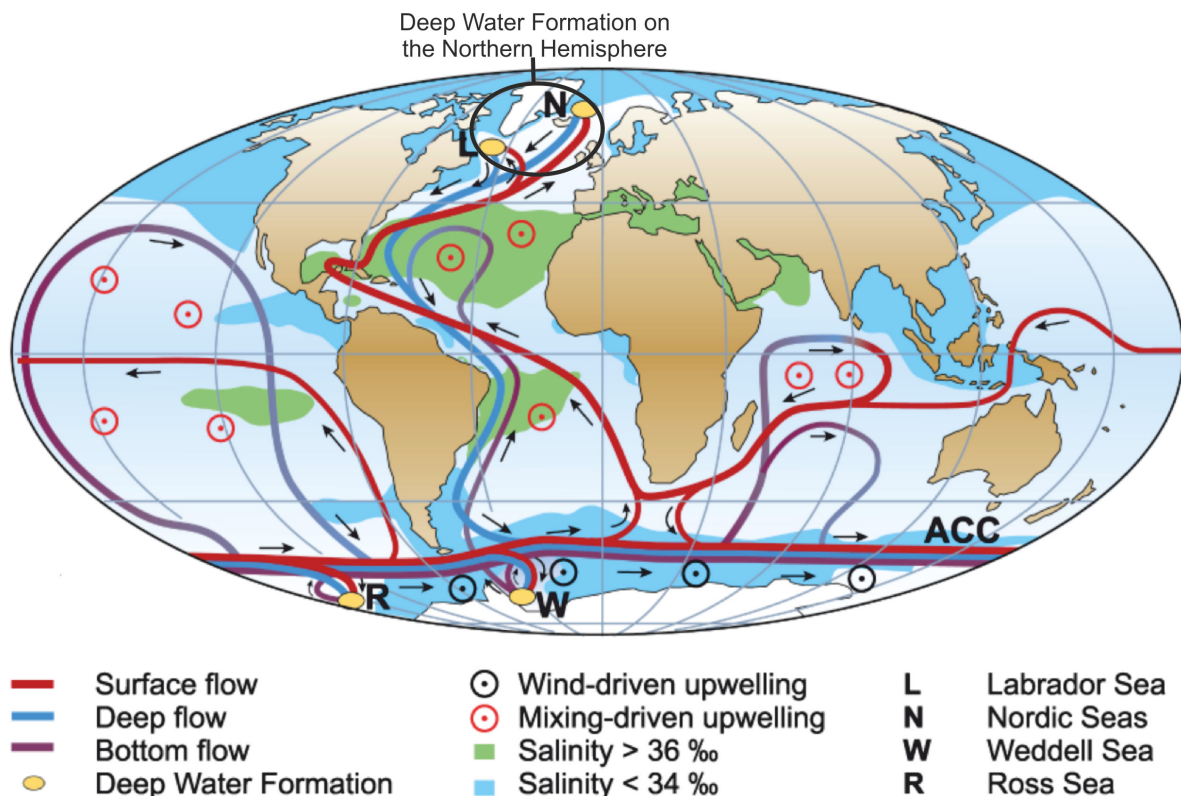

Figure 1.1. Schematic sketch of the global Thermohaline Circulation modified from Kuhlbrodt *et al.* (2007).

A unique location to investigate the deep branch of the North Atlantic THC is the Eirik Drift. It lies 200 km south of Greenland closely downstream of the deep-water formation region of the Northern Hemisphere (Fig. 1.2). The deep water produced in the Nordic Seas has to pass the Eirik Drift as the thermohaline deep current is bound to the slope of Greenland due to Coriolis force (Quadfasel and Käse, 2007). At present, the deep-water produced in the Greenland Sea combines with Arctic Ocean water masses and overflows the sill between Greenland and Iceland (~620 m) as Denmark Strait Overflow Water (DSOW; Fig. 1.2; Hansen and Østerhus, 2000; Quadfasel and Käse, 2007). Deep-water from the Norwegian Sea spills mainly through the Faroe-Conduit (Faroe-Shetland Channel and Faroe Bank Channel; ~840 m) as Iceland-Scotland Overflow Water (ISOW) and circulates around the Reykjanes Ridge to the east coast of Greenland (Fig. 1.2; Hansen and Østerhus, 2000; Quadfasel and Käse, 2007). Both overflows entrain deep-water formed in the Labrador Sea (Labrador Sea Water (LSW) 700-1500 m depth; Fig. 1.2) and modified Antarctic Bottom Water (Lower Deep Water (LDW) > 3000 m depth) while descending into the North Atlantic (Fig. 1.2; Hansen and Østerhus, 2000; Quadfasel and Käse, 2007). DSOW and ISOW meet at the east coast of Greenland and combine to the Western Boundary Undercurrent (WBUC; also referred to as Deep Western Boundary Current (DWBC)), which constitutes the deep limb of the North Atlantic THC. The WBUC is a contour intensified deep current, which transports ISOW at a core depth of ~2000 m and DSOW at a core depth of ~3000 m off Cape Farewell (Dickson and Brown, 1994; Schmitz, 1996). The Eirik Drift lies within the pathway of the present WBUC as its crest slopes from the southern Greenland margin to ~3500 m in the WSW. The topographically guided WBUC changes its direction and divides into a more complex flow system of different branches while overflowing the Eirik Drift and entering the Labrador Sea (Fig. 1.2; Hunter *et al.*, 2007b). Little is known about pathways and causes of the division of the WBUC here and its investigation will help to improve our understanding of the complex system of the North Atlantic THC.

The Eirik Drift lies at the entrance of the Labrador Sea (Fig. 1.2). The Labrador basin is over 2000 m deep and flanked by continental shelves to the southwest, northwest and northeast and limited by the Davis Strait (< 700 m) to the north (Fig. 1.2). The southeastern drift flank borders on the Irminger Sea (Fig. 1.2). The Irminger Sea is flanked by the Greenland shelf to the west, Denmark Strait to the north and Reykjanes Ridge to the east (Fig. 1.2). The geological evolution of this area started with sea-floor spreading between Greenland and Labrador ~61 Ma ago (Chalmers and Pulvertaft, 2001). A re-orientation of the spreading axis was observed ~56-53 Ma ago, at the same time when sea-floor spreading between Greenland and Europe began (Chalmers and Pulvertaft, 2001). The spreading in the Labrador Basin ceased ~33 Ma ago (Srivastava and Roest, 1999). The main structural components in the eastern Labrador Sea resulting from this opening history are NE-SW orientated fracture zones, the Leif Fracture Zone in the southeast and the Farewell Fracture Zone in the northeast, which underlies the Eirik Drift (Fig. 1.2a). The basement highs associated with the Farewell Fracture Zone are suggested to have influenced the drift build-up and the morphology of the drift (Hillaire-Marcel *et al.*, 1994; Hunter *et al.*, 2007b).

First relevant overflows from northern sourced deep-water into the North Atlantic were reported for the Faroe Conduit in Early Miocene (Stoker *et al.*, 2005), for the Iceland-Faroe Ridge ~13-11 Ma, and for the Denmark Strait ~7 Ma (Fig. 1.2; Bohrmann *et al.*, 1990). Therefore, northern sourced deep-water flow could have affected the Eirik Drift region since then, but the existing stratigraphy assessed the onset of drift building at ~4.5 Ma (Arthur *et al.*, 1989). Certainly, the Eirik Drift has been built under the influence of deep-water currents of Nordic Sea origin. Therefore, the sedimentary structure of the Eirik Drift has been shaped by the deep currents and bears information about changes in pathways and strength of the North Atlantic deep circulation in changing climate conditions.
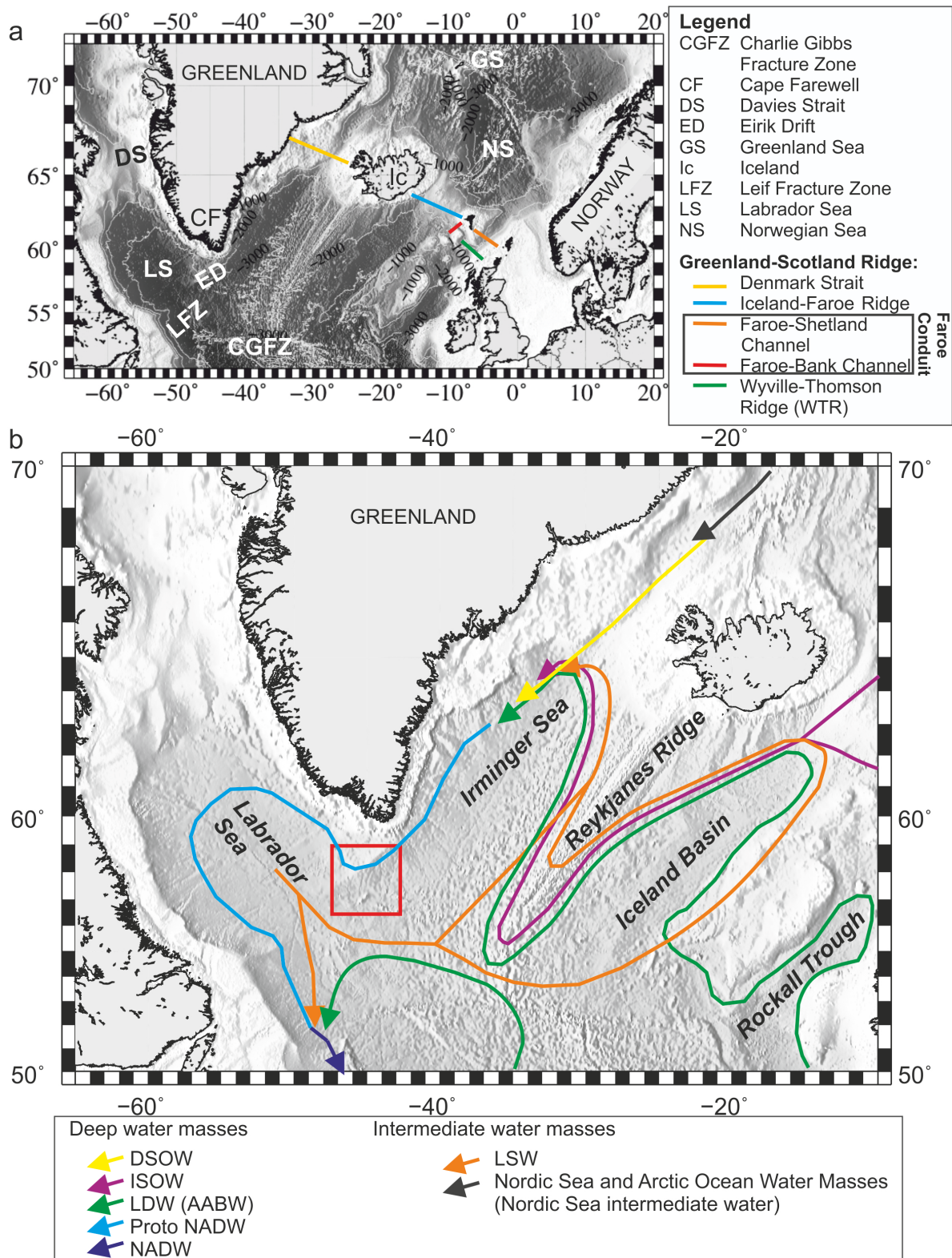
Figure 1.2. Satellite-derived bathymetry map (Smith and Sandwell, 1997) of the northern North Atlantic. (a) Basins, ridges and fracture zones in the northern North Atlantic. (b) Water mass contribution to the WBUC. The red box shows the study area (Fig. 2.1). DSOW: Denmark Strait Overflow Water; ISOW: Iceland-Scotland Overflow Water; LDW (Lower Deep Water; AABW: Antarctic Bottom Water; NADW: North Atlantic Deep Water; LSW: Labrador Sea Water. Modified from Müller-Michaelis *et al.* (2013).

3

For a detailed analysis of the sedimentary structure of the Eirik Drift, which could reveal more details about pathways and intensity of the WBUC south of Greenland, the Alfred-Wegener-Institut, Helmholtz-Zentrum für Polar- und Meeresforschung, gathered high-resolution seismic reflection data in 2009. The seismic lines connected four scientific drill sites: ODP (Ocean Drilling Program) Leg 105 Site 646 and IODP (Integrated Ocean Drilling Program) Expedition 303 Sites 1305, 1306 and 1307. With the combination of seismic and geological borehole data it should be possible to answer questions about the paleocirculation at the Eirik Drift in the context of global climate changes. The results should reveal modifications of the deep THC branch at the Eirik Drift during climate changes in the past considering its unique location closely downstream of the deep-water formation regions of the Northern Hemisphere. The observed seismic structures can be interpreted with regard to contour current pathways and intensity (Faugères and Stow, 2008; Faugères *et al.*, 1999; Nielsen *et al.*, 2008; Rebesco and Stow, 2001; Stow *et al.*, 2002). The Eirik Drift is classified as a mounded, giant elongated, detached drift (Fig. 1.3; Faugères *et al.*, 1999; Stow *et al.*, 2002). The main features of this drift type comprise: a) Detached, elongated, mounded drifts usually prograde in the initial flow direction and therefore, their crests are found parallel to the prevailing deep current direction. b) The depocenters are always found to the right of the deep current core on the Northern Hemisphere due to Coriolis force. c) Drift deposits of detached, elongated, mounded drifts are typically lenticular in shape with bedding thickening at the drift axis and converging internal reflectors towards the flank(s) of the intensified deep current core location (Fig. 1.3; Faugères *et al.*, 1999; Stow *et al.*, 2002). In a nutshell, by identifying erosional and depositional centers in the seismic data, the pathways of the deep currents, which shaped the Eirik Drift, are revealed and changes in erosional/depositional style can then be linked to changes in deep-current intensity.
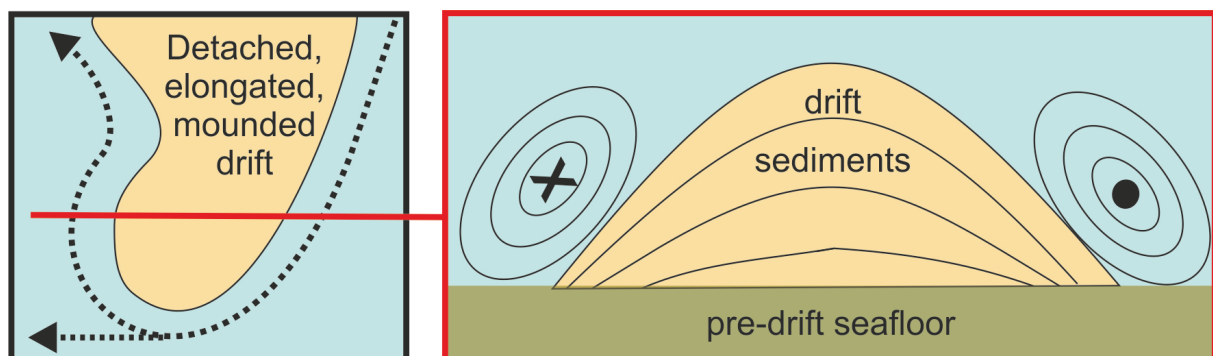
Figure 1.3. Simplified sketch of a detached, elongated, mounded drift with the main depositional sedimentary features and inferred deep-current direction according to Coriolis force on the Northern Hemisphere. The left panel shows a plan view of a deep current (black arrows) flowing around a margin corner. The red line indicates the location of the cross-section displayed on the right. Modified after Rebesco and Stow (2001).

In the first part of my PhD-thesis I correlated the scientific borehole data with the newly collected high-resolution seismic reflection data. This allows an interpretation of the seismic structures at the Eirik Drift in combination with geological information from the drill sites. I revised the seismostratigraphic concept of Arthur *et al.* (1989). The results were published in Müller-Michaelis *et al.* (2013) and answer the following questions:

- What is the detailed structure of the Eirik Drift?
- For which period can the first impact of deep-water circulation recorded at the Eirik Drift be identified?

For the second part of my PhD-thesis I use the revised seismostratigraphic concept of Müller-Michaelis *et al.* (2013) for a more detailed analysis of the sedimentary structures and the distribution of the depocenters for all seismic (sub)units. This resulted in the reconstruction of

the paleocirculation at the Erik Drift. The results have been submitted (04/2013) and in revision (11/2013, moderate revision advised) in Müller-Michaelis and Uenzelmann-Neben (2013, in revision) and answer the following questions:

- Can the development of the WBUC be reconstructed for this region?
- Have modifications in the WBUC been documented in the sediment transport? In what way did oceanographic modifications affect the sedimentary sequences?
- Can oceanographic modifications observed locally be linked to major changes in the North Atlantic climate?

For the third part of my PhD-thesis the method of seismic oceanography was applied to the seismic data aiming at imaging the present WBUC at the Erik Drift. Seismic data can provide a high lateral resolution of thermohaline structures within the ocean (Holbrook *et al.*, 2003; Ruddick, 2003). So far, all seismic oceanography studies have been conducted of the upper ocean (< 1500 m depth). This study therefore constitutes the first seismic oceanography analysis in the deeper ocean. Even though the data acquisition was not designed for this purpose, I tried to gather structural information about the present WBUC at the Erik Drift. The results have been submitted (11/2013) to Müller-Michaelis and Uenzelmann-Neben (2013, submitted) and deal with the questions:

- Can deep currents of depths > 1500 m be studied with the seismic oceanography method?
- Does the observation of the WBUC in seismic reflection data improve the knowledge gained by classical physical oceanography methods?
- Can we identify and track the present WBUC at the Erik Drift? Does our observation of the present WBUC support our interpretation from the past?

The major aim of the analysis of the high-resolution seismic reflection data from the Erik Drift has been a detailed reconstruction of the WBUC in this region in the past and at present. The results should reveal the close interactions of different paleoclimate conditions and changes of the WBUC and the results from the present should proof our interpretation of the past. The knowledge about modifications of the WBUC in changing climate conditions will contribute to an extended understanding of the THC and should help to improve future climate models.

2 Datasets

2.1 Seismic reflection data

The new geophysical data that are analyzed in this study were collected during research vessel Maria S. Merian cruise MSM12/2 in 2009 (Uenzelmann-Neben, 2009). ~2000 km of high-resolution multichannel seismic reflection data were acquired to analyze the internal structure of the sediment cover at the Eirik Drift (Fig. 2.1). The seismic signal was produced by four GI-guns© with a volume of about 1.4 l each, composed of a generator chamber (0.72 l volume) and an injector chamber (1.68 l volume). The GI-guns© were fired every 10 s, which corresponds to a shot spacing of approximately 25 m. The injector chambers were triggered with a 33 ms delay to suppress the bubble. The reflected waves from the subsurface were in-sea collected by a 3000 m long SERCEL SEAL© streamer consisting of 240 hydrophones and a lead-in cable length of 191 m (Fig. 2.2). The on-board acquisition system (SERCEL SEAL©) received and stored the seismic data with a sample interval of 1 ms along with the navigation data specified by GPS (Global Positioning System). The seismic lines intersect four ODP and IODP scientific boreholes in this area (Fig. 2.1).
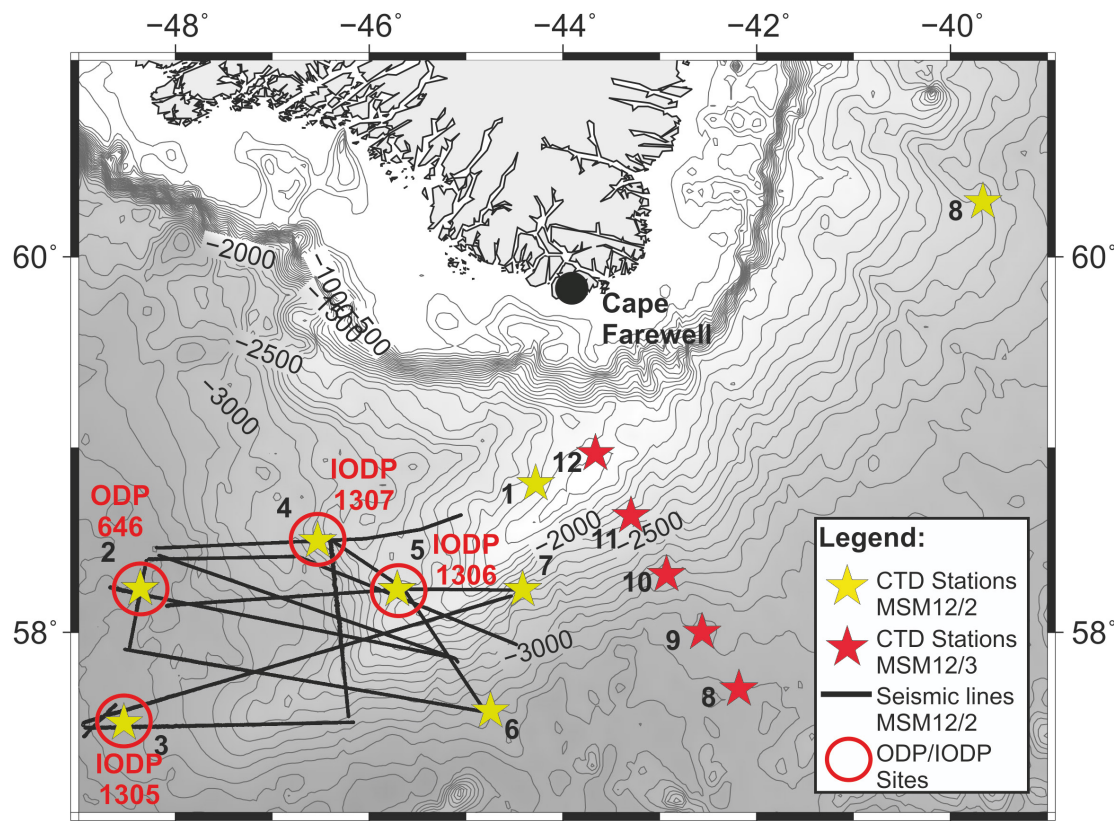
Figure 2.1. Satellite bathymetric map (Smith and Sandwell, 1997) of the study area showing the location of the seismic lines (black lines). The red circles indicate the locations of the drill sites ODP Leg 105 Site 646 (Shipboard Scientific Party, 1987) and IODP Expedition 303 Sites U1305, U1306 and U1307 (Channell *et al.*, 2010). The stars mark the locations of the CTD stations of the Maria S. Merian cruises MSM12/2 (yellow stars) and MSM12/3 (red stars; by courtesy of Rhein (2011)).
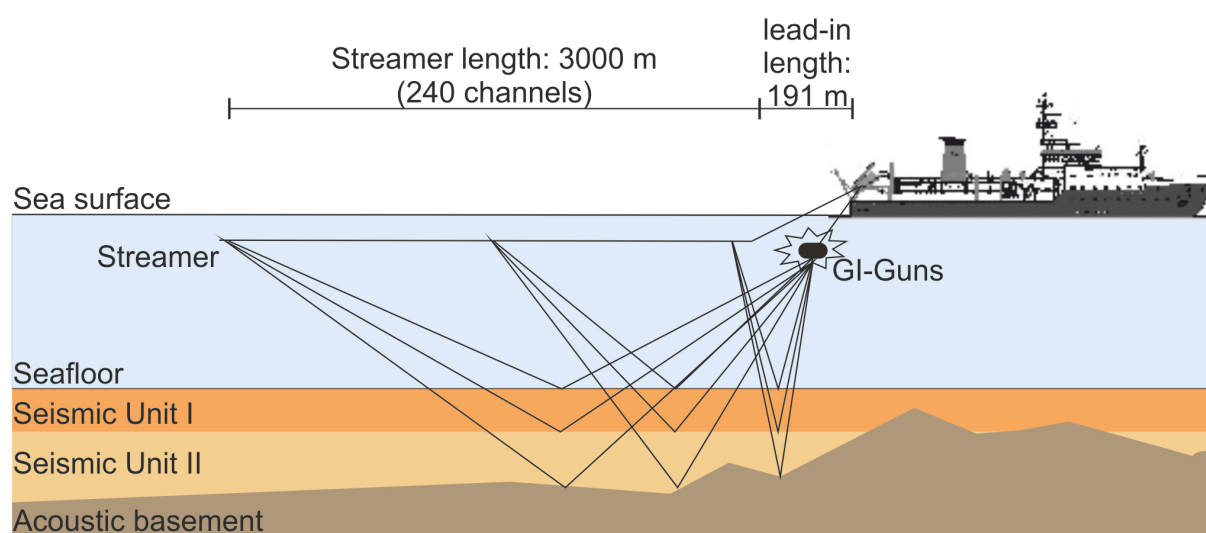
Figure 2.2. Simplified sketch of the seismic reflection data acquisition. Ray pathways for only three channels are depicted as an example. The acquisition geometry of the RV Maria S. Merian cruise MSM12/2 comprised an active streamer length of 3000 m with 240 digital channels (hydrophones) and a lead-in cable length of 191 m.

2.2 Scientific borehole data

For the interpretation of the seismic reflection data of the Eirik Drift, I additionally used the existing geological borehole data of the four drill sites intersected by the seismic lines: ODP (Ocean Drilling Program) Leg 105 Site 646 (Shipboard Scientific Party, 1987) and IODP (Integrated Ocean Drilling Program) Expedition 303 Sites U1305, U1306, and U1307 (Channell *et al.*, 2010). Their locations are shown in Figure 2.1. The drill core data can be tied to the seismic reflection data, which helps to determine age estimations. To correlate the geological information with the high-resolution seismic reflection data, the physical properties density and P-wave velocity from the drill site data are needed (see Ch. 3.1.2). The measurements of the physical properties can be conducted downhole at the drill site or at the recovered core. At the recovered core there are the possibilities to measure the physical properties at the whole core with a multi-sensing track tool (MST) or at discrete locations at the split core (Blum, 1997). The relevant information about water depth, core recovery, age, measured depth and measurement techniques provided from the four ODP/IODP Sites are summarized in Table 2.1. The processing of the physical property data will be explained further in chapters 3.1.2 and 3.1.3.

Table 2.1.
Summarized information about the ODP/IODP drill sites. W.d.: Water depth; msbf: meters below seafloor; res.: resolution; Exp.: Expedition; MST: Multi-sensing track tool. For location see Fig. 2.1.

Drill Site	W.d. [m]	recovery [m]	age [Ma]	location in study area	measured bulk density			measured P-wave velocity		
					tool	depth [mbsf]	res. [m]	tool	depth [mbsf]	res. [m]
ODP Leg 105 Site 646	3450	766.7	8.60	W	MST	0.006 - 758.9	0.006	downhole	209 - 745	0.15
								split core	4.3 - 758	6 - 77
IODP Exp. 303 Site 1305	3459	295.0	1.77	SW	MST	0.05 - 287.5	0.05	MST	0.35 - 115.2	0.05
IODP Exp. 303 Site 1306	2274	309.3	1.95	NE	MST	0.05 - 179.9	0.05	MST	0.15 - 179.3	0.05
IODP Exp. 303 Site 1307	2575	162.6	3.58	N	MST	0.05 - 154.5	0.05	MST	0.25 - 154.2	0.05

2.3 Conductivity-Temperature-Depth (CTD) probe data

A Sea-Bird© SBE 9/11 profiling instrument measured conductivity, temperature and pressure. The depth is determined by the pressure and the salinity by the conductivity. The CTD was fixed on a Sea-Bird© 24 position carousel with a Sea-Bird© altimeter and Ocean Test Equipment Niskin bottles for water samples. It was lowered by winch to approx. 10 m above sea bottom. The profiles were recorded during the down- and up-cast by a Sea-Bird© 11+ V2 deck unit. The casts were initiated and terminated on deck. Water samples were taken for calibration of the conductivity sensor. The salinity of the water samples was measured by salinometer. Eight CTD casts were conducted during the MSM12/2 cruise for the calibration of the multibeam bathymetry tool (Fig. 2.1). For the interpretation I used the MSM12/2 CTD casts #4, #5, and #7 (Fig. 2.1; Table 2.2). A cross-section of five CTD casts of the following cruise MSM12/3 (CTD #8-12; Fig. 2.1; Table 2.2; by courtesy of Rhein (2011)) was also used. 12x5 l Niskin bottles were attached to the frame during MSM12/2 CTD casts. The setup of MSM12/3 CTD casts comprised 22x10 l Niskin bottles and additionally a Sea-Bird© SBE 43 dissolved oxygen sensor and a LADCP (Lowered Acoustic Doppler Current Profiler). The CTD data were used for the interpretation of the seismic data with respect to seismic oceanography. This method will be further explained in chapter 3.2 and the results are presented in chapter 7.

Table 2.2.
Summarized information about the CTD casts used.

Cruise	Cast	Date	Time	Latitude	Longitude	Depth [m]
MSM12/2	#4	2009/07/02	05:36	58° 30.34' N	046° 24.05' W	2565
MSM12/2	#5	2009/07/02	14:48	58° 14.23' N	045° 38.54' W	2259
MSM12/2	#7	2009/07/07	07:19	58° 14.32' N	044° 24.87' W	2372
MSM12/3	#8	2009/07/18	12:00	57° 40.55' N	042° 11.15' W	3295
MSM12/3	#9	2009/07/18	16:00	57° 59.99' N	042° 33.53' W	3196
MSM12/3	#10	2009/07/18	19:52	58° 18.96' N	042° 55.51' W	2909
MSM12/3	#11	2009/07/18	23:45	58° 38.49' N	043° 18.00' W	2153
MSM12/3	#12	2009/07/19	03:07	58° 57.99' N	043° 40.01' W	1616

3 Methods

In this chapter I explain the methods I used for the interpretation of the seismic reflection data. In subsection 3.1 I focus on the sub-seafloor seismic reflection data as the seismic survey was designed to investigate the structure and geometry of the Eirik Drift in a paleoceanographic and paleoclimatic context. I will explain the seismic data processing (Ch. 3.1.1), the conversion of geological borehole data to synthetic seismograms (Ch. 3.1.2), and the interpretation resulting from the correlation of the synthetic seismograms with the seismic data (Ch. 3.1.3). Based on the correlation of seismic and borehole data I developed a refined seismostratigraphic concept and revised the onset of deep-current activity at the Eirik Drift to Miocene age, which was published in Müller-Michaelis *et al.* (2013) (see Ch. 5). By means of the depocenter outlines and (re)distribution and the internal seismic reflection characteristics of each seismic unit I derived the pathways and intensity of the WBUC at the Eirik Drift and developed a model for the paleo-deep-current activity in the northern Northeast Atlantic since the Miocene. These results are presented in Müller-Michaelis and Uenzelmann-Neben (2013 (in revision)) (see Ch. 6).

In subsection 3.2 I concentrate on the seismic data of the water column in the area of the Eirik Drift and introduce the seismic oceanography method for studies of the present day deep circulation. I explain the differences and challenges in seismic data processing (Ch. 3.2.1), and the processing of the CTD data for my interpretation (Ch. 3.2.2). I tracked pathway and structure of the present upper core of the WBUC at the Eirik Drift by means of the reflections resulting from thermohaline fine structure due to mixing processes at the boundary of the intensified deep current core in the water column. These results are introduced in Müller-Michaelis and Uenzelmann-Neben (2013 (submitted)) (see Ch. 7).

3.1 Sediment drift data

3.1.1 Seismic data processing

Processing of the seismic data started with geometry definition invoking the ship's navigational data. The data were sorted to Common Depth Point (CDP) with a CDP spacing of 25 m. A precise velocity analysis was carried out by picking the seismic velocities every 50 CDPs. The determined stacking velocity was used for normal moveout (NMO) correction, which reduced the differences in travel time from a reflecting surface to the source-to-geophone distance. The CDPs were stacked and a time-migration with the stacking velocity field was carried out (Omega-X migration; Yilmaz, 2001). Bandpass filtering with tapering (Hanning window) with the boundaries 20-25 Hz and 200-250 Hz was applied to the data for display. The data processing was conducted by using the FOCUS/Disco software from PARADIGM©.

3.1.2 Conversion of ODP/IODP logs to synthetic seismograms

The calculation of synthetic seismograms of the ODP/IODP drill site data enables the correlation of the seismic data with geological information. The reflection coefficient is governed by the contrast in acoustic impedance, which is the product of density and velocity. The basic information about bulk density and sonic velocity logs provided for the ODP/IODP sites are listed in Table 2.1. For the IODP Expedition 303 Sites the logs of these physical properties were measured on whole-round core sections run through a MST and led to bulk density and seismic velocity data with a resolution of 0.05 m (Expedition 303 Scientists, 2006). The bulk density of ODP Leg 105 Site 646 was also conducted through a MST and supplied a resolution of 0.006 m (Srivastava *et al.,* 1989). No P-wave velocity data derived from a MST whole-round core is provided for ODP Leg 105 Site 646, and the sonic velocity measured at the split core has a poor resolution in irregular intervals varying between 6 and 77 m (Table 2.1). However, downhole measurements conducted with a long spacing Sonic

Tool provide seismic P-wave velocity data with a resolution of 0.15 m but only in the interval 208.788 to 744.931 mbsf (Table 2.1; Srivastava *et al.,* 1989). Therefore, I complemented the downhole loggings with the laboratory measurements at the split core (red line in Fig. 3.1a). The following processing steps are displayed using the example of ODP Leg 105 Site 646 in Figure 3.1. From the original data logs (Fig. 3.1a) I removed loops and spurious data, extrapolated the data to the starting depth of 0 mbsf and interpolated for missing data. The data was depth-time-converted using the P-wave velocity data and the data were resampled to 1 ms to fit to the sample rate of the seismic data (Fig. 3.1b). Then, I calculated the reflection coefficients for each ODP/IODP Site and applied a convolution with a 70 Hz Ricker wavelet (Ricker, 1953) to create the synthetic seismograms (Fig. 3.1c). The convolution of the reflection coefficients with an artificial Ricker wavelet yields better results than synthetics obtained by application of a wavelet estimated from the seismic data (Wildeboer Schut and Uenzelmann-Neben, 2006). The frequency of 70 Hz was chosen as applied Ricker wavelets of lower frequencies bore a loss of resolution while higher frequency wavelets introduced reflectors to the synthetic seismograms (Fig. 3.1c), which are not observed in the seismic data. The data were resampled with the General Mapping Tool (GMT©). Data processing was conducted in FOCUS/DISCO (PARADIGM©) with the stand-alone programs loginit and logproc. No filters were applied to the synthetic seismograms.
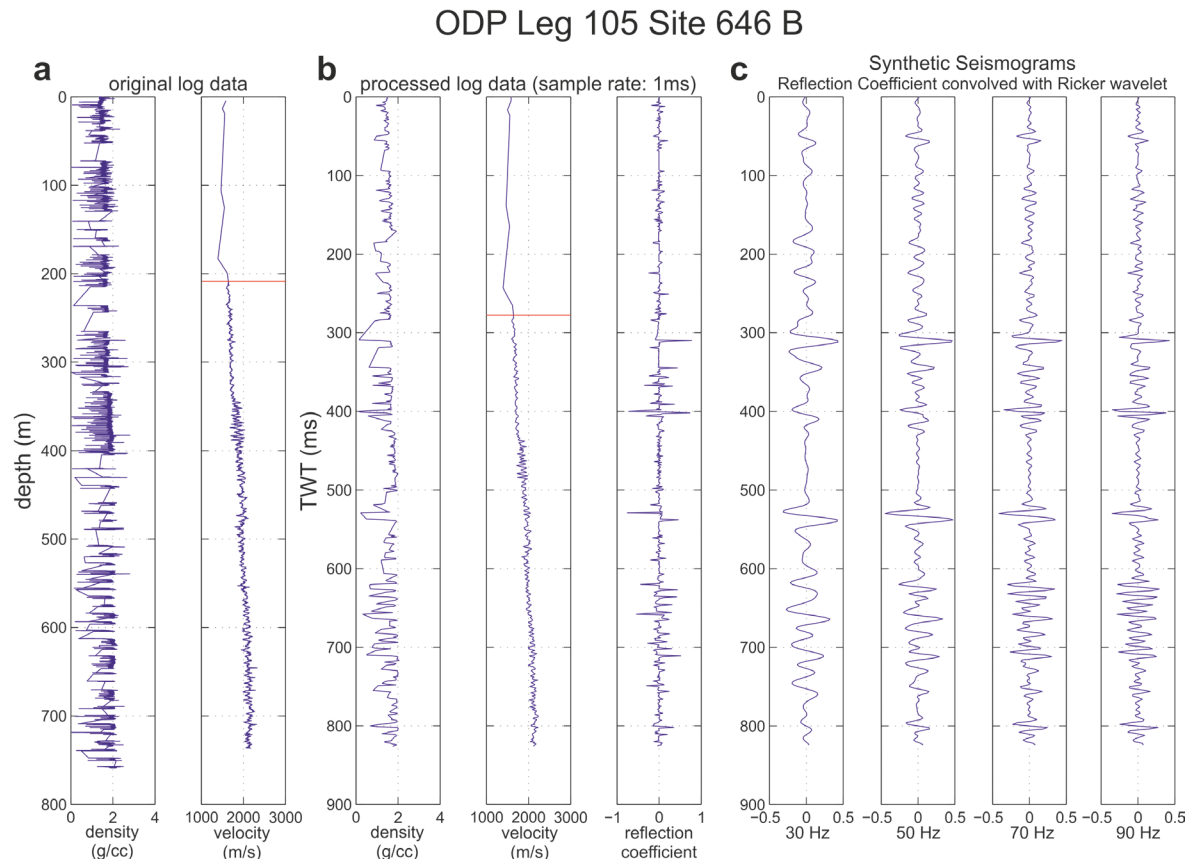
Figure 3.1. ODP Leg 105 Site 646 data. (a) Original density (left) and velocity (right) log data vs. depth. (b) Processed density (left) and velocity (middle) data and the calculated reflection coefficient (right) vs. TWT. (c) Convolution of the reflection coefficient with 30 Hz, 50 Hz, 70 Hz, and 90 Hz Ricker wavelets yields synthetic seismograms.

3.1.3 Correlation and interpretation of synthetic seismograms and seismic data

The prominent reflectors in the synthetic seismograms are correlated to the high amplitude reflections observed in our seismic data following the seismostratigraphic concept of Arthur *et al.* (1989) at ODP Leg 105 Site 646 (Fig. 3.2). Three reflectors, A1, A2 and A3, were

added to the stratigraphy because significant changes in reflection characteristics were observed (Fig. 3.2). These reflectors were dated by means of the sedimentation rate at ODP Leg 105 Site 646 (Müller-Michaelis *et al.*, 2013).

The processed seismic reflection data were uploaded and interpreted on a Landmark Seisworks 2D © system. I tracked and picked the seismic horizons throughout the complete seismic reflection data set and calculated the depths of the seismic horizons and the seismic unit thicknesses. The depth information as well as the unit thickness were gridded and displayed with the General Mapping Tool (GMT©). The depocenters were defined by the root mean square (rms) value of the thickness of each seismic unit, i.e. unit thickness values above the rms value were defined as depocenters. The horizon depths, the depocenter locations as well as reflector terminations observed in the seismic lines were used to analyze the distribution of the sedimentary units at the Eirik Drift in relation to the paleo deep current activity (Ch. 5 and 6).
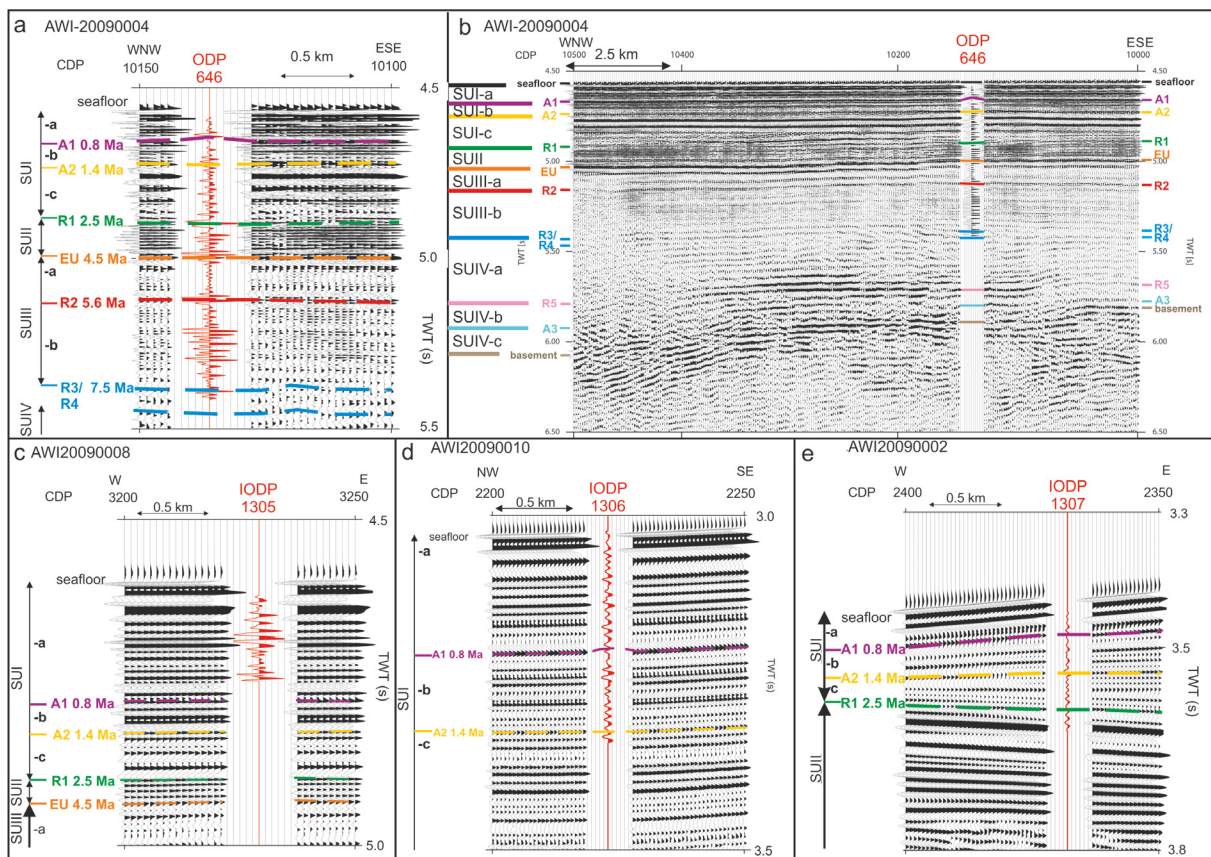
Figure 3.2. Correlation of the synthetic seismograms of each drill site with the seismic reflection data. (a) ODP Leg 105 Site 646 seismogram (red) incorporated to seismic line AWI-20090004 (CDP 10100 to 10150 vs. TWT 4.5 to 5.5 s). (b) Subsection of seismic line AWI-20090004 (CDP 10000 to 10500 vs. TWT 4.5 to 6.5 s) with the incorporated ODP Leg 105 Site 646 data. (c) IODP Exp. 303 Site U1305 seismogram (red) incorporated to seismic line AWI-20090008 (CDP 3200 to 3250 vs. TWT 4.5 to 5.0 s). (d) IODP Exp. 303 Site U1306 synthetic seismogram (red) incorporated to seismic line AWI-20090010 (CDP 2200 to 2250 vs. TWT 3.0 to 3.5 s). (e) IODP Exp. Site U1307 synthetic seismogram (red) incorporated to seismic line AWI-20090002 (CDP 2350 to 2400 vs. TWT 3.3 to 3.8 s). SUI-SUIV: Seismic Units; A1-A3, R1-R5, EU: Seismic horizons. Modified after Müller-Michaelis *et al.* (2013).

3.2 Seismic oceanography

3.2.1 Seismic oceanography data processing

Seismic oceanography is a promising method of using seismic reflection data for oceanographic reasons as the high spatial resolution can create detailed images of thermohaline structure in the ocean (Holbrook *et al.*, 2003; Ruddick *et al.*, 2009). So far, seismic oceanography analyses have been conducted solely in the upper ocean (< 1500 m) (e.g. Biescas *et al.*, 2008; Buffett *et al.*, 2009; Krahmann *et al.*, 2008; Nandi *et al.*, 2004; Papenberg *et al.*, 2010; Pinheiro *et al.*, 2010; Tsuji *et al.*, 2005). This is due to two major problems, which arise from investigating the deeper ocean: Firstly, the increasing signal loss in large water depths of the already weak reflections amplitude caused by thermohaline structures. Secondly, the high amplitude seafloor reflection can disturb or even destroy the signal of the much weaker thermohaline reflections in the water column above during stacking or migration processing steps. To preserve the amplitudes in the water column the pre-stack data processing was therefore conducted for each single shot. The conventional processing steps of geometry definition, zero-phase filtering and static shift were applied to the seismic reflection data (Fig. 3.3a). The seafloor was picked and the amplitudes below were reduced to the amplitudes of the water column (Fig. 3.3b). An automatic picking algorithm was used to find the maximum amplitude, which was assumed to be congruent with the seafloor reflection. However, in some parts of each profile higher amplitudes are found below the seafloor and thus, the picks had to be checked and corrected manually. The direct wave energy that has not undergone a reflection was suppressed by means of a Median filter (Figs. 3.3b and c). For this purpose a copy of the data panel was shifted so that the direct wave is flattened to horizontal. A weighted moving average was performed over the shifted panel to emphasize events with the specified moveout and suppress events with other moveouts. Then, the panel was shifted back and subtracted from the original data and thus the direct wave was removed (Fig. 3.3c). Noisy traces were removed from the shots, which were then CDP sorted. Normal move-out (NMO) correction was applied and the data were stacked. A location dependent, weighted mean of the sound velocity profiles of the MSM12/2 CTD stations was used for the NMO correction. Using the measured velocity yields results of a similar good quality as a handpicked velocity model and is an improvement over a fixed sound velocity value (Fortin and Holbrook, 2009). A lateral running mix to increase the signal to noise ratio of the data was applied as well as a gain to the profile for display to visualize the thermohaline reflections. The data processing was carried out with the open source seismic utilities package SEISMIC UNIX.
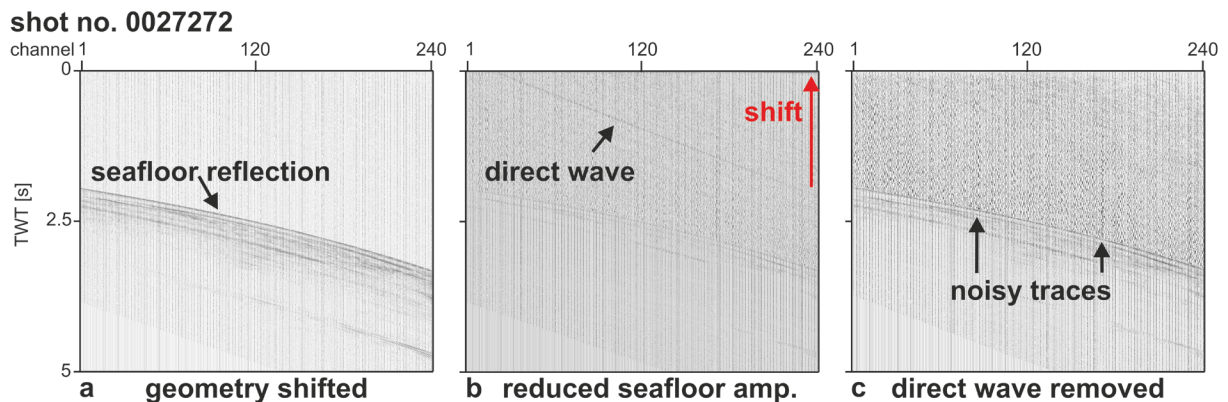
Figure 3.3. Single-shot processing example for shot no. 0027272. 240 channels vs. 0-5 s TWT. (a) Geometry shifted shot. Seafloor reflection is highlighted. (b) Shot with reduced amplitudes (amp.) of the seafloor and below. The direct wave is highlighted and its shift for the direct wave removal by Median filter is indicated in red. (c) Shot after direct wave removal. Noisy traces are highlighted.

3.2.2 CTD data processing

Temperature, salinity and pressure data of each CTD cast were used to calculate the sound velocity after Chen and Millero (1977). The sound velocity was then used for the depth-time conversion of the data. Analogue to the generation of synthetic seismograms from drill logs (Ch. 3.1.2) the data was resampled to the seismic sample rate of 1 ms, the reflection coefficients were calculated using the acoustic impedance contrast and the synthetic seismograms were computed by convolution with a 70 Hz Ricker wavelet. To display the synthetic seismograms to the temperature-depth profiles of the CTD casts the synthetic seismograms were converted back to the depth domain (Fig. 3.4). The CTD data processing was carried out with MATLAB MathWorks© software
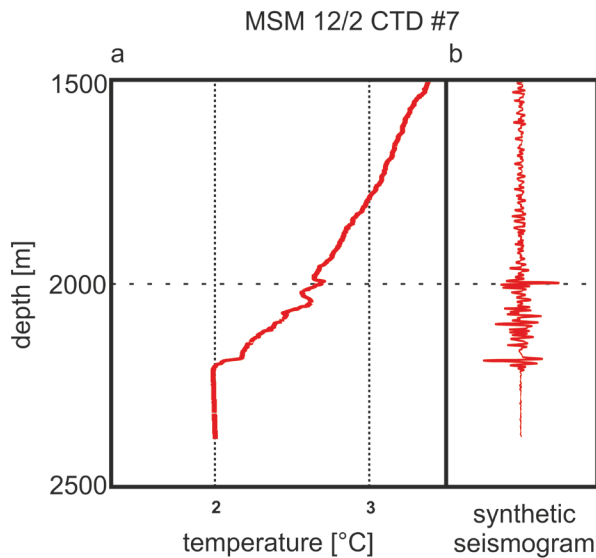
Figure 3.4. Example of MSM12/2 CTD #7 in the depth range 1500-2500 m (for location see Fig. 2.1).
(a) Temperature vs. depth profile.
(b) Synthetic seismogram calculated from the CTD data.

4 Contributions to scientific publications

Here, I present a brief summary of each of the scientific publications, which comprise this PhD project in order to report the individual contributions of each of its authors. The publications are included in full in chapters 5 - 7. The datasets used and the applied processing steps and methods have been explained in chapters 2 (Datasets) and 3 (Methods), respectively.

4.1 A revised Early Miocene age for the instigation of the Eirik Drift offshore southern Greenland: Evidence from high-resolution seismic reflection data

Müller-Michaelis, A., Uenzelmann-Neben, G., Stein, R., 2013 A revised Early Miocene age for the instigation of the Eirik Drift, offshore southern Greenland: Evidence from high-resolution seismic reflection data. Marine Geology. doi:10.1016/j.margeo.2013.04.012.

This publication (see Ch. 5) consits of a seismostratigraphic analysis of the Eirik Drift. The base of this study is the incorporation of high-resolution multichannel seismic reflection data collected in 2009 with geological information from ODP Leg 105 Site 646 (Shipboard Scientific Party, 1987) and IODP Expedition 303 Sites U1305, U1306 and U1307 (Channell *et al.*, 2010). We refined and corrected the pre-existing seismostratigraphic concept by Arthur *et al.* (1989). We reassessed the onset of drift building at the Eirik Drift to the Early Miocene (prior: Early Pliocene (Arthur *et al.*, 1989)), i.e. we could evidence a much earlier influence of deep-water circulation at the Eirik Drift. This knowledge is important for paleoceanographic and paleoclimatic studies in the North Atlantic, as the present deep-water circulation at the Eirik Drift is a main contributor to the global Thermohaline Circulation, which is closely connected to the world's climate.

I defined the geometry and conducted CDP sorting, velocity analysis, NMO correction, time migration and filtering of the seismic reflection data. I calculated the synthetic seismograms out of the density and P-wave velocity logs from the drill sites. I correlated the synthetic seismograms with the seismic reflection data. I identified and defined seismic horizons, tracked and picked them throughout the complete seismic reflection data set. I calculated the depths of the seismic horizons and the seismic unit thicknesses and wrote the manuscript. Dr. Uenzelmann-Neben supervised the project and was Chief Scientist during MSM12/2. Prof. Dr. Stein was also participant of the MSM12/2 cruise and helped me with the interpretation of the geological borehole data (see Ch. 5.4.2). All authors revised the manuscript and contributed to the results in several discussions.

4.2 Development of the Western Boundary Undercurrent at the Eirik Drift related to changing climate since the early Miocene

Müller-Michaelis, A. and Uenzelmann-Neben, G., 2013 (in revision). Development of the Western Boundary Undercurrent at the Eirik Drift related to changing climate since the early Miocene. Deep-Sea Research Part I (submitted 04/2013; in revision 11/2013, moderate revisions advised).

In this publication (see Ch. 6), I used my refined seismostratigraphic concept (Müller-Michaelis *et al.*, 2013) to reconstruct the deep Paleocirculation at the Eirik Drift. Changes of strength and pathways of the WBUC in a changing climate were revealed by analyzing the morphology of each seismic horizon, the thickness, location and orientation of the overlying depocenters and the internal reflection characteristics of each seismic unit. We observe a

strong WBUC at the Eirik drift during warm climates and at the beginning of cooling phases. A weak WBUC is observed during enhanced cooling phases accompanied by Northern Hemisphere Glaciation. We concluded that the deep-water formation regions as well as the deep current system of the North Atlantic shifted south during cold climate phases with enhanced ice extent at the Nordic Seas and that the main deep-water route just affected the Eirik Drift during warmer climate.

I defined the geometry and conducted CDP sorting, velocity analysis, NMO correction, time migration and filtering of the seismic reflection data. I calculated the synthetic seismograms out of the density and P-wave velocity logs from the drill sites. I correlated the synthetic seismograms with the seismic reflection data. I identified and defined seismic horizons, tracked and picked them throughout the complete seismic reflection data set and calculated the depths of the seismic horizons and the seismic unit thicknesses. I developed a deep circulation model for the northern North Atlantic and wrote the manuscript. Dr. Uenzelmann-Neben supervised the project and was Chief Scientist during MSM12/2. She revised the manuscript and contributed to the results in several discussions.

4.3 Using seismic reflection data to reveal high-resolution structure and pathway of the upper Western Boundary Undercurrent core at the Eirik Drift

Müller-Michaelis, A. and Uenzelmann-Neben, G. (submitted 11/2013). Using seismic reflection data to reveal high-resolution structure and pathway of the upper Western Boundary Undercurrent core at the Eirik Drift. Geophysical Research Letters (submitted 11/2013).

In this study (see Ch. 7), the seismic oceanography method was applied to the seismic data. We were able to identify and track the structure of the present upper WBUC core at the Eirik Drift. This is the first seismic oceanography study, which has been able to resolve thermohaline fine structure in depths > 1500 m. We showed that discrete classical oceanographic measurements (CTDs) are not able to resolve the structure of the WBUC core in detail like the seismic oceanography method can. We evidenced the WBUC pathways suggested by Müller-Michaelis and Uenzelmann-Neben (2013 (in revision)) and the influence of the changing topography over the Eirik Drift to the pathway and structure of the deep-current core.

I applied the conventional seismic data processing steps of geometry definition, zero-phase filtering and static shift to the shot-sorted seismic data. For the investigation of seismic oceanographic structures in greater depth directly at the seafloor, I additionally picked the seafloor amplitude in shot gathers and reduced the amplitudes below to that of the amplitudes within the deepest part of the water column. I removed the direct wave energy before I conducted CDP sorting, NMO correction and stacking of the data. For the NMO correction I calculated a weighted mean of the sound velocity recorded in the MSM12/2 CTD casts. I applied a lateral running mix filter and a gain to the data for display to increase the signal to noise ratio and visualize the thermohaline fine structure reflections. I identified pathway and structure of the upper WBUC core in the seismic data and wrote the manuscript. Dr. Uenzelmann-Neben supervised the project and was Chief Scientist during MSM12/2. She revised the manuscript and contributed to the results in several discussions.

5 First paper: Miocene development of the Eirik Drift

5.1 Abstract

The Eirik Drift lies on the continental slope south of Greenland, where it has been formed under the influence of Northern Component Water (NCW). NCW flow is an essential part of the global Thermohaline Circulation (THC), which is closely connected to the world's climate. Changes in pathways and intensity of NCW flow bear information about modifications of the North Atlantic THC in a changing climate. There is some disagreement about when deep-current controlled sedimentation at the Eirik Drift started. While the onset of drift building was previously dated as early Pliocene or late Miocene in age we suggest that the effect of large-scale current deposition had been initiated by at least 19-17 Ma based on the seismostratigraphic analysis of sedimentary structures identified in a set of high-resolution seismic reflection data. This assumption of an early Miocene onset of NCW flow is supported by regional evidence regarding the breaching of the Greenland-Scotland Ridge, which is documented in several erosional unconformities within the North Atlantic. After the onset of deep-current controlled sedimentation at the Eirik Drift, two major changes in the deep-current system are revealed during the Miocene: At the mid- to late Miocene boundary (12-10 Ma) and at 7.5 Ma.

5.2 Introduction

The global Thermohaline Circulation (THC) is closely connected to major changes in Earth's climate (Dickson and Brown, 1994). The surface branch of the THC transports heat and freshwater around the world's oceans and interacts with the overlying atmosphere through surface fluxes (Schmitz, 1996). The formation of deep water in the basins of the northern North Atlantic, Arctic and Antarctic is a mechanism driving the global THC (Dickson and Brown, 1994; Schmitz, 1996). The Eirik Drift, located offshore southern Greenland is built under the influence of the deep-water currents originating as overflows from the Nordic Sea deep-water formation regions (North Atlantic Deep Water (NADW)) (Fig. 5.1; e.g. Arthur *et al.*, 1989; Hunter *et al.*, 2007a; Wold, 1994). Therefore, the sedimentary structures and packages of the Eirik Drift archive changes in strength and direction of these deep-water currents. As the NADW flow is today's main contributor to the lower branch of the North Atlantic THC, decoding of these deep-water currents yields information about the development of the global THC (Schmitz, 1996).

Even though it is certain that the Eirik Drift was built under the influence of these deep-water currents (e.g. Arthur *et al.*, 1989; Wold, 1994; Hunter *et al.*, 2007a,b), the timing of the onset of development of the Eirik Drift remains ambiguous. Arthur *et al.* (1989) suggested that the "modern" pattern of deep circulation in the Labrador Sea was established some time in the late Miocene (8.2-7.5 Ma), but they dated the onset of deep current-controlled deposition at 4.5 Ma. By investigating accumulation rates of sediment drifts in the northern North Atlantic, Wold (1994), however, found that drift building at the Eirik Drift may have started 7-8 Ma ago. The study regarding the North Atlantic deep circulation by Wright and Miller (1996) is based on the findings of Wold (1994), but dates the onset of drift accumulation at Eirik Drift at 5-6 Ma. This date of onset of drift building at the Eirik Drift is used in further investigations by several authors (e.g. Wright, 1998; Cramer *et al.*, 2009; Miller *et al.*, 2009). On the other hand, recent works of Hunter *et al.* (2007a) and Hunter *et al.* (2007b) based their investigations at the Eirik Drift on the interpretation from Arthur *et al.*

(1989) with the onset of deep-current controlled sedimentation at 4.5 Ma. In this study, we aim to reappraise the question of the timing of the onset of drift accumulation at Eirik Drift on the basis of an analysis of a tight grid of newly collected seismic reflection data. We incorporate these seismic data with geological information and age-models of Ocean Drilling Program (ODP)/Integrated Ocean Drilling Program (IODP) drill sites, including ODP Leg 105 Site 646 and IODP Expedition 303 Sites U1305, U1306 and U1307 in a bid to better define the inception of drift growth offshore southern Greenland (Figs. 5.1 and 5.2).

5.3 Settings

5.3.1 Geological settings and drift morphology

The Labrador Sea basin is about 900 km wide and opens to the SE into the North Atlantic (Fig. 5.1; Chalmers and Pulvertaft, 2001). This basin formed as a consequence of continental rifting between Greenland and Labrador, which commenced during the Late Cretaceous (anomaly 27, ~63 Ma) (Chalmers and Pulvertaft, 2001), but had ceased by ~35 Ma ago (Srivastava and Roest, 1999). The Eirik Drift is located in the eastern part of the Labrador Sea, south of the southern tip of Greenland (Fig. 5.1). Two narrow parallel WSW-trending basement ridges, which formed during the rifting process between about 61 and 40 Ma (Mueller *et al.*, 2008), underlie the Eirik Drift (Fig. 5.2; Le Pichon *et al.*, 1971; Srivastava and Arthur, 1989). These basement elevations are believed to have controlled the onset of drift building in this region (Srivastava and Arthur, 1989; Hunter *et al.*, 2007b). At present, the main Eirik Drift crest extends from a water depth of 1500 m in the NE to ~3600 m, and extends a total length of 360 km in the SW over these basement ridges (Fig. 5.2; Hunter *et al.*, 2007a). The Eirik Ridge is classified as a detached giant elongated drift formed under the influence of deep contour currents (e.g. Stow *et al.*, 1998; Faugères *et al.*, 1999). Hunter *et al.* (2007a) reported three NW-trending subsidiary ridges, which extend to the NW from the main drift crest (Fig. 5.2).

The Greenland-Scotland-Ridge (GSR; Fig. 5.1a) is the gateway for northern-sourced deep-water into the northern North Atlantic. Therefore, its formation and subsidence history is important for the evolution of the Eirik Drift but has yet to be fully understood. The western part of the GSR between Greenland and Iceland is called the Denmark Strait (Fig. 5.1a). Here, first significant overflow was observed at ~7 Ma (Bohrmann *et al.*, 1990) and the present sill depth lies at ~620 m (Hansen and Østerhus, 2000). The eastern part of the GSR is a complex ridge-channel-system (Fig. 5.1). The Iceland-Faroe-Ridge with a present maximum sill depth of ~480 m (Hansen and Østerhus, 2000) experienced first significant overflows at ~13-11 Ma (Bohrmann *et al.*, 1990). The deepest part of the GSR is the Faroe Conduit (~840 m), a pathway through the Faroe-Shetland Channel into the Iceland Basin via the Faroe Bank Channel (Fig. 5.1; Hansen and Østerhus, 2000). The Faroe Conduit developed in early Miocene and is suggested as the first true deep-water connection between the Nordic Seas and the Atlantic (Stoker *et al.*, 2005). Sufficient subsidence of the GSR with first overflows at the distal eastern part of the GSR into the Rockall Trough (Fig. 5.1) is suggested for the early Oligocene (Davies *et al.*, 2001). The sill between the Faroe-Shetland Chanel and the Rockall Trough is called Wyville-Thomson Ridge and has a present sill-depth of ~600 m (Fig. 5.1; Hansen and Østerhus, 2000). The main deep-water connection of the Arctic Ocean to the Nordic Seas, the Fram Strait, occurred concomitant with the development of the Faroe Conduit (Ehlers and Jokat, 2013).
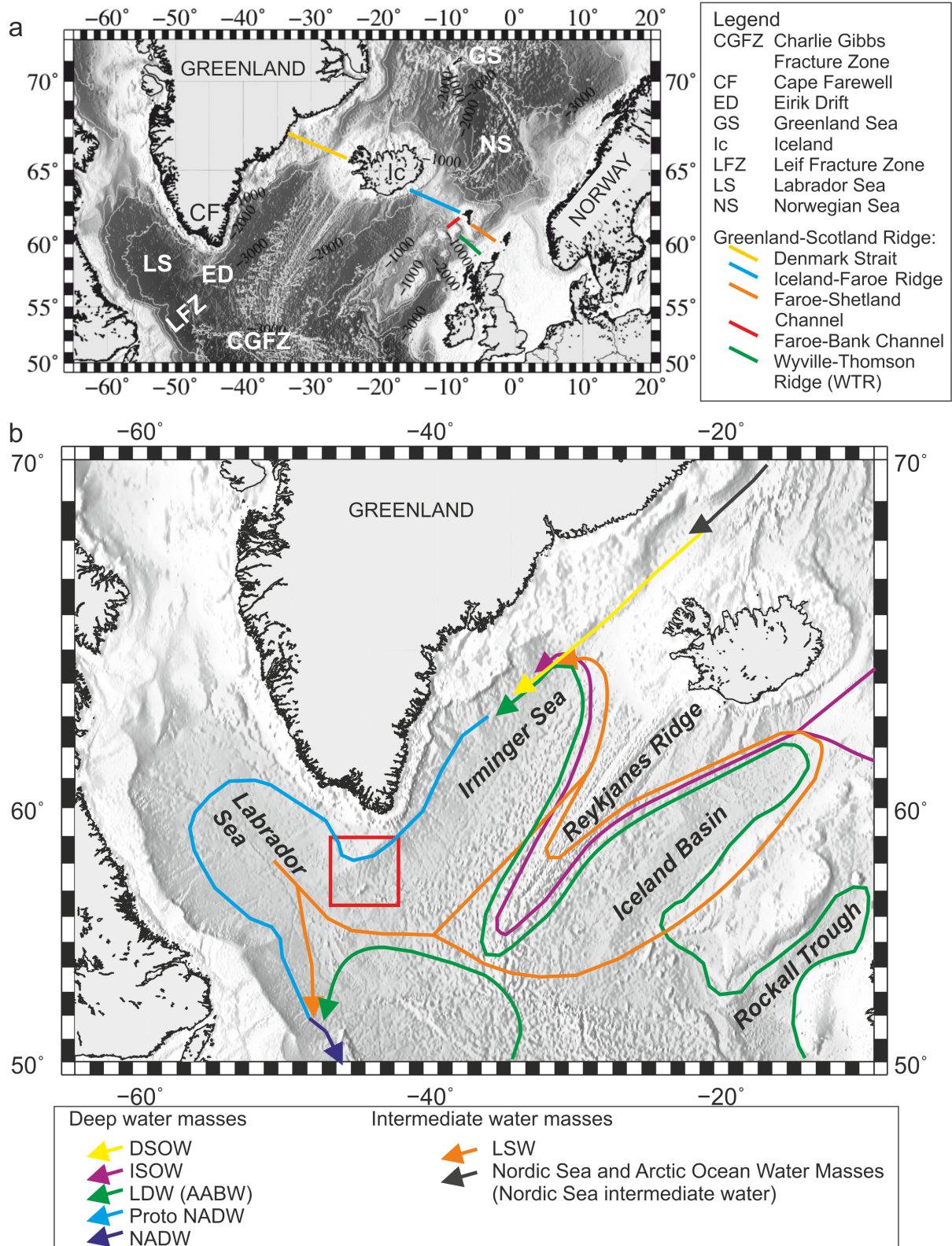
Figure 5.1. Satellite-derived bathymetry map (Smith and Sandwell, 1997) of the North Atlantic. (a) Basins, ridges and fracture zones in the northern North Atlantic (see text for description). (b) Water mass contribution to the formation of the North Atlantic Deep Water (modified from Schmitz, 1996; see text for description). The red box shows the study area (see Fig. 5.2). Water mass abbreviations: DSOW, Denmark Strait Overflow Water; ISOW, Iceland Overflow Water; LDW, Lower Deep Water; AABW, Antarctic Bottom Water; NADW, North Atlantic Deep Water; LSW, Labrador Sea Water.
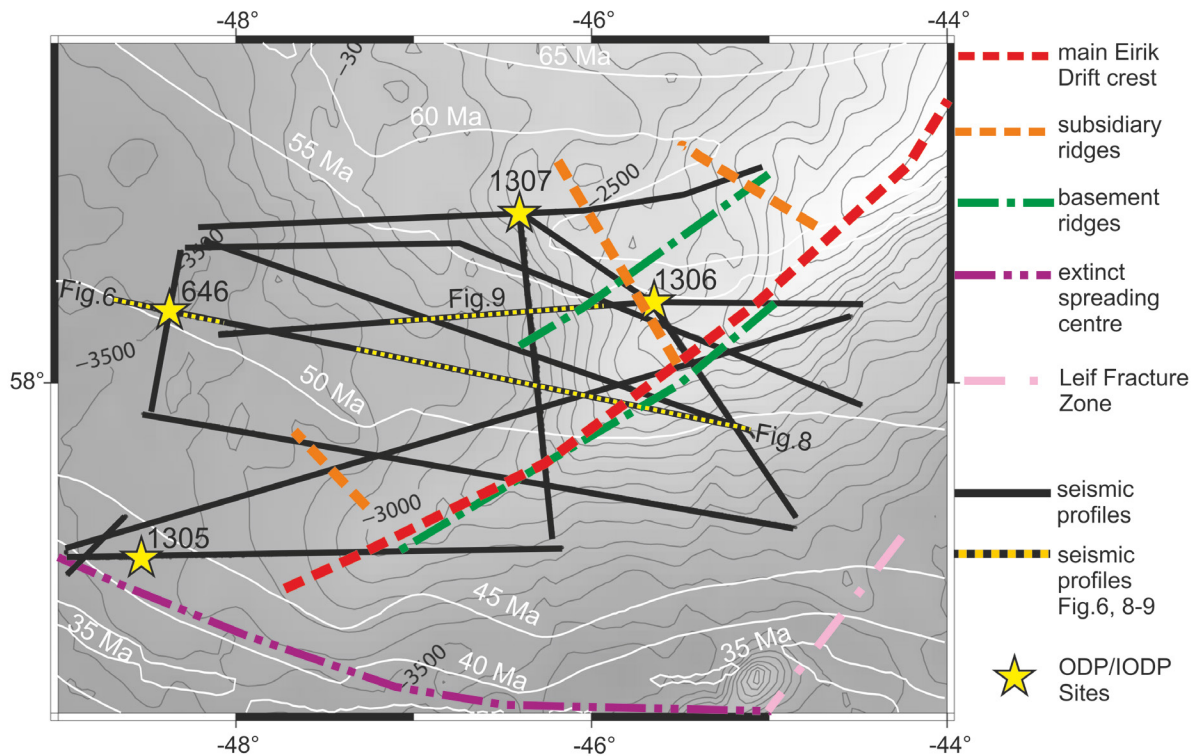
Figure 5.2. Satellite-derived bathymetry map (Smith and Sandwell 1997; red box in Figure 5.1b) showing the location of the seismic lines (black lines). The dashed yellow seismic lines are displayed in Figs. 5.6, 5.8, and 5.9. The yellow stars show ODP Leg 105 Site 646 (Shipboard Scientific Party, 1987a) and IODP Expedition 303 Sites U1305, U1306 and U1307 (Channell *et al.*, 2010). The dashed red line shows the NE-SW trending crest of the main Eirik Drift. The dashed orange lines indicate the 3 secondary ridges described by Hunter *et al.* (2007a and b). The dashed green lines mark the location of the two NE-SW trending basement ridges. The purple dashed line indicates the location of the extinct spreading center of the Labrador Sea Basin. The pink dashed line shows the Leif Fracture Zone. The white contour lines mark the oceanic basement age (Mueller *et al.*, 2008).

5.3.2 Present-day Oceanographic setting

At present, the Western Boundary Undercurrent (WBUC) is the active deep current in the vicinity of the Eirik Drift. In this region, it is located between the 1900 m and 3000 m isobaths and composed of four main water masses: Denmark Strait Overflow Water (DSOW), Iceland Scotland Overflow Water (ISOW), Labrador Sea Water (LSW) and modified Antarctic Bottom Water (AABW) (Dickson and Brown, 1994; Schmitz, 1996). Convective mixing in the Greenland and Norwegian Seas together with Arctic Ocean outflow forms Nordic Sea intermediate and deep water (Fig. 5.1; Hansen and Østerhus, 2000). These overspill the shallow Greenland-Scotland Ridge (GSR) via the Denmark Strait (~620 m; DSOW) and the Iceland-Scotland Ridge (ISOW), mainly through the Faroe-Conduit (~840 m) (Fig. 5.1; Hansen and Østerhus, 2000). While descending into the northern North Atlantic, these overflows entrain LSW and Lower Deep Water (LDW) (Fig. 5.1). LSW is formed by convective overturning in the Labrador Sea and is found at depths between 700 and 1500 m off the east coast of Greenland (Fig. 5.1; Dickson and Brown, 1994; Schmitz, 1996). LDW is modified AABW. It flows northward from its formation point in the Antarctic as bottom current (below 3000 m) and entrains ambient waters on its way (Dickson and Brown, 1994; Schmitz, 1996). The overflows, including the entrained water masses, together form the WBUC off the east coast of Greenland (Fig. 5.1; Dickson and Brown, 1994; Schmitz, 1996). ISOW forms the upper layer of the WBUC with a core depth around 2000 m and DSOW forms the lower layer with a core depth around 3000 m off Cape Farewell (Dickson and Brown, 1994; Schmitz, 1996). The WBUC entrains more surrounding water masses on its

way through the Labrador Basin and is modified to North Atlantic Deep Water (NADW) (Fig. 5.1; Hansen and Østerhus, 2000). NADW is the main contributor to the lower limb of the present day North Atlantic THC (Dickson and Brown, 1994; Schmitz, 1996). As the composition and pathways of the ancient northern-sourced deep-water are not well known, the precursor of the present NADW is called Northern Component Water (NCW).

5.4 Data and Methods

5.4.1 Seismic Reflection Data

In 2009, the Alfred Wegener Institute for Polar and Marine Research gathered ~ 2000 km of high-resolution seismic reflection data in the area of the Eirik Drift south of Greenland with the German research vessel Maria S. Merian (Fig. 5.2). Four GI-guns©, with a volume of about 1.4 l each, were used as a seismic source. Each of the GI-guns© consisted of a generator chamber (0.72 l volume) that produced the seismic signal, and an injector chamber (1.68 l volume), which was triggered with a 33 ms delay to suppress the bubble. The GI-guns© were fired every 10 s (corresponding to a shot-spacing of approximately 25 m), producing signals with frequencies of up to 300 Hz. Data with a sample interval of 1 ms were received using a high-resolution seismic data acquisition system (SERCEL SEAL©), consisting of both on-board and in-sea equipment. The total active streamer length was 3000 m, consisting of 240 channels, and additionally a lead-in cable length of 191 m. Navigation data were specified by GPS (Global Positioning System).

Processing of the seismic reflection data comprised geometry definition using the ship's navigation data, and Common Depth Point (CDP) sorting with a CDP spacing of 25 m. A precise velocity analysis (every 50 CDP) was carried out and used for normal moveout correction. After stacking, a time-migration was carried out (Omega-X migration) (Yilmaz, 2001). Band filtering with tapering (Hanning window) with the boundaries 20-25 Hz and 200-250 Hz, but no AGC (Automatic Gain Control) was applied to the data for display.

5.4.2 ODP / IODP data

The seismic survey was designed to image the seismic reflection geometry of the Eirik Drift and intersect four ODP and IODP scientific boreholes in the area (Fig. 5.2). The following description of ODP Leg 105 Site 646 (ODP 646) is derived from Srivastava *et al.* (1989) and Cremer (1989); results from IODP Expedition 303 Sites U1305 - U1307 are taken from Channell *et al.* (2010), Channell *et al.* (2006), Expedition 303 Scientists (2006) and Shipboard Scientific Party (2005).

5.4.2.1 ODP Leg 105 Site 646 (ODP 646)
ODP 646 lies in the west of the study area at a water depth of 3450 m (Fig. 5.2). The borehole recovered 766.7 m of dominantly fine-grained, terrigenous sediments, which comprise two major lithological units ranging back to the Late Miocene (Fig. 5.3). For the entire drilled sequence sedimentation rates average about 9.1 cm/ka.

5.4.2.2 IODP Expedition 303 Site U1305 (IODP 1305)
IODP 1305 is located 82.2 km south of ODP 646, in the SW corner of our study area at a water depth of 3459 m (Fig. 5.2). A single Quaternary lithologic unit of 295 m was obtained (Fig. 5.3), which documents the last 1.77 Ma and is dominated by varying mixtures of terrigenous components and biogenic material. The mean sedimentation rate for the drilled sequence is assumed to be 17.3 cm/ka using biostratigraphic and magnetostratigraphic data.

5.4.2.3 IODP Expedition 303 Site U1306 (IODP 1306)

IODP 1306 is located in the NE of the study area (Fig. 5.2) at a water depth of 2274 m. Drilling at IODP 1306 proved sediment as old as 1.95 Ma at a depth of 309.3 m. The single lithological unit consists of Quaternary terrigenous and biogenic sediments (Fig. 5.3), which are gradationally interbedded at scales of a few meters or less. The mean sedimentation rate for the drilled sequence was estimated to be 18 cm/ka by means of biostratigraphic and magnetostratigraphic data.
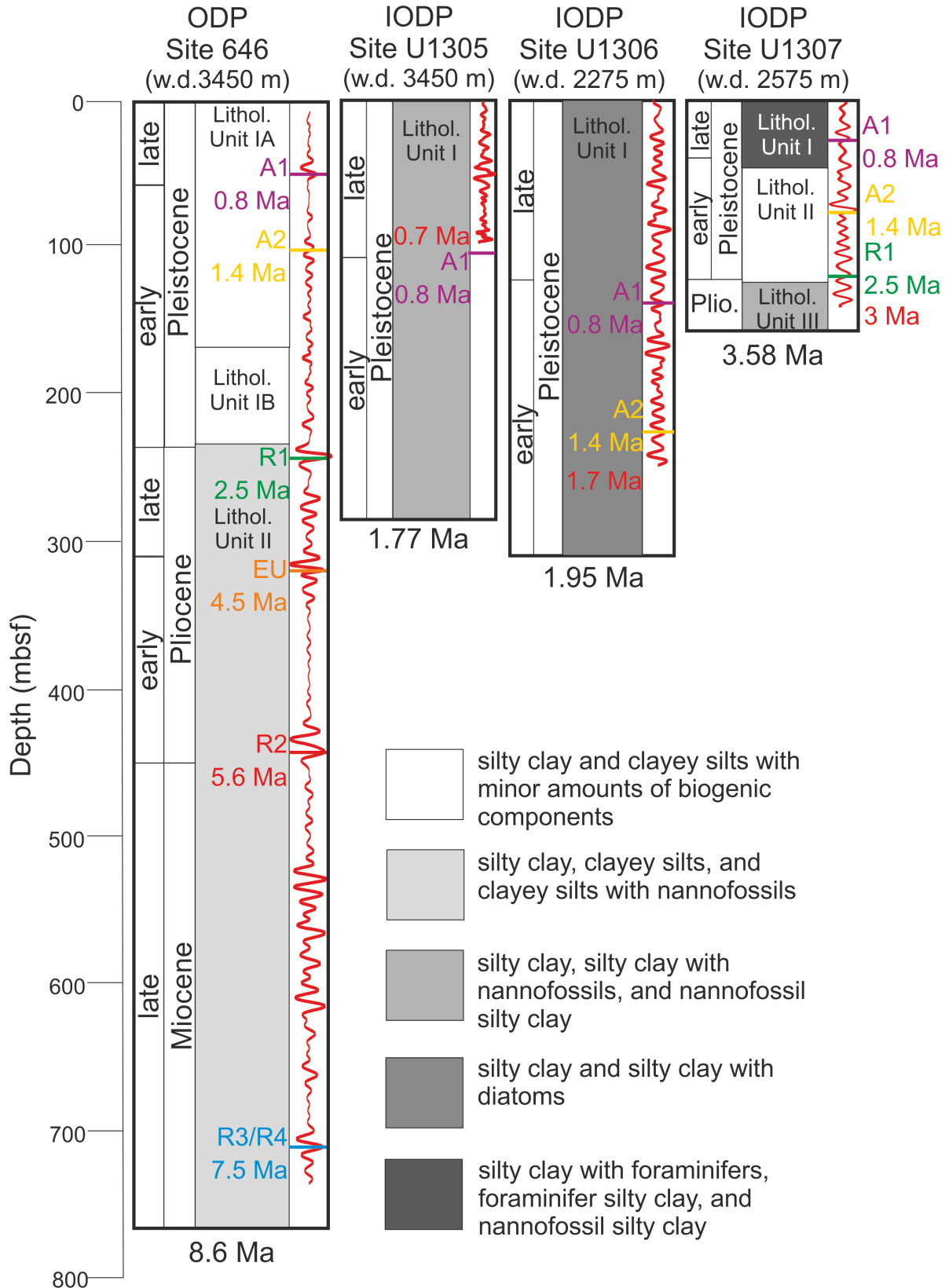
5.4.2.4 IODP Expedition 303 Site U1307 (IODP 1307)

IODP 1307 is located 53 km northwest of IODP 1306 (Fig. 5.2) at a water depth of 2575 m. This borehole cored 162.6 m of Upper Pliocene-Holocene sediments that comprise 3 lithologic units extending back to 3.58 Ma with variations in input of terrigenuous and biogenic components (Fig. 5.3). Apart from one possible hiatus (1.2-1.4 Ma; ~56-61 mbsf) the sedimentary record at IODP 1307 appears continuous with a mean sedimentation rate of 4.8 cm/ka.

5.4.2.5 Conversion of ODP/IODP logs to synthetic seismic data

Density and P-wave velocity data from the drill sites are needed to calculate synthetic seismograms, which enable a correlation of the seismic data with geological information (database: http://www-odp.tamu.edu/ or http://brg.ldeo.columbia.edu/data/odp/leg105/646B/). For ODP 646 Gamma ray attenuation (GRA) measurements with the whole core multi-sensing track tool (MST) provide GRA Bulk density data with a resolution of 0.006 m extending from 0.006 to 758.948 mbsf (Fig. 5.4a). Sonic velocity measurements of the split core are provided with only a very low resolution (in irregular intervals in the order of tens of meters). Downhole measurements conducted with a long spacing Sonic Tool provide seismic P-wave velocity data with a resolution of 0.15 m but only in the interval 208.788 to 744.931 mbsf. Therefore, a complementary combination of the downhole loggings and the laboratory measurements of the split core is used and spurious P-wave velocity data (<1400 m/s) are removed. The resulting P-wave velocity log is shown in Figure 5.4a. The black line marks the boundary between low-resolution split core measurements in the upper 208 m and the high-resolution downhole log.

The physical properties of IODP 1305 - 1307 were measured on whole-round core sections run through a MST and led to bulk density and seismic velocity data with a resolution of 0.05 m. Unfortunately, P-Wave velocity measurements are not available for the same depth range as the density logs; hence, the synthetic seismograms do not cover the total depth drilled (Fig. 5.3). Data processing comprised elimination of loops and spurious data, extrapolation to the starting depth of 0 mbsf and interpolation (resampling) for missing data and adjusting the sample intervals. A depth-time-conversion using the P-wave velocity data (sonic log) was carried out and the data were resampled to 1 ms to fit to the sample rate of our seismic data. Acoustic impedance and the reflection coefficients were computed. Wildeboer Schut and Uenzelmann-Neben (2006) showed that the convolution of the reflection coefficients with an artificial Ricker wavelet (Ricker, 1953) yields better results than synthetics obtained by application of a wavelet estimated from the seismic data. Therefore, Ricker wavelets in the frequency range between 20 and 250 Hz were applied to the reflection coefficients. The applied Ricker wavelets of lower frequencies bear a loss of resolution while high-frequency wavelets introduce reflectors, which are not observed in the seismic data. The convolution of the reflectivity series with a 70 Hz Ricker wavelet correlated best with the seismic data and therefore was used to generate the synthetic seismograms. The processed density and velocity data, the calculated impedance, reflection coefficients and the resulting synthetic traces in time domain (TWT) for all sites are shown on the right in Fig. 5.4 (5.4b: ODP 646; 5.4d: IODP 1305; 5.4f: IODP 1306; 5.4h: IODP 1307). No filters were applied to the synthetic seismograms.

Figure 5.3. Summary of litholigic units as a function of depth [mbsf] of the four drilling locations ODP Leg 105 Site 646 (Shipboard Scientific Party, 1987b) and IODP Expedition 303 Sites U1305, U1306 and U1307 (Expedition 303 Scientists, 2006). The red curves show the penetration depth of the synthetic seismograms calculated for each drill site using the density and P-wave velocity measurements. The colored lines show the horizons as identified in Fig. 5.5 and listed in Table 5.1. Please note we use the updated definitions of the early Pliocene (5.332–3.6 Ma), late Pliocene (3.6–2.588 Ma), and early Pleistocene (2.588–0.781 Ma) (Gibbard *et al.*, 2010). W.d. Water depth.
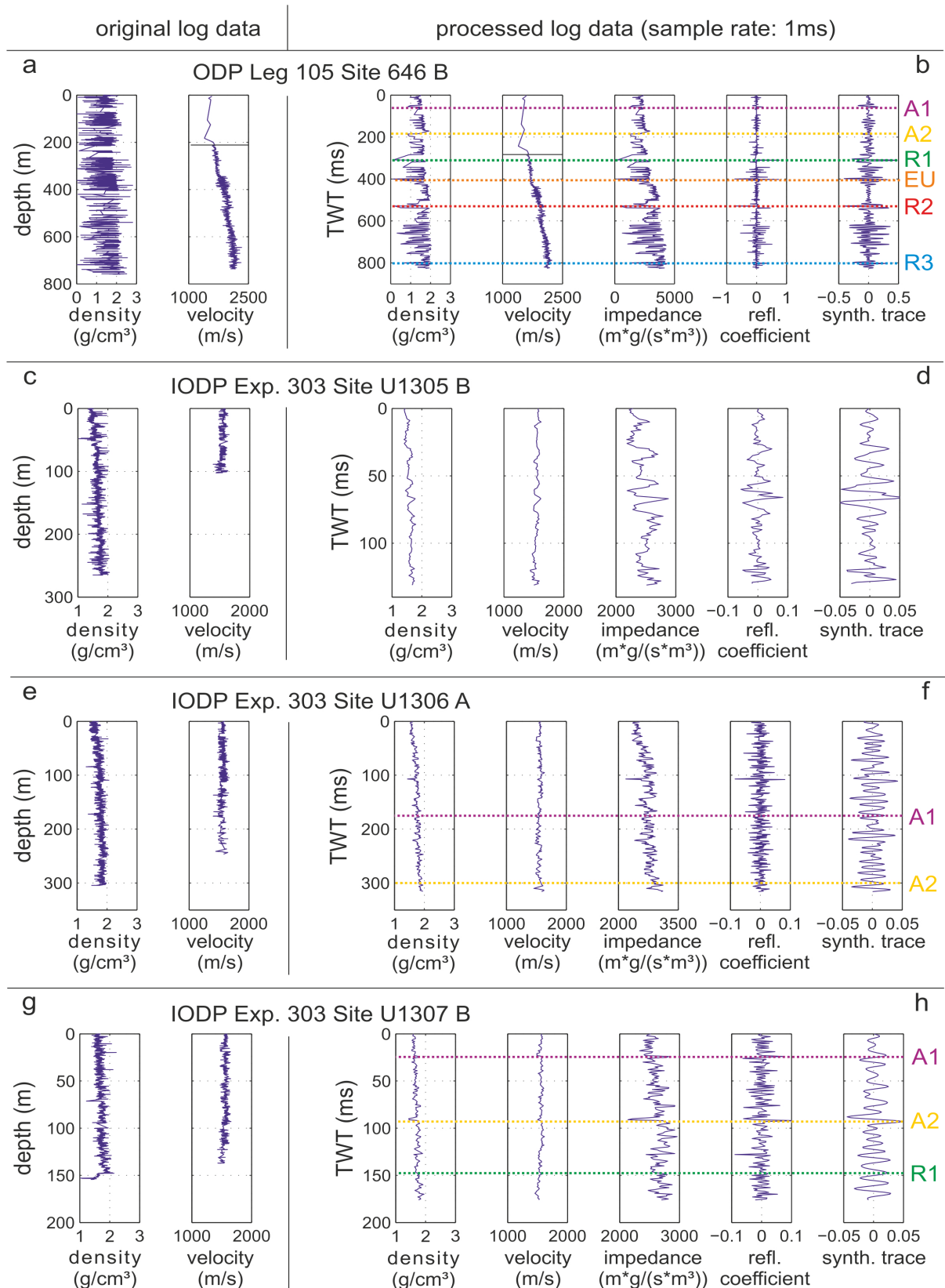
Figure 5.4. Original (left) and processed (right) Multi Sensor Track (MST) log data of the four drilling locations ODP Leg 105 Site 646 (a, b) and IODP Expedition 303 Sites U1305 (c, d), U1306 (e, f) and U1307 (g, h). The original log data on the left show density and P-wave velocity versus depth [m]. The processed data on the right show density, P-wave velocity, impedance, the reflection coefficient and the synthetic seismogram as result of the convolution of the reflection coefficient with a 70 Hz Ricker wavelet versus two-way-traveltime [TWT]. The colored lines show the horizons as identified in Fig. 5.5 and listed in Table 5.1.

5.5 Results

5.5.1 Correlation of geological and seismic data and seismostratigraphic model

The synthetic seismic data are compared and correlated with the recorded seismic data and thus, age control of the seismic data is possible (Fig. 5.5). Following the stratigraphy defined by Arthur *et al.* (1989), we identified horizon R1 (4.9 s TWT; Fig. 5.5a and b), an erosional unconformity which marks the boundary between seismic units SUII and SUIII (5.0 s TWT; Fig. 5.5a and b), horizon R2 (5.1 s TWT; Fig. 5.5a and b), reflector doublet R3/R4 (5.4 s and 5.45 s TWT; Fig. 5.5a and b) and below penetration depth horizon R5 (5.7 s TWT; Fig. 5.5b) and the basement reflector (5.9 s TWT; Fig. 5.5b) at the location of ODP 646 (Table 5.1). Three additional horizons were defined at ODP 646 (Fig. 5.5a and b; Table 5.1). Two horizons, A1 (4.65 s TWT; Fig. 5.5a and b) and A2 (4.7 s TWT; Fig. 5.5a and b), were defined within unit SUI, and horizon A3 (5.8 s TWT, Fig. 5.5b) within unit SUIV (Table 5.1). We extrapolated the identified and defined horizons at ODP 646 to our whole seismic grid. The synthetic seismograms of the shallow sites IODP 1305-1307 were also correlated with the seismic data (Fig. 5.5c-e). Using the sedimentation rates of each borehole proved to be consistent with our extrapolation of the upper horizons (Fig. 5.5c-e).
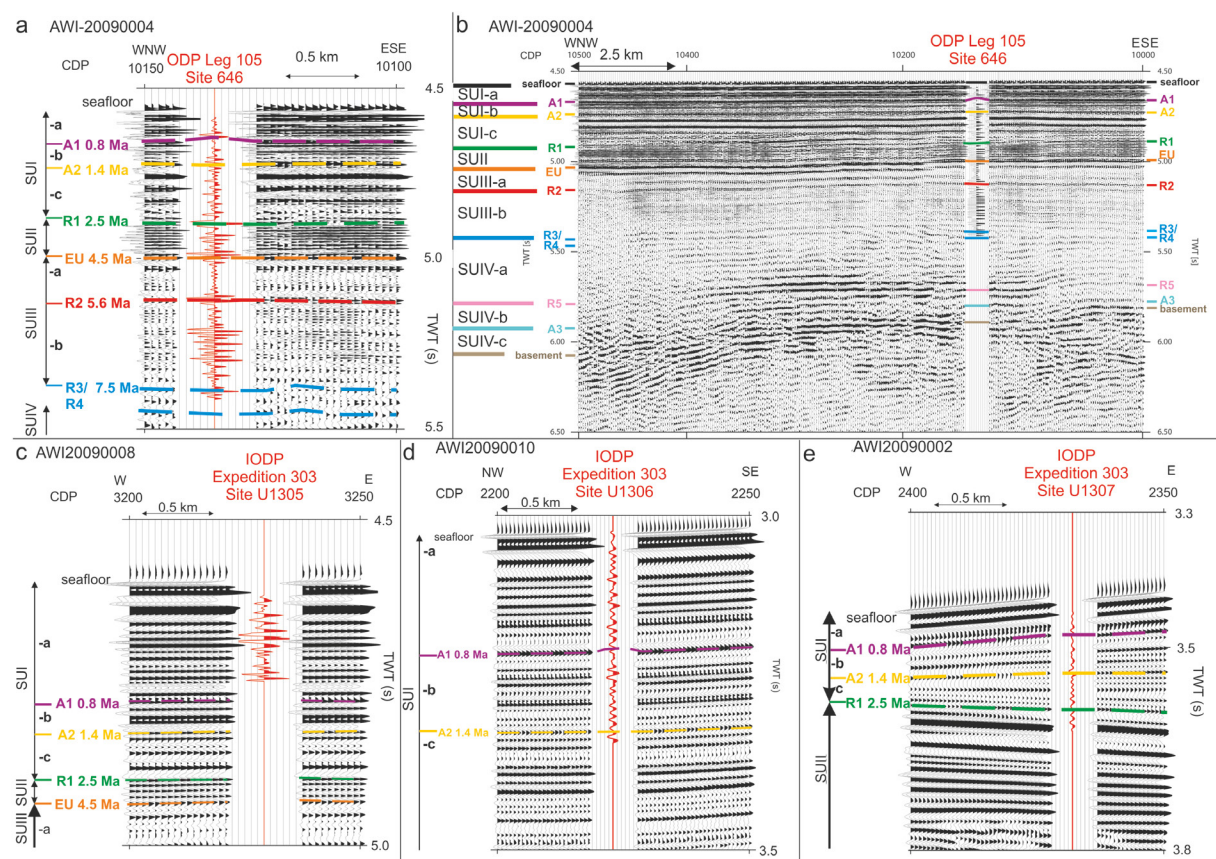
Figure 5.5. Correlation of the synthetic seismograms of each drill site with the seismic reflection data. (a) ODP Leg 105 Site 646 seismogram (red) incorporated to seismic line AWI-20090004 (CDP 10100 to 10150 vs. TWT 4.5 to 5.5 s). (b) Subsection of seismic line AWI-20090004 (CDP 10000 to 10500 vs. TWT 4.5 to 6.5 s) with the incorporated ODP Leg 105 Site 646 data. (c) IODP Exp. 303 Site U1305B seismogram (red) incorporated to seismic line AWI-20090008 (CDP 3200 to 3250 vs. TWT 4.5 to 5.0 s). (d) IODP Exp. 303 Site U1306A synthetic seismogram (red) incorporated to seismic line AWI-20090010 (CDP 2200 to 2250 vs. TWT 3.0 to 3.5 s). (e) IODP Exp. Site U1307B synthetic seismogram (red) incorporated to seismic line AWI-20090002 (CDP 2350 to 2400 vs. TWT 3.3 to 3.8 s). Seismic Units (SUI-IV) and horizons (A1-A3, R1-R5, EU) as listed in Table 5.1.

The definition of Seismic Units and the description of their seismic characteristics outlined in the following and summarized in Table 5.1 are conducted in the vicinity of ODP 646 in the western part of the study area (Fig. 5.6).

5.5.1.1 Seismic Unit I

Unit SUI corresponds to Lithologic Unit I (Fig. 5.3) and extends from the seafloor to medium- to high-amplitude horizon R1 (Fig. 5.5a and b; Fig. 5.6). Unit SUI is 270 to 400 ms thick and characterized by high amplitude reflections that are parallel to subparallel to the seafloor (Fig. 5.6). The lithological texture of unit SUI is marked by scattered coarse particles up to cobble size, which disappear at its base (Cremer, 1989). This base, horizon R1, is dated to 2.5 Ma, and related to the onset of major ice rafting around the Pliocene/Pleistocene boundary (Arthur *et al.*, 1989). The division into two lithologic subunits, IA and IB (Fig. 5.3), is based on a lower carbonate content (< 10 wt%) and a higher content of granule-sized particles in the lower lithologic subunit IB (Cremer, 1989). This subdivision is not used for our seismostratigraphic model.

We defined medium- to high-amplitude horizons A1 and A2 within unit SUI (Fig. 5.5a and b; Fig. 5.6). The sedimentation rate at ODP 646 was used to date these horizons. Horizon A1 lies at the boundary from Early to Mid-Pleistocene (0.8 Ma; Fig. 5.3). Subunit SUI-a, embedded between the seafloor and horizon A1, is 100 ms TWT thick and comprises continuous high-amplitude parallel reflections (Fig. 5.6). Subunit SUI-b extends between the high-amplitude horizons A1 and A2, which is dated at 1.4 Ma. Subunit SUI-b is also about 100 ms TWT thick, but characterized by medium amplitude, narrow-spaced (<0.01 s TWT), continuous to discontinuous, parallel reflections (Fig. 5.5a and b; Fig. 5.6). Subunit SUI-c is bordered by horizon A2 at the top and medium- to high-amplitude horizon R1 at the base. It comprises the lower part of Lithologic subunit IA and Lithologic subunit IB (Fig. 5.3). Subunit SUI-c thins from 200 ms TWT in the west to 100 ms TWT in the east (Fig. 5.6). The broad-spaced (0.04 s TWT), continuous to discontinuous, parallel to subparallel internal reflections increase in amplitude from its base to the top and converge towards the east (Fig. 5.5a and b; Fig. 5.6).

5.5.1.2 Seismic Unit II

Unit SUII is bordered by horizon R1 at the top and the erosional unconformity EU at the bottom, which appears as a high-amplitude horizon. Here, changes in grain size, sorting (Cremer, 1989) and foraminiferal assemblages (Kaminski *et al.*, 1989) were observed. Arthur *et al.* (1989) defined the base of Unit SUII, which is dated at 4.5 Ma, as the basal unconformity of the drift. Unit SUII is 100-140 ms thick, rises from the west to the east and consists of many narrow-spaced (<0.01 s TWT), continuous high amplitude reflections (Fig. 5.5a and b; Fig. 5.6).

5.5.1.3 Seismic Unit III

Unit SUIII extends between the erosional unconformity and the reflection doublet R3/R4 and thickens from 350 ms TWT in the west to 550 ms TWT in the east (Fig. 5.6). The basal reflection doublet R3/R4 consists of two medium- to high-amplitude, continuous to discontinuous reflections with a mean spacing of ~50 ms TWT (Fig. 5.5a and b; Fig. 5.6; Figs. 5.8-5.9). Unit SUIII is subdivided by the medium amplitude horizon R2 (Fig. 5.5a and b; Fig. 5.6). Horizon R2 as well as reflection doublet R3/R4 mark changes in the carbonate content (Kaminski *et al.*, 1989).

Subunit SUIII-a is dated at 4.5-5.6 Ma (Arthur *et al.*, 1989) and thickens from 100 ms TWT in the west to 300 ms TWT in the east. Amplitudes of, and spacing between, the internal reflections increase towards the top of subunit SUIII-a (Fig. 5.5a and b; Fig. 5.6). In the east, reflector truncations are observed at the erosional unconformity (Fig. 5.6). Subunit SUIII-b is between 150 and 300 ms TWT thick and consits of narrowly spaced (<0.01 s

TWT) parallel to subparallel mainly low amplitude reflections (Fig. 5.5a and b; Fig. 5.6). Subunit SUIII-b is dated as 5.6-7.5 Ma (Arthur *et al.*, 1989).

5.5.1.4 Seismic Unit IV

Unit SUIV is bordered at the top by the medium- to high-amplitude reflector doublet R3/R4, which is underlain by many diffractions, and the irregular acoustic basement horizon that forms the top of the oceanic crust between 5.8 and 6.2 s TWT (Fig. 5.6). The thickness of unit SUIV varies between 350 and 700 ms TWT due to the roughness of the basement. The top reflector doublet R3/R4 is dated at 7.5 Ma (Arthur *et al.*, 1989). The basement underlying the region of ODP 646 is dated 50-51 Ma (Fig. 5.2; Mueller *et al.*, 2008).

Unit SUIV is subdivided by the internal horizons R5 and A3, which lie beneath the drilling penetration depth of site ODP 646 (Fig. 5.5b; Fig. 5.6). Using the sedimentation rate of the upper part of unit SUIV, the ages of horizons R5 and A3 are estimated as middle Miocene (10-12 Ma) and early Miocene (17-19), respectively. However, considering the age of the underlying basement, the sedimentation rate within unit SUIV must be much lower and/or there must be hiatuses within this unit. The age estimation of these horizons will be discussed in detail later. Horizon R5 lies within a band of 3-4 high-amplitude reflections at depth between 5.6 and 5.7 s TWT. Besides this band and the top reflector doublet R3/R4, subunit SUIV-a consits of low amplitude, parallel to subparallel reflections and is 200 to 300 ms TWT thick (Fig. 5.6). Subunit SUIV-b lies between the high-amplitude horizons R5 and A3. Subunit SUIV-b thins from 250 ms TWT in the west to 50 ms TWT in the east, where the low- to medium amplitude internal reflections converge (Fig. 5.6). Horizon A3 lies mainly closely above the acoustic basement reflection (50-100 ms TWT), but terminates against basement highs and lies almost horizontally above basement troughs (Fig. 5.6). Therefore, subunit SUIV-c varies in thickness from 0 to 250 ms TWT. Subunit SUIV-c appears almost acoustically transparent.

5.5.2 Detailed description of the Miocene Unit SUIV

For a detailed investigation of the different sedimentary environments at the Eirik Drift, we tracked the horizons from the acoustic basement to the seafloor and computed the different unit and subunit thicknesses. In this study, we want to concentrate on unit SUIV and therefore on the early stages of drift development during the Miocene. The drift development after 7.5 Ma (horizon R3/R4) will be the focus of further studies. In Fig. 5.7 the outlines of the interface horizons (left) and the (sub)unit thicknesses (right) of unit SUIV are depicted. Interface depth values shallower than its root mean square (rms) value are defined to represent topographic highs of the horizon in question (Fig. 5.7 left). A depocenter is defined as the part of the thickness maps which is thicker than the rms value (Fig. 5.7 right).

The seismic basement represents the top of the oceanic crust, which on all seismic sections appears as a high-amplitude reflection with an irregular, hummocky topography, characterized by several local highs (Figs. 5.6, 5.7a, 5.8-5.9). The rms depth of the basement lies at ~5500 ms TWT (Fig. 5.7a). Its outline encircles smaller basement elevations in the NW, SW, and the NE corner of the study area with a branch extending towards the basement highs in the SW (Fig. 5.7a). These basement highs are aligned along the axes of the WSW-trending basement ridges (Fig. 5.7a; Le Pichon *et al.*, 1971; Srivastava and Arthur, 1989). The basement slopes from the NE at ~3800 ms TWT to the WSW at ~6500 ms TWT (Fig. 5.7a).

Unit SUIV lies above the seismic basement (Fig. 5.7b), with its top being formed by reflector doublet R3/R4 of late Miocene age (Arthur *et al.*, 1989). Horizon doublet R3/R4 slopes from 3260 ms TWT in the ENE to 5670 ms TWT in the WSW (Fig. 5.7c). Due to the irregular basement below (Fig. 5.7a) the thickness of unit SUIV is highly variable ranging from 0 to 1570 ms TWT (Fig. 5.7b). The part of unit SUIV with a thickness > 860 ms TWT is

Table 5.1.
Refined seismic stratigraphy and reflector nomeclature at ODP Leg 105 Site 646.

Geological record from ODP 646			Age [Ma]	Reflector/ unit name	Depth at ODP 646 [ms TWT]	Thickness (min/max) [ms TWT]	Seismic characteristic
late	Pliocene	Lithol. Unit IA		SUI-a		100/100	continuous high amplitude reflctions, parallel to subparallel to seafloor
			0.8	A1	456		**High-amplitude reflector**
early				SUI-b		100/100	continuous to discontinuous, narrowly-spaced, parallel medium amplitude reflections
			1.4	A2	470		**High-amplitude reflector**
		Lithol. Unit IB		SUI-c		100/200	wide-spaced, continuous to discontinuous, parallel to subparallel reflections, upward increase in amplitudes
late	Pliocene	Lithol. Unit II	2.5	R1	490		**Medium- to high amplitude reflector**
				SUII		100/140	narrowly-spaced, continuous high-amplitude reflections / unit rises from W to E
early			4.5	EU	500		**Erosional unconformity high-amplitude reflector reflector truncation**
				SUIII-a		100/300	upward increase in amplitudes and reflector spacing / unit thickens from W to E
late	Miocene		5.6	R2	510		**Medium-amplitude reflector**
				SUIII-b		150/300	narrowly-spaced, parallel to subparallel, low-amplitude reflections
			7.5/ 8.1	R3/ R4	540/ 545		**medium- to high-amplitude reflector doublet**
				SUIV-a		200/300	parallel to subparallel, low-amplitude reflections
			10-12	R5	570		**band of 3-4 high-amplitude reflections**
				SUIV-b		50/250	converging, low- to medium-amplitude reflections / unit thins from W to E
			17-19	A3	580		**High-amplitude reflector**
				SUIV-c		0/250	almost acoustically transparent
			40-60	basement	590		**irregular basement topography**

defined as its depocenter. This depocenter covers the SE study area with two branches extending to the WNW and N (Fig. 5.7b). The depocenter appears attached to the SW flank of topographic high of the basement partly crossing the lower part of the topographic high in the south (Fig. 5.7a and b). Unit SUIV is subdivided into 3 subunits SUIV-a, -b and -c by the internal high-amplitude reflectors A3 and R5 (Table 5.1; Figs. 5.7, 5.8 and 5.9).

The oldest subunit SUIV-c (Fig. 5.7d) extends from the basement to horizon A3. Horizon A3 slopes from 4130 ms TWT in the NE to 6250 ms TWT in the WSW (Fig. 5.7e). Generally, the continuous, medium- to high-amplitude horizon A3 lies close (50–200 ms TWT) over the basement (Figs. 5.6, 5.8 and 5.9) and therefore, the topographic high of horizon A3 lies mainly on top of the topographic high of the basement in the NE (Fig. 5.7a

and e). However, horizon A3 terminates against several basement highs and runs horizontally over deeper basement troughs (Figs. 5.6, 5.8 and 5.9). The thickness of subunit SUIV-c thus varies between 0 and 384 ms TWT and we observe a number of smaller depocenters with a thickness of >140 ms TWT distributed over the study area (Fig. 5.7d). These small depocenters coincide mainly with the topographic lows of the basement horizon (Fig. 5.7a). Apart from the top reflector A3 of medium- to high-amplitude, subunit SUIV-c appears semi-transparent (Figs. 5.8–5.9).

Above subunit SUIV-c, subunit SUIV-b (Fig. 5.7f) extends to its top reflector R5. Horizon R5 slopes from 3900 ms TWT in the NE to 5950 ms TWT in the WSW (Fig. 5.7g). The topographic high of horizon R5 is located in the NE branching towards the SW in the southern central study area (Fig. 5.7g). In comparison to the basal horizon A3, the topographic high of top reflector R5 is shifted to the east and obliquely elongated to the SW in its shape (Fig. 5.7e and g). The topographic low of horizon R5 in the west is almost homogenous and lies between 5500 and 6000 ms TWT (Fig. 5.6; Fig. 5.7g). In this western part of the study area, the internal low- to medium-amplitude reflections of subunit SUIV-b are parallel to subparallel (Fig. 5.6). The main depocenter of subunit SUIV-b is found in the SE part of the study area with a maximum sediment thickness of 900 ms TWT (Fig. 5.7f). Its wavy outline lies at a depth of 435 ms TWT, and it appears plastered onto the southern flank of horizon A3's topographic high (Fig. 5.7e and f). Here, subunit SUIV-b is lenticularly shaped (Figs. 5.8-5.9). The internal reflections of SUIV-b show low-angle downlaps to the basal horizon A3 and diverge towards the east (Figs. 5.8-5.9). The low amplitudes of the internal reflections increase towards the medium- to high-reflection band near the top (Figs. 5.8-5.9). Top horizon R5 lies within this band of higher reflections, and a number of vertical to sub-vertical faults are observed (Figs. 5.8-5.9).
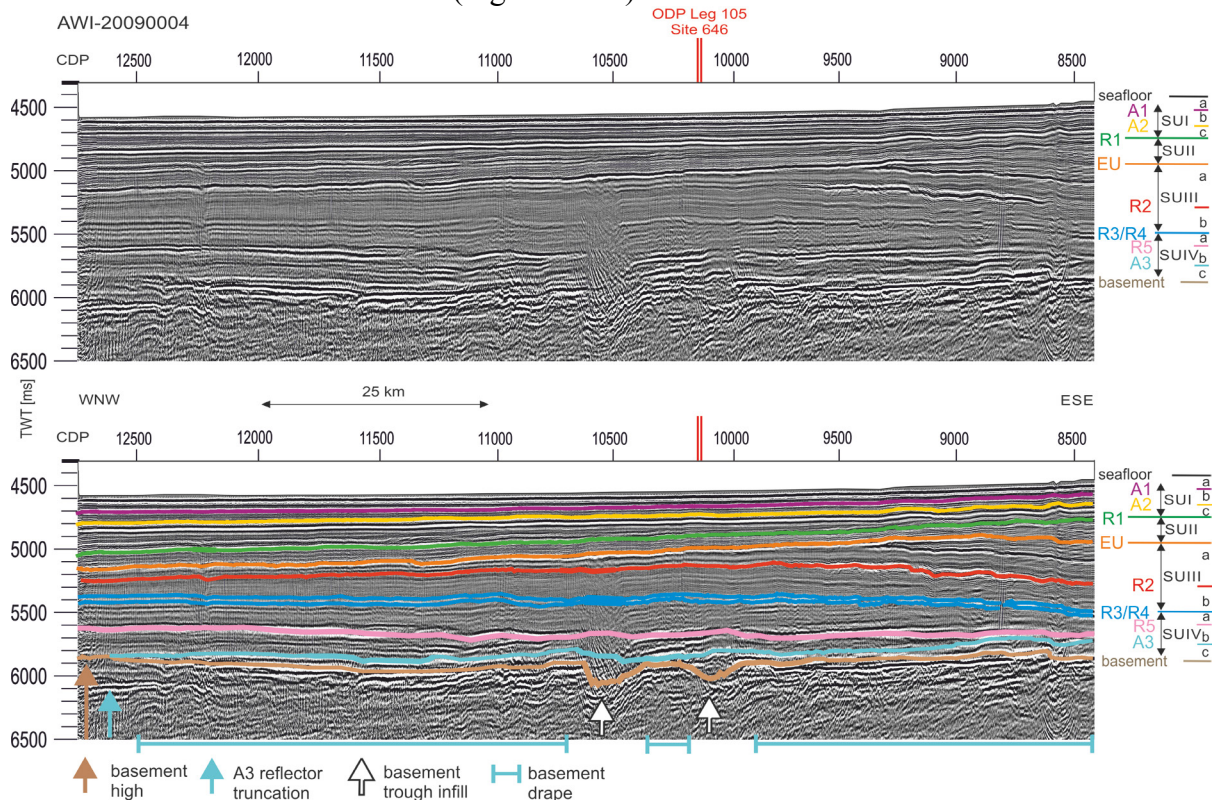
Figure 5.6. Uninterpreted (top) and interpreted (bottom) subsection of line AWI-20090004 (CDP 8400 to 12780 vs. TWT 4300 to 6500 ms). This correlation and extrapolation of the seismic horizons is the base of the seismostratigraphic model (Table 5.1). SUI-SUIV: Seismic Units I-IV (subunits: -a, -b, -c). Horizons: A1 (magenta; 0.8 Ma), A2 (yellow; 1.4 Ma), R1 (green; 2.5 Ma), erosional unconformity EU (orange; 4.5 Ma), R2 (red; 5.6 Ma), reflection doublet R3/R4 (blue; 7.5 Ma), R5 (pink; ~11 Ma), A3 (cyan; ~19 Ma) and basement (brown; ~50 Ma).

The uppermost subunit SUIV-a is bounded by horizon R5 below and horizon doublet R3/R4 at the top. Its thickness varies between 50 and 940 ms TWT (Fig. 5.7h). The depocenter of subunit SUIV-a comprises sediments thicker than 430 ms TWT and is located in the SE part of the study area (Fig. 5.7h). Two branches extend to the WSW and NW (Fig. 5.7h). The depocenter lies on top of the southern flank of reflector R5's topographic high partly extending into the adjacent topographic lows (Fig. 5.7g and h). The internal reflections of subunit SUIV-a are of low amplitudes in the center of the unit and of medium- to high-amplitude near the top and bottom (Fig. 5.8-5.9). Within the depocenter subunit SUIV-a appears lentincularly shaped, and it comprises diverging internal reflections (Figs. 5.8-5.9). Subunit SUIV-a is of almost homogenous thickness elsewhere, and the internal reflections are parallel to subparallel (Fig. 5.6).

5.6 Discussion

The Miocene unit SUIV has been poorly investigated but is of great interest as the investigation of paleocurrents is fundamental for our present understanding of the oceans climate history. Our key objective in this study was to address the question as to whether or not there are indications for the onset of current-controlled sedimentation of the Eirik Drift before 7.5 Ma. Seismic characteristics typical of current-controlled sedimentation and contourite drifts have been described by several authors (e.g. McCave and Tucholke, 1986; Faugères *et al.*, 1999; Stow *et al.*, 2002; Faugères and Stow, 2008; Nielsen *et al.*, 2008), and key observational criteria are summarised below:

1. Major changes in depositional style from non-current dominated to current dominated regime and vice versa cause high- to moderate amplitude reflections.
2. Initiation of a strong deep current is accompanied by non-deposition/erosion.
3. Erosional unconformities are characterized by a single continuous high- to moderate amplitude reflector of regional to semi-regional extent. Commonly, the onset of deep current-controlled sediment accumulation is marked by a basal unconformity.
4. Internal reflections commonly show low-angle downlap onto these basal erosional unconformities.
5. An indication for drift deposits is their thickness, which exceeds that of the adjacent sediment cover. However, morphology, location and internal reflection characteristics of thick sediment deposits have to be investigated to distinguish drift deposits from mass-transport deposits.
6. Drift deposits are found along-slope in contrast to mass-transport deposits, which are observed in down-slope direction.
7. The stronger mean flow of the deep-current core at the steeper drift flank causes erosion and/or reduced net accumulation.
8. Higher sediment accumulation is found at the comparatively tranquil sides of the deep-current core.
9. The geometries of the internal seismic units are lenticular or sigmoidal shaped, due to the above-mentioned regulations of erosion and accumulation at sediment drifts.

Several different types of sediment drifts can be distinguished and their overall shape and geometry are due to an interplay of different boundary conditions: the location and its topography, the current velocity and variability, the amount and type of sediment available, and the time span at which the deep-current was active. The Eirik Drift is classified as a detached elongated, mounded drift. These are distinctly mounded and elongated in shape.
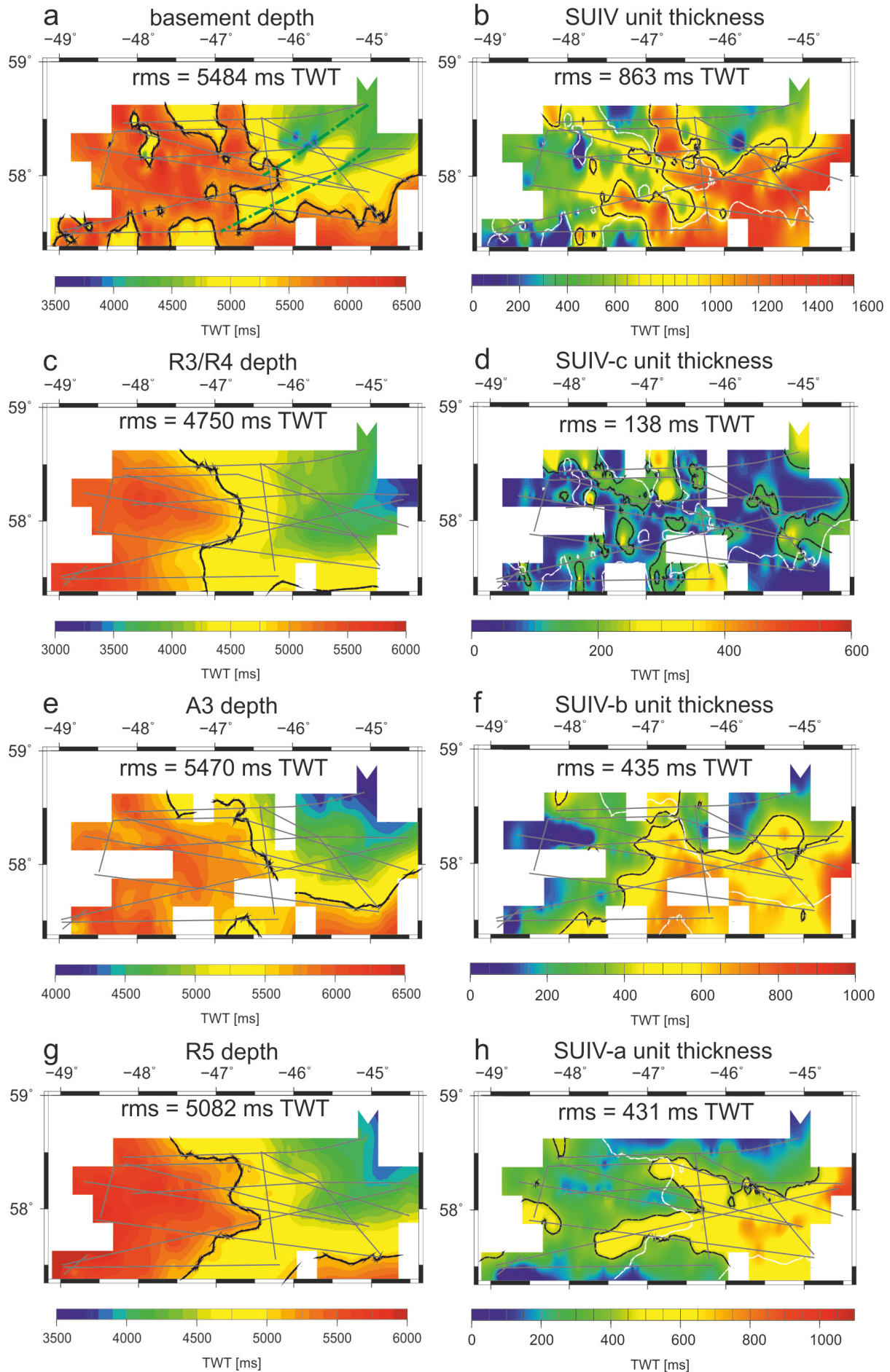
One of the principal controls on the morphology of a detached elongated, mounded drift appears to be the form of the pre-existing seafloor, which controls and directs the various contour-following branches of the deep current. Elongated detached drifts usually prograde in

the direction of the initial flow and their crests are found parallel to the prevailing deep current direction, but progradation can also lead to parts of the drift being elongated almost perpendicular to the margin. This is the case for the Eirik Drift in response to a change to the margin's trend as the intensity of the deep current is commonly related to the steepness of the slope with intensification of the current core at steeper slopes and weaker currents at gentle slopes. For detached elongated drifts in the Northern Hemisphere the higher sediment accumulation is found always to the right of the current core due to Coriolis force. Currents directed oppositely at both drift flanks yield in increased sedimentation at the drift axis. Subsidiary drift crests can be found in the downcurrent flank. Drift deposits are lenticular in shape with the bedding thickening at the drift axis and thinning towards either both drift flanks or the flank where the flow is fastest. At the thinner parts the internal reflections converge while diverging internal reflections are found at the areas of increased accumulation at the drift axis. Thus, the internal reflections describe a uniform pattern of continuous low to medium amplitude reflections that tend to follow the main drift morphology.

By means of the extended stratigraphy assessed at site ODP 646, we identified Miocene unit SUIV and divided it into 3 subunits. We observed that the depocenter of unit SUIV appears attached to the SW flank of the topographic high of the basement (Fig. 5.7a and b). The thicker sequence at the elevated basement flank compared to the thinner sequence at the basement topographic lows in the west of the study area is a strong indication for deep current controlled deposition (McCave and Tucholke, 1986; Faugères *et al.*, 1999; Stow *et al.*, 2002; Faugères and Stow, 2008; Nielsen *et al.*, 2008). To confirm the assumption that deep current-controlled sedimentation started during deposition of unit SUIV and to identify its onset, the subunits of unit SUIV are investigated in more detail below.

The oldest subunit SUIV-c overlies basement. Its top horizon A3 onlaps on several basement highs (Figs. 5.8-5.9). The small, patch-like distributed depocenters of subunit SUIV-c lie mainly in the topographic lows of the basal basement horizon and are interpreted as an infill of the irregular basement topography (Fig. 5.7a and d). Therefore, the top horizon A3 shows a smoothed morphology compared to the underlying basement horizon (Fig. 5.7a and e). This points to a drape of the underlying basement reflector during deposition of subunit SUIV-c. The seismic transparency of subunit SUIV-c indicates that the depositional conditions for the sedimentation were tranquil and stable.

In contrast to subunit SUIV-c, the upper subunits SUIV-b and -a show distinct depocenters, which are attached to (SUIV-b; Fig. 5.7f) or lie on top of (SUIV-a; Fig. 5.7h) the topographic highs of their basal interfaces (Fig. 5.7e and g). The development of depocenters at the topographic highs of their basal interfaces indicates that no uniform sedimentation during deposition of subunits SUIV-b and -a occurred. The location of the depocenters at the SE flanks of the topographic highs of the basal interfaces suggests that the main control on the deposition is related to a contour current flowing around the pre-existing seafloor contours (Fig. 5.7e-h). The depocenters are lenticular shaped and comprise diverging internal reflections (Figs. 5.8-5.9). This is typical for detached elongated, mounded contourite drifts as the bedding thickens at the drift axis but thins at the drift flanks. This is due to the location of the deep-current core and the effect of Coriolis force (McCave and Tucholke, 1986; Faugères *et al.*, 1999; Stow *et al.*, 2002; Faugères and Stow, 2008; Nielsen *et al.*, 2008). The thin parts indicate erosion and/or less sedimentation and are interpreted as the locations of the intense deep current cores, while the thicker parts with the diverging internal reflections denote the drift axis with increased sedimentation in the relatively tranquil zones to the right of the stronger deep current core (McCave and Tucholke, 1986; Faugères *et al.*, 1999; Stow *et al.*, 2002; Faugères and Stow, 2008; Nielsen *et al.*, 2008). Thus, the combination of thickness, location, orientation, shape and internal reflections of the depocenters all suggest that deep-current-controlled sedimentation was responsible for the deposition of subunits SUIV-b and -a. In addition, subunit SUIV-c and the lower part of subunit SUIV-b appear acoustically

a basement depth

rms = 5484 ms TWT

TWT [ms]

b SUIV unit thickness

rms = 863 ms TWT

TWT [ms]

c R3/R4 depth

rms = 4750 ms TWT

TWT [ms]

d SUIV-c unit thickness

rms = 138 ms TWT

TWT [ms]

e A3 depth

rms = 5470 ms TWT

TWT [ms]

f SUIV-b unit thickness

rms = 435 ms TWT

TWT [ms]

g R5 depth

rms = 5082 ms TWT

TWT [ms]

h SUIV-a unit thickness

rms = 431 ms TWT

TWT [ms]

transparent but their interface horizon A3 is of high amplitude and continuous apart from its interruption due to basement elevations (Figs. 5.6, 5.8-5.9). This change in reflection characteristics may be due to a change in sediment supply and/or composition or changes in strength and/or location of the deep current system. There is no drilled sedimentary record of the main part of unit SUIV and therefore, changes in sediment composition cannot be confirmed or excluded. Horizon A3 shows the characteristics of a basal unconformity (single, continuous high-amplitude reflectors of regional to subregional extent). These basal unconformities represent strong, initial pulses of deep contour currents, which are often connected with erosional hiatuses (McCave and Tucholke, 1986; Faugères *et al.*, 1999; Stow *et al.*, 2002; Faugères and Stow, 2008; Nielsen *et al.*, 2008). We observed low-angle downlaps at horizon A3, which are also typical for erosional unconformities (Fig. 5.8-5.9) (Faugères *et al.*, 1999; Nielsen *et al.*, 2008; Stow *et al.*, 2002). Therefore, we suggest horizon A3 marks the onset of drift building at the Eirik Drift.

Even though we interpret both subunits SUIV-b and -a as the result of deep-current controlled deposition, there are some differences between these two subunits. The topographic high of the basal horizon A3 has a semicircle appearance in the NE corner of the study area (Fig. 5.7e). The topographic high develops to a NE-SW directed, elongated slope at horizon R5 (Fig. 5.7g) and a more ENE-WSW orientated slope at horizon doublet R3/R4 (Fig. 5.7c). This is interpreted as elongation and progradation of the Eirik Drift towards the WSW. The depocenter of subunit SUIV-b lies in the SE part of the study area attached to the SW flank of the topographic high of its basal interface A3 (Fig. 5.7e-f). Deep-current cores flow at isobaths and Coriolis force accounts for deposition to the right of the deep-current cores in the Northern Hemisphere. The combination of the basal interface outline and the location of the depocenter of subunit SUIV-b infers a deep-current core at a contour below the rms value of 5470 ms TWT of the basal interface A3 (Fig. 5.7e-f). It suggests a deep-current core, which flows SW beyond our study area and turns to a NNW directed flow along the western depocenter outline (Fig. 5.7f). The depocenter of subunit SUIV-a lies mainly on top of its basal horizon R5 (Fig. 5.7g-h). The branches of the depocenter, which extend to the NW and WSW indicate a meandering, NW directed deep-current core (Fig. 5.7h) roughly following the undulations of the rms outline of R5's topographic high at 5082 ms TWT (Fig. 5.7g). Therefore, we assume that the deep-current core responsible for deposition of subunit SUIV-a lies at shallower depth than before.

The internal reflections of subunit SUIV-b are of low amplitude. The amplitudes increase towards the top horizon R5, which is found within a band of 3-4 high amplitude reflections (Fig. 5.8-5.9). Changes in the deep current system and/or of the supplied sediment can create changes in the impedance contrast, which yields higher amplitude reflectors like these. The faults observed within the high-reflection band surrounding R5 bear analogy to diagenetically induced polygonal fault system due to their swarm-like and apparently layer-bound appearance (Cartwright, 2011). However, diagenetic processes and their typical

Figure 5.7. Contour maps of horizon depth (left) and (sub-)unit thickness (right) of unit SUIV. The grey lines show the locations of the seismic profiles. The black lines indicate the root mean square (rms) depth (left) and rms thickness (right), respectively. The rms depth outline of the topographic high of the basal horizon is added in the (sub-)unit thickness plots (right) as white lines. (a) Basement depth, rms=5484 ms TWT. The green, dashed lines mark the location of the two NE-SW trending basement ridges (cf. Fig. 5.2). (b) Total unit thickness SUIV, rms=863 ms TWT, white line: outline of the topographic high of the basement. (c) Horizon doublet R3/R4 depth, rms=4750 ms TWT. (d) Subunit SUIV-c thickness, rms=138 ms TWT, white line: outline of the topographic high of the basement. (e) Horizon A3 depth, rms=5470 ms TWT. (f) Subunit SUIV-b thickness, rms=435 ms TWT, white line: outline of the topographic high of A3. (g) Horizon R5 depth, rms=5082 ms TWT. (h) Subunit SUIV-a unit thickness, rms=431 ms TWT, white line: outline of the topographic high of R5.
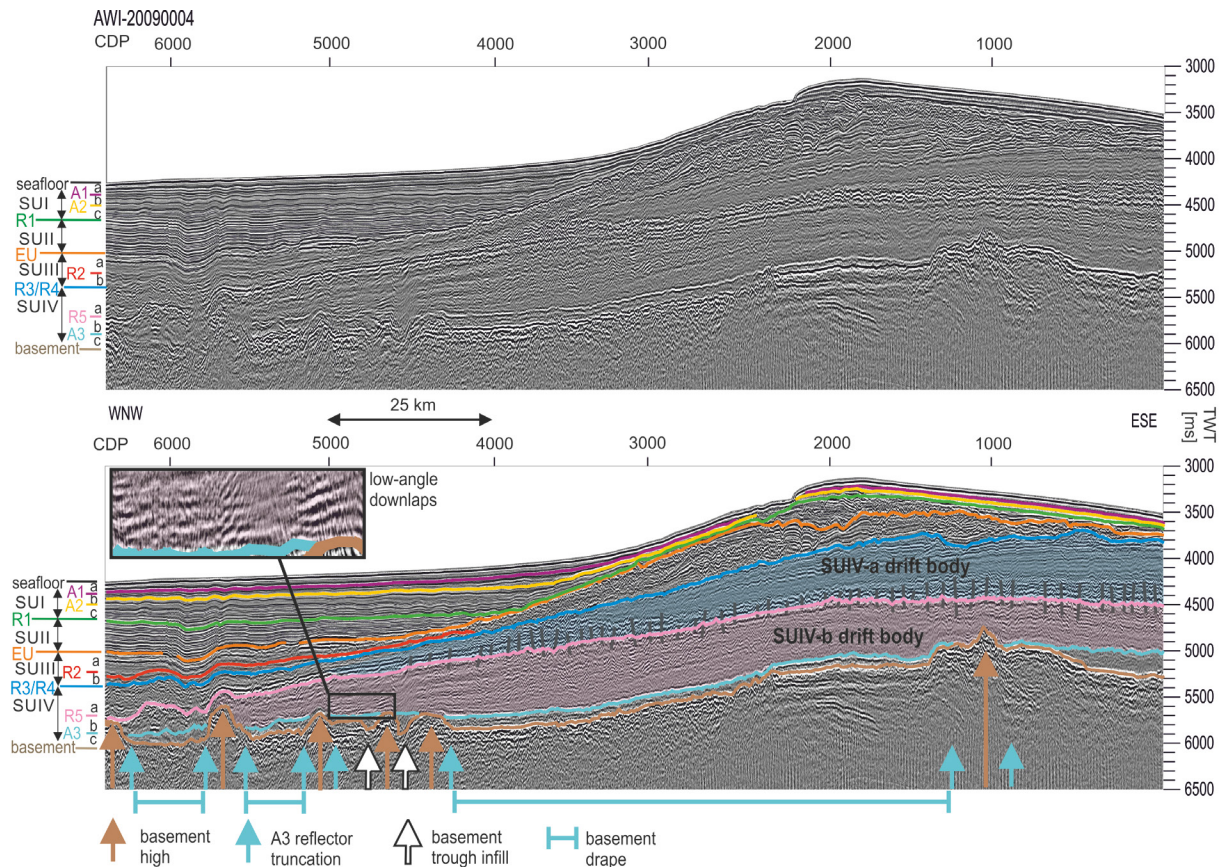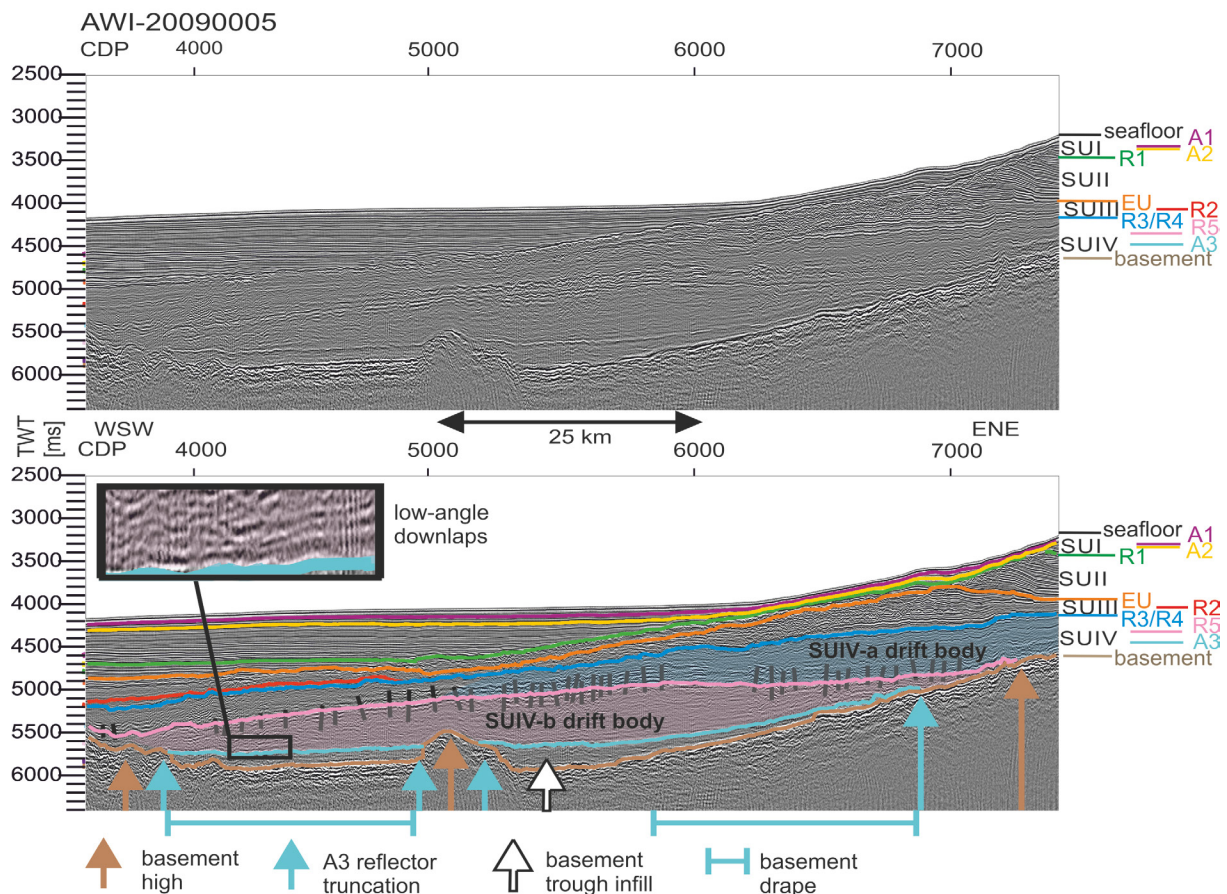
Figure 5.8. Uninterpreted (top) and interpreted (bottom) subsection of line AWI-20090004 (CDP 50 to 6500 vs. TWT 3000 to 6500 ms). For location see Fig. 5.2. Horizons: A1 (magenta; 0.8 Ma), A2 (yellow; 1.4 Ma), R1 (green; 2.5 Ma), erosional unconformity EU (orange; 4.5 Ma), R2 (red; 5.6 Ma), reflection doublet R3/R4 (blue; 7.5 Ma), R5 (pink; ~11 Ma), A3 (cyan; ~19 Ma) and basement (brown; ~~51 Ma). Pink and blue transparent patches highlight drift bodies within subunit SUIV-b and SUIV-a, respectively.

polygonal planform geometry (Cartwright, 2011) cannot be confirmed due to the lack of geological information and seismic 3-D data. Fluids moving within the sediment, possibly initiated by changing sedimentation rates, or varying current strength and directions, may also cause these vertical to sub-vertical small-scale faults. In combination with the observed shifts of the depocenters and the concluded changes in the deep-current core depth from subunit SUIV-b to SUIV-a, we assume a change in deep-current system at horizon R5.

In the following, we try to set the onset of drift building in the correct chronological context, even though we have no direct age control of borehole data. The top reflector doublet R3/R4 of seismic unit SUIV was dated as 7.5 Ma (Arthur *et al.*, 1989) and marks changes in carbonate content (Kaminski *et al.*, 1989). The suggested onset of NCW overflow at the Denmark Strait (DSOW) at ~7 Ma (Bohrmann *et al.*, 1990) might account for these changes. In addition, Kaminski *et al.* (1989) found evidence for corrosive, southern-sourced bottom water in the lowermost sedimentary record at ODP 646, i.e. below horizon R3/R4 (8.1-8.6 Ma). Hence, it was concluded, that no NCW flow was active at the Eirik drift prior to formation of reflector doublet R3/R4 at 7.5 Ma (Arthur *et al.*, 1989; Kaminski *et al.*, 1989). Several authors reported a phase of high NCW production from around 12.5 Ma to the Pliocene with minor interruptions around 9 Ma and 7 Ma (Wright and Miller, 1996; Wright, 1998; Poore *et al.*, 2006). These studies link the deep-water circulation in the North Atlantic to the subsidence history of the Greenland-Scotland-Ridge by investigating the Iceland mantle plume activity in combination with carbon and/or oxygen records in sediment cores. We suggest these short interruptions of the prevailing NCW flow to account for the formation of the reflector doublet R3/R4 and the 9 Ma event to have been responsible for the record of

Figure 5.9. Uninterpreted (top) and interpreted (bottom) subsection of line AWI-20090005 (CDP 3600 to 7400 vs. TWT 2500 to 6500 ms). For location see Fig. 5.2. Horizons: A1 (magenta; 0.8 Ma), A2 (yellow; 1.4 Ma), R1 (green; 2.5 Ma), erosional unconformity EU (orange; 4.5 Ma), R2 (red; 5.6 Ma), reflection doublet R3/R4 (blue; 7.5 Ma), R5 (pink; ~11 Ma), A3 (cyan; ~19 Ma) and basement (brown; ~53 Ma). Pink and blue transparent patches highlight drift bodies within subunit SUIV-b and SUIV-a, respectively.

corrosive southern-sourced deep-water at ODP 646 at 8.1-8.6 Ma. The medium- to high amplitude reflections found below horizon R3/R4 may be also a result of this variability of NCW flow around 9 Ma. Subunit SUIV-a comprises low-amplitude reflections indicating sedimentation under uniform conditions, i.e. no major changes in sediment supply and/or deep-current intensity occurred.

We estimate the age of horizon R5 at 10-12 Ma, which we derived from extrapolation of sedimentation rates at the lower part of ODP 646. This estimate correlates well with the onset of a phase of high NCW production at ~12.5 Ma (Wright and Miller, 1996; Wright, 1998; Poore *et al.*, 2006), a drift accumulation phase generally observed in the northern North Atlantic at ~13 Ma (Miller and Tucholke, 1983; Wold, 1994) and the formation of several erosional unconformities in the northern North Atlantic at 10-13 Ma (Wold, 1994; Wright and Miller, 1996). Hatton and Snorri Drift started to develop at around 13 Ma (Wold, 1994). This happened at the same time when the first significant overflows were observed at the Iceland-Faroe-Ridge ~13-11 Ma (Bohrmann *et al.*, 1990). The high reflection band with its swarm-like faults observed in our data (Fig. 5.8-5.9) is similar to the widespread occurrence of a hummocky reflection zone above a relatively reflector-free or low-amplitude section at the US Atlantic continental rise (Mountain and Tucholke, 1985; McMaster *et al.*, 1989; Locker and Laine, 1992). These reflection characteristics were identified below reflector Merlin by Mountain and Tucholke (1985), inferred to represent the initialized stabilization of drift deposits in the western North Atlantic ~10-12 Ma ago. Horizon G of McMaster *et al.* (1989) is concordant with reflector Merlin. Geological drilling results in combination with seismic

data revealed, that an interval of deep-current erosion at 11.5-12 Ma caused horizon G (Muza and Covington, 1987; McMaster *et al.*, 1989). Locker and Laine (1992) linked their horizon X (10.5 Ma) with reflector Merlin. They stated that the hummocky seismic facies developed as a result of widespread reworking of sediments by deep contour currents as proposed by Mountain and Tucholke (1985). The hydrological event, which caused the formation of horizon Merlin/G/X in the eastern North Atlantic, was synchronous with a sharp rise in sea level (Haq *et al.*, 1987). Based on the similarity of the reflection characteristics of horizon Merlin/G/X and horizon R5, we confirm the suggested date of horizon R5 (10-12 Ma) and the assumption that horizon R5 represents a change in the deep-current system at the Eirik Drift.

Using sedimentation rates determined at ODP 646, horizon A3 appears to be of middle Miocene age. The production of NCW was disabled between 15 and 12.5 Ma due to increased Iceland mantle plume activity and a resulting uplift of the Greenland-Scotland-Ridge (Miller and Tucholke, 1983; Wright and Miller, 1996). The elimination of NCW production during this phase probably yielded much lower sedimentation rates and therefore has to be taken into account in the age estimation for horizon A3. We therefore suggest that horizon A3 is more likely of early Miocene age (19-17 Ma), when initiation of strong NCW fluxes (20-19 Ma; Wright and Miller, 1996) formed widespread erosional unconformities in the northern North Atlantic (Table 5.2; Dingle *et al.*, 1982; Masson and Kidd, 1986; McCave *et al.*, 1980; McCave and Tucholke, 1986; Miller and Tucholke, 1983; Stoker *et al.*, 2001) and drift accumulation at Bjorn and Gardar Drift started (Miller and Tucholke, 1983; Wright and Miller, 1996). This is in accordance to the development of the deep-water connection through the Faroe Conduit in early Miocene (Stoker *et al.*, 2005) and the opening of the Fram Strait for a deep-water exchange of the Arctic Ocean to the Nordic Seas (Ehlers and Jokat, 2013).

Subunit SUIV-c underlying horizon A3 was deposited in a tranquil environment. The basement is 40-61 Ma in age and therefore ~20-40 Ma older than the estimated age of horizon A3. The mean sedimentation rate of subunit SUIV-c would be < 10 ms TWT/m.y. and significantly decreased compared to the mean sedimentation rates of subunits SUIV-b (70 ms TWT/m.y.) and SUIV-a (120 ms TWT/m.y.). The question arises whether a tranquil environment would account for such low sedimentation rates or whether horizon A3 might represent a sedimentary hiatus. Due to its reflection characteristics (a single continuous high- to moderate amplitude reflector of regional to semi-regional extent with low-angle downlaps), horizon A3 was identified as the basal unconformity of the drift, which represents strong, initial pulses of deep contour currents. These often are connected with erosional hiatuses. The observed low-angle downlaps at horizon A3 suggest erosion (Fig. 5.8-5.9). Therefore, we interpret horizon A3 as a sedimentary hiatus due to erosion at the onset of intense NCW flux. However, as there is no drilled sedimentary record of the main part of unit SUIV, the assumption of a sedimentary hiatus at horizon A3 cannot be confirmed.

Table 5.2.

North Atlantic erosional unconformities of late Early Miocene age.

Reflector age	Reflector name	Region	Citation
19-18 Ma	"Challanger"	Porcupine Bank	Dingle *et al.* (1982)
Late Early Miocene	Regional reflector	Faroe-Shetland region	Stoker *et al.* (2005)
Late Early Miocene	"C20"	Rockall Trough	Stoker *et al.* (2001)
17 Ma	"Green"	Southern Rockall Trogh	Mason and Kidd (1986)
17 Ma	"IR"	Gardar Drift	McCave *et al.* (1980)
17-16 Ma	"R2"	Rockall, Gloria Drift, Baffin Bay	Miller and Tucholke (1983)

5.7 Conclusion

A new set of high-resolution seismic reflection data has been interpreted with respect to the build-up of the Eirik Drift. We have refined the seismostratigraphic concept of Arthur *et al.* (1989) adding horizons A1 (0.8 Ma), A2 (1.4 Ma) and A3 (17-19 Ma) and dating horizon R5 (10-12 Ma). Our study suggests that the onset of drift building was instigated in the early Miocene (17-19 Ma), which contrasts with the hypotheses by Arthur *et al.* (1989) and Wold (1994), who inferred a drift build-up after ~4.5 Ma and after ~7-8 Ma, respectively.

Our proposed history of sedimentation within the Miocene seismic unit SUIV at the Eirik Drift is as follows:

- Until 19-17 Ma sedimentation at the Eirik Drift was not deep-current controlled; deposition of subunit SUIV-c took place in a tranquil and stable environment.
- Horizon A3 is identified as the basal erosional unconformity of the Eirik Drift and is dated 19-17 Ma, when initiation of strong NCW fluxes occurred, as is documented in several erosional unconformities and drifts in the northern North Atlantic. Horizon A3 presumably represents also a sedimentary hiatus due to enhanced erosion. This onset of strong NCW fluxes follows the development of the Faroe Conduit in early Miocene (Stoker *et al.*, 2005) and the onset of deep-water exchange at the Fram Strait (Ehlers and Jokat, 2013).
- Onset of drift building is documented by deposition of unit SUIV-b under the influence of strong NCW fluxes, which were inhibited between 15-12.5 Ma.
- Changes in the deep-current velocity presumably formed the high-amplitude reflection-band surrounding horizon R5 at 12-10 Ma along with a renewed onset of NCW flow. At that time (~13-11 Ma) the first significant overflows at the Iceland-Faroe-Ridge were observed (Bohrmann *et al.*, 1990).
- Drift elongation and progradation to the WSW under the influence of shallower NCW flow is suggested by the sedimentary record of unit SUIV-a.
- Reflection doublet R3/R4 (7.5 Ma) and the medium- to high amplitude reflections found below this horizon are ascribed to the minor interruptions of NCW flow at 7 and 9 Ma. Presumably, the suggested onset of overflows over the Denmark Strait (~7 Ma; Bohrmann *et al.*, 1990) are documented by horizon R3.

In this study, we concentrated on the development of the Eirik Drift during the Miocene to show that drift building at the Eirik Drift started much earlier than previously thought. The refined seismostratigraphic concept will be used in further studies to define a model for the development of pathways and intensity of the NCW flow over the Erik drift during Neogene and Quaternary.

5.8 Acknowledgements

5.9 References

Arthur, M.A., Srivastava, S.P., Kaminski, M., Jarrard, R.D., Osler, J., 1989. Seismic Stratigraphy and History of Deep Circulation and Sediment Drift Development in Baffin Bay and the Labrador Sea. In: Srivastava, S.P., Arthur, M., Clement, B., et al. (Eds.), Scientific Results. Ocean Drilling Program, College Station, TX, USA, 957-988.

Bohrmann, G., Henrich, R., Thiede, J., 1990. Miocene to Quaternary Paleoceanography in the Northern North Atlantic: Variability in Carbonate and Biogenic Opal Accumulation. In: Bleil, U., Thiede, J. (Eds), Geological History of the Polar Oceans: Arctic versus Antarctic. Springer, Netherlands, 647-675.

Cartwright, J., 2011. Diagenetically induced shear failure of fine-grained sediments and the development of polygonal fault systems. Marine and Petroleum Geology 28, 1593-1610.

Chalmers, J.A., Pulvertaft, T.C.R., 2001. Development of the continental margins of the Labrador Sea – a review. In: Wilson, R.C.L., Whitmarsh, R.B., Froitzheim, N. (Eds.), Non-volcanic rifting of the continental margins: a comparison of evidence from land and sea. Geological Society London, UK, 77-105.

Channell, J.E.T., Kanamatsu, T., Sato, T., Stein, R., Alvarez Zarikian, C.A., Malone, M.J., Expedition 303/306 Scientists, 2006. Proceedings of the Intergrated Ocean Drilling Program. vol 303/306. Expeditions Report North Atlantic Climate.

Channell, J.E.T., Sato, T., Kanamatsu, T., Stein, R., Alvarez Zarikian, C.A., 2010. Expedition 303/306 synthesis: North Atlantic climate. In: Channell, J.E.T., Kanamatsu, T., Sato, T., Stein, R., Alvarez Zarikian, C.A., Malone, M.J., Expedition Scientists (Eds.), Proceedings of the Integrated Ocean Drilling Program. Integrated Ocean Drilling Program, College Station, TX, USA.

Cramer, B.S., Toggweiler, J.R., Wright, J.D., Katz, M.E., Miller, K.G., 2009. Ocean overturning since the Late Cretaceous: Inferences from a new benthic foraminiferal isotope compilation. Paleoceanography 24, PA 4216, doi:10.1029/2008PA001683.

Cremer, M., 1989. Texture and Microstructure of Neogene-Quaternary Sediments, ODP Sites 645 and 646, Baffin Bay and Labrador Sea. In: Srivastava, S.P., Arthur, M., Clement, B., et al. (Eds.), Scientific Results. Ocean Drilling Program, College Station, TX, USA.

Davies, R., Cartright, J., Pike, J., Line, C., 2001. Early Oligocene initiation of North Atlantic Deep Water formation. Nature 410, 917-920.

Dickson, R.R., Brown, J., 1994. The production of North Atlantic Deep Water: Sources, rates, and pathways. Journal of Geophysical Research 99, 12319-12341.

Dingle, R.V., Megson, J.B., Scrutton, R.A., 1982. Acoustic Stratigraphy of the sedimentary succession west of Porcupine Bank, N.E. Atlantic Ocean: A preliminary account. Marine Geology 47, 17-35.

Ehlers, B.-M., Jokat, W., 2013. Paleo-bathymetry of the northern North Atlantic and consequences for the opening of the Fram Strait. Marine Geophysical Research, doi:10.1007/s11001-013-9165-9.

Expedition 303 Scientists, 2006. Expedition 303 summary. In: Channell, J.E.T., Kanamatsu, T., Sato, T., Stein, R., Alvarez Zarikian, C.A., Malone, M.J., Expedition Scientists (Eds.), Proc. IODP. Integrated Ocean Drilling Program Management International, College Station, TX, USA, 30.

Faugères, J.C., Stow, D.A.V., Imbert, P., Viana, A.R., 1999. Seismic Features Diagnostic of Contourite Drifts. Marine Geology 162, 1-38.

Faugères, J.C., Stow, D.A.V., 2008. Contourite Drifts: Nature, Evolution and Controls. In: Rebesco, M. and Camerlenghi, A. (Eds.), Contourites. Elsevier, Amsterdam, the Netherlands, 259-288.

Gibbard, P.L., Head, M.J., Walker, M.J.C., 2010. Formal ratification of the Quaternary System/Period and the Pleistocene Series/Epoch with a base at 2.58 Ma. Journal of Quaternary Science 25, 96-102.

Hansen, B., Østerhus, S., 2000. North Atlantic–Nordic Seas exchanges. Progress in Oceanography 45, 109-208.

Haq, B.U., Hardenbol, J., Vail, P.R., 1987. Chronology of fluctuating sea levels since Tirassic. Science 235, 1156-1167.

Hunter, S., Wilkinson, D., Louarn, E., McCave, I.N., Rohling, E., Stow, D.A.V., Bacon, S., 2007a. Deep western boundary current dynamics and associated sedimentation on the Eirik Drift, Southern Greenland Margin. Deep-Sea research I 54, 2036-2066.

Hunter, S., Wilkinson, D., Stanford, J., Stow, D.A.V., Bacon, S., Akhmetzhanov, A.M., Kenyon, N.H., 2007b. The Eirik Drift: A long-term barometer of North Atlantic deepwater flux south of Cape Farewell, Greenland. In: Viana, A.R., Rebesco, M. (Eds.), Economic and Palaeoceanographic Significance of Contourite Deposits. Geological Society, London, UK, 245-263.

Kaminski, M.A., Gradstein, F.M., Scott, D.B., Mackinnon, K.D., 1989. Neogene benthic foraminifer biostratigraphy and deep-water history of Sites 645, 646, and 647, Baffin Bay and Labrador Sea. In: Srivastava, S.P., Arthur, M., Clement, B., et al. (Eds.), Scientific Results. Ocean Drilling Program, College Station, TX, USA, 731-756.

Le Pichon, X., Hyndman, R.D., Pautot, G., 1971. Geophysical Study of the Opening of the Labrador Sea. Journal of Geophysical Research 76, 4724-4743.

Locker, S.D., Laine, E.D., 1992. Paleogene-Neogene depositional history of the middle U.S. Atlantic continental rise: mixed turbidite and contourite depositional systems. Marine Geology 103, 137-164.

Masson, D.G., Kidd, R.B., 1986. Revised Tertiary seismic Stratigraphy of the southern Rockall Trough. Initial Reports Deep Sea Drilling Project 94, TX, USA, 1117-1126.

McCave, I.N., Tucholke, B.E., 1986. Deep Current-Controlled Sedimentation in the Western North Atlantic. In: Vogt, P.R., Tucholke, B.E. (Eds.), The Geology of North America - The Western North Atlantic Region. Geological Society of America, Boulder, USA, 451-468.

McCave, I.N., Lonsdale, P.F., Hollister, C.D., Gardner, W.D., 1980. Sediment transport over the Hatton and Gardar contourite drifts. Journal of Sedimentary Research 50, 1049-1062.

McMaster, R.L., Locker, S.D., Laine, E.D., 1989. The early Neogene continental rise off the eastern United States. Marine Geology 87, 137-163.

Miller, K.G., Tucholke, B.E., 1983. Development of Cenozoic Abyssal Circulation south of the Greenland-Scotland Ridge. In: Bott, M.H.P., Saxov, S., Talwani, M., Thiede, J. (Eds.), Structures and Development of the Greenland-Scotland Ridge - New Methods and Concepts. Plenum Press, New York and London, 549-589.

Miller, K.G., Wright, J.D., Katz, M.E., Wade, B.S., Browning, J.V., Cramer, B.S., Rosenthal, Y., 2009. Climate threshold at the Eocene-Oligocene transition: Antarctic ice sheet influence on ocean circulation. In: Koeberl, C., Montanari, A. (Eds.), The Late Eocene Earth-Hothouse, Icehouse, and Impacts. Geological Society of America Special Paper, USA, 169-178.

Mountain, G.S., Tucholke, B.E., 1985. Mesozoic and Cenozoic Geology of the U.S. Atlantic continental slope and rise. In: Poag, C.W. (Ed.), Geologic Evolution of the United States Atlantic Margin. Van Nostrand Reinhold Company, New York, USA, 293-341.

Mueller, R.D., Sdrolias, M., Gaina, C., Roest, W.R., 2008. Age, spreading rates, and spreading asymmetry of the world's ocean crust. Geochemistry Geophysics Geosystems 9.

Muza, J.P., Covington, J.M., 1987. Neogene calcareous nannofossils from Deep Sea Drilling Project Site 603, lower continental rise, western North Atlantic: Biostratigraphy and correlations with magnetic and seismic stratigraphy. In: van Hinte, J.E., Wise Jr, S.W., et al. (Eds.), Initial Reports Deep-Sea Drilling Project 93, USA, 593-616.

Nielsen, T., Knutz, P.C., Kuijpers, 2008. Seismic Expression of Contourite Depositional Systems. In: Rebesco, M. and Camerlenghi, A. (Eds.), Contourites. Elsevier, Amsterdam, the Netherlands, 301-321.

Poore, H.R., Samworth, R., White, N.J., Jones, S.M., McCave, I.N., 2006. Neogene overflow of Northern Component Water at the Greenland-Scotland Ridge. Geochemistry Geophysics Geosystems 7, No. 6, Q06010, doi:10.1029/2005GC001085.

Ricker, N., 1953. The form and laws of propagation of seismic wavelets. Geophysics 18, 10-40.

Schmitz, W.J., Jr., 1996. On the World Ocean Circulation: Volume I - Some Global Features / North Atlantic Circulation, Technical Report. Woods Hole Oceanographic Institution, Woods Hole, MA, USA.

Shipboard Scientific Party, 2005. Ice sheet-ocean atmosphere interactions on millenial timescales during the late Neogene-Quaternary using a paleointensity-assisted chronology for the North Atlantic. IODP Expedition 303 preliminary report. Integrated Ocean Drilling Program, College Station, TX, USA.

Shipboard Scientific Party, 1987a. Site 646. In: Srivastava, S.P., Arthur, M., Clement, B., et al. (Eds.), Init. Repts. Ocean Drilling Program, College Station, TX, USA, 419-674.

Shipboard Scientific Party, 1987b. Explanatory Notes: ODP Leg 105, Baffin Bay and Labrador Sea. In: Srivastava, S.P., Arthur, M., Clement, B., et al. (Eds.), Init. Repts. Ocean Drilling Program, College Station, TX, USA, 21-41.

Smith, W.H.S., Sandwell, D.T., 1997. Global Sea Floor Topography from Satellite Altimetry and Ship Depth Soundings. Science 277, 1956-1962.

Srivastava, S.P., Arthur, M.A., 1989. Tectonic Evolution of the Labrador Sea and Baffin Bay: Constraints Imposed by Regional Geophysics and Drilling Results from Leg 105. In: Srivastava, S.P., Arthur, M., Clement, B., et al. (Eds.), Scientific Results. Ocean Drilling Program, College Station, TX, USA, 989-1009.

Srivastava, S.P., Arthur, M.A., Clement, B., et al (Eds.), 1989. Proceedings ODP, Scientific Results, 105. Ocean Drilling Program, College Station, TX, USA.

Srivastava, S.P., Roest, W.R., 1999. Extent of oceanic crust in the Labrador Sea. Marine and Petroleum Geology 16, 65-84.

Stoker, M.S., Hoult, R.J., Nielsen, T., Hjelstuen, B.O., Laberg, J.S., Shannon, P.M., Praeg, D., Mathiesen, A., van Weering, T.C.E., McDonnell, A., 2005. Sedimentary and oceanographic responses to early Neogene compression on the NW European margin. Marine and Petroleum Geology 22, 1031-1044.

Stoker, M.S., van Weering, T.C.E., Svaerdborg, T., 2001. A mid- to late Cenozoic tectostratigraphic framework for the Rockall Trough. In: Shannon, P.M., Haughton, P., Corcoran, D. (Eds), The Petroleum Exploration of Ireland's Offshore Basins-Geological Society, London, UK, Special Publication 188, 411-438.

Stow, D.A.V., Faugères, J.-C., Viana, A., Gonthier, E., 1998. Fossil contourites: a critical review. Sedimentary Geology 115, 3-31.

Stow, D.A.V., Faugères, J.-C., Howe, J.A., Pudsey, C.J., Viana, A.R., 2002. Bottom currents, contourites and deep-sea sediment drifts: current state-of-the-art. In: Stow, D.A.V., Pudsey, C.J., Howe, J.A., Faugères, J.-C., Viana, A.R. (Eds.), Deep-water contourite

systems: Modern drifts and ancient series. Geological Society of London, London, UK, 7-20.

Wildeboer Schut, E., Uenzelmann-Neben, G., 2006. Tying seismic data to geologic information from core data: An example from ODP Leg 177. Geo-Marine Letters 26, 235-248.

Wold, C.N., 1994. Cenozoic Sediment Accumulation on Drifts in the Northern North Atlantic. Paleoceanography 9, 917-941.

Wright, J.D., 1998. Role of the Greenland-Scotland Ridge in Neogene climate changes. In: Crowley, T.J., Burke, K. (Eds.), Tectonic Boundary Conditions for Climate Reconstructions. Oxford University Press, Oxford, UK, 192-211.

Wright, J.D., Miller, K.G., 1996. Control of North Atlantic Deep Water Circulation by the Greenland-Scotland Ridge. Paleoceanography 11, 157-170.

Yilmaz, Ö., 2001. Seismic Data Analysis. Society of Exploration Geophysicists, Tulsa, USA.

6 Second paper: Paleocirculation of the Western Boundary Undercurrent at the Eirik Drift

6.1 Abstract

The Eirik Drift lies on the slope south of Greenland, where it has been formed under the influence of the Western Boundary Undercurrent (WBUC) closely downstream of its origin region, the deep-water formation centers of the Nordic Seas. Therefore, the sediment record at the Eirik Drift documents changes in pathways and intensity of the WBUC. These changes reflect changes in deep-water formation in the Nordic Seas and are therefore coupled with climate changes. Based on the seismostratigraphic analysis of sedimentary structures identified in a set of high-resolution seismic reflection data, we were able to reconstruct the paleocirculation of the WBUC at the Eirik Drift since the Micoene. In conflict to our expectations, we observed a strong WBUC during warm climate conditions, and in phases of climate cooling with enhanced sea-ice extent we found weak WBUC influence at the Eirik Drift. We suggest a southward shift of the deep-water formation region along with a shift of the deep current system during the cool phases. This implies that the main North Atlantic deep-water route just affected the Eirik Drift during warm phases and that during cool phases solely weak branches of the circulation system overflowed the Eirik Drift.

6.2 Introduction

Growing interest in climate research and the coupled ocean-atmosphere interactions has led to numerous studies of the modern and ancient global ocean Thermohaline Circulation (THC), which is closely linked to the earth's climate. Via the upper branch of the THC the surface ocean stores and transports heat and freshwater around the globe. It interacts with the overlying atmosphere through surface fluxes of heat and freshwater (Schmitz, 1996; Van Aken, 2007). The compensating counterpart is a reversed deep ocean circulation. This deep circulation is fed by North Atlantic Deep Water (NADW). NADW formation is the driving mechanism for the THC (Schmitz, 1996; Van Aken, 2007). Thus, NADW production and circulation is of highest importance for the global THC and the global climate (Dickson and Brown, 1994; Schmitz, 1996). It is therefore indispensable for any kind of climate research to understand the principles of the interplay of changes in NADW circulation and climate. Here, we want to contribute to the understanding of the development of this complex interplay by investigating changes in the deep circulation of the northern North Atlantic, closely downstream of the present NADW formation region. From their formation regions in the Nordic Seas and Labrador Sea the NADW components meet southeast of Greenland and combine to the Western Boundary Undercurrent (WBUC; Fig. 6.1). The Eirik Drift south off Greenland is a sediment drift, which lies directly in the pathway of the present WBUC (Arthur *et al.*, 1989; Hunter *et al.*, 2007a; Müller-Michaelis *et al.*, 2013; Wold, 1994). We aim for a better understanding of the development of the ancient WBUC by investigating the sedimentary structure of the Eirik Drift. Information about the development of strength and direction of the WBUC should help to decipher onset and changes in ancient NADW formation and its origin regions. Little is known about the composition of ancient deep water formed in the Nordic Seas, and it is therefore referred to as Northern Component Water (NCW). Our findings will lead to an improved understanding of interactions of NCW production and flow and climate changes.

We have analyzed high-resolution multichannel seismic reflection data of the Eirik Drift, gathered in 2009, in combination with geological information of four ODP/IODP sites. In this study we focus on a detailed reconstruction of interface outlines and depocenter geometries of the Eirik Drift. The location and orientation of the depocenters and their interface outlines will help to assess a model of the paleocurrents in the vicinity of the Eirik Drift. The changes in pathways and strength of the paleocirculation will be discussed with respect to the changes in climate.

6.3 Background and Settings

6.3.1 Oceanographic setting
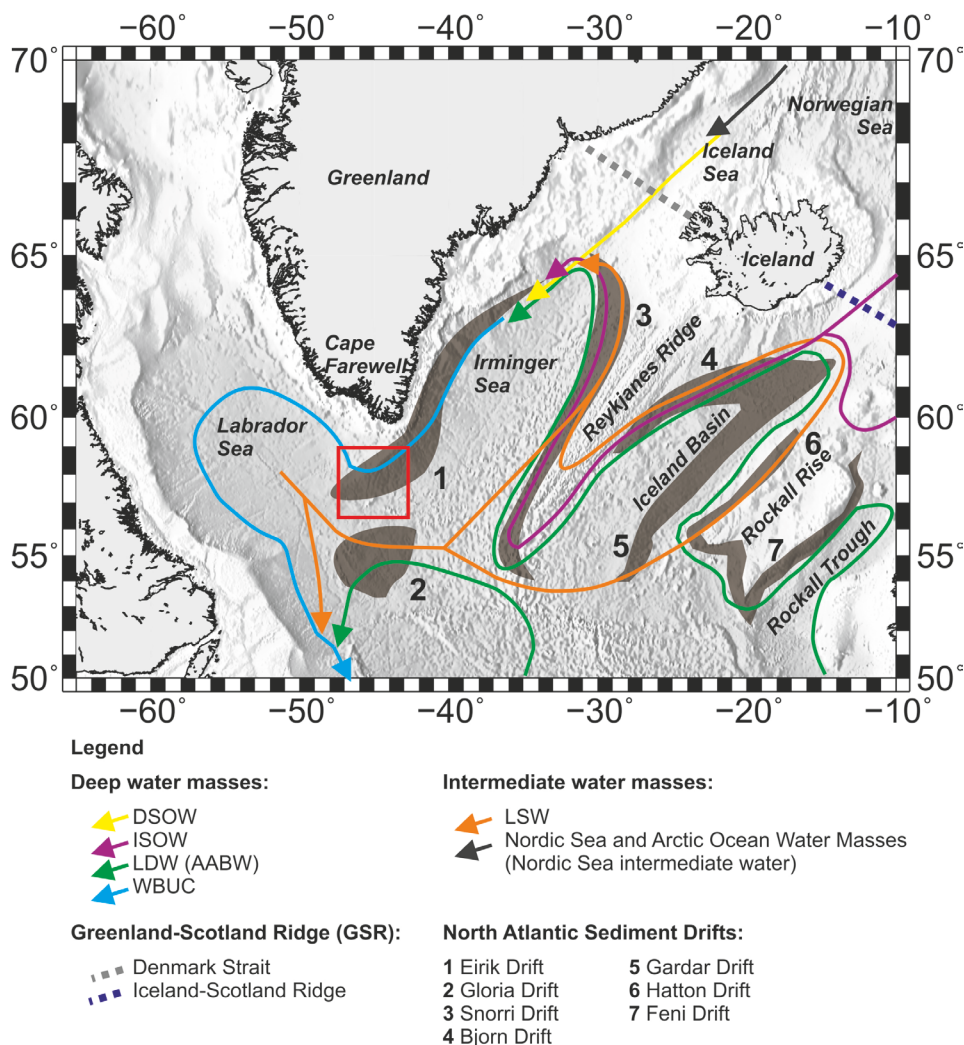
Figure 6.1. Satellite bathymetry map (Smith and Sandwell, 1997) including basins, ridges, sediment drifts and prevailing deep-current system of the North Atlantic (modified from Müller-Michaelis *et al.* (2013); sediment drifts after Faugères *et al.* (1999)). The present Western Boundary Undercurrent (WBUC) at the Eirik Drift transports Denmark Strait Overflow Water (DSOW), Iceland-Scotland Overflow Water (ISOW), Lower Deep Water (LDW; also: modified Antarctic Bottom Water AABW) and Labrador Sea Water (LSW) (modified from Schmitz, 1996). The red box shows the study area (see Fig. 6.2).

The THC is driven by deep-water formation due to thermohaline convection (Dickson and Brown, 1994; Schmitz, 1996). Present deep-water formation is conducted in a bipolar mode

in the polar regions of both the Northern and Southern Hemisphere (Van Aken, 2007). On the Southern Hemisphere shelf ice convection is dominant, but on the Northern Hemisphere the open ocean convection due to atmospheric cooling prevails (Van Aken, 2007). Open ocean convection is assisted by cyclonic surface ocean circulation, which helps to destabilize the stratification of the surface ocean (Van Aken, 2007). The prevailing wind system induces the cyclonic gyres to the surface ocean. Therefore, interactions of atmosphere and the surface ocean through surface fluxes form the necessary preconditions for open ocean convection. The deep-water formation regions on the Northern Hemisphere comprise the Nordic Seas, i.e. the Greenland Sea and the Norwegian Sea, and the Labrador Sea (Fig. 6.1; Kuhlbrodt *et al.*, 2007; Quadfasel and Käse, 2007). In these regions, sufficient atmospheric cooling and cyclonic surface ocean gyres allow convective mixing to greater depths of the deep basins. The deep-water formed in the Nordic Seas spills over the Greenland-Scotland-Ridge (GSR) as dense overflows (Fig. 6.1) (Quadfasel and Käse, 2007; Van Aken, 2007). The overflows as well as the deep water formed in the Labrador Sea recirculate around the Irminger and Labrador basins and entrain different amounts of ambient water (Fig. 6.1; Quadfasel and Käse, 2007). Therefore, the water masses differ in their characteristics, especially in their densities, and are divided into Labrador Sea Water (LSW), Iceland Scotland Overflow Water (ISOW) and Denmark Strait Overflow Water (DSOW; Fig. 6.1; Dickson and Brown, 1994; Schmitz, 1996). These water masses meet at the southeast coast of Greenland. Here, they combine to the North Atlantic Western Boundary Undercurrent (WBUC), a deep, equatorward flow along the western continental slope (Dickson and Brown, 1994; Schmitz, 1996). It is crucial to notice that here the initial North Atlantic WBUC is a complex flow system of overlying water masses of different densities. This system appears as a uniform current at regions with relatively uniform continental slopes and no distinct topographic barriers. In regions of a more complex topography, especially at a margin corner like Cape Farewell, this flow might split up into different strands following different depth contours according to their core depth. Away from its origin, the water masses mix, and south of the Grand Banks (~48° N) DSOW and ISOW are not distinguishable anymore and are referred to as NADW (Smethie and Fine, 2001). In the vicinity of the Eirik Drift the WBUC comprises Upper Labrador Sea Water (ULSW) in water depths of 700 to 1300 m, Classical Labrador Sea Water (CLSW) between 1300 and 2500 m, ISOW between 2500 and 3500 m, and DSOW beneath 3500 m (Pickart, 1992). The deep water, which was formed in the Nordic Seas and northern North Atlantic in former times, differs in composition from the modern NADW due to changing tectonic and climatic conditions. Deep water produced in the Nordic Seas prior to the modern NADW is therefore referred to as Northern Component Water (NCW).

6.3.2 Geological and Paleoceanographic Background

The Labrador Sea has been formed by rifting between Greenland and Labrador during the Late Cretaceous (Chalmers and Pulvertaft, 2001; Srivastava and Arthur, 1989). Active sea-floor spreading ceased ~35 Ma ago (Srivastava and Roest, 1999). Approximately at the same time (~35-33 Ma) the bipolar mode of the THC with the onset of deep-water formation in the Nordic Seas established (Via and Thomas, 2006). The cause for the distribution of Northern Component Water (NCW) is presumably the subsidence of the Greenland-Scotland-Ridge (GSR; Fig. 6.1; Via and Thomas, 2006). This is the topographic barrier between the Nordic Seas and the northern North Atlantic. The western part of the GSR between Iceland and Greenland is called Denmark Strait with a present sill depth of ~600 m (Fig. 6.1; Wright and Miller, 1996). The eastern part of the GSR is the Iceland-Scotland-Ridge (Fig. 6.1), which in fact is a complex ridge system. The Iceland-Faroe-Ridge with an actual sill depth of ~400 m forms the western part of the Iceland-Scotland-Ridge (Wright and Miller, 1996). At its eastern part the Faroe-Shetland-Channel forms the deepest part of the GSR with ~1000 m depth. It is connected to the Irminger Basin of the northern North Atlantic through the N-S orientated

Faroe-Bank-Channel at ~800-1000 m depth and this connection is also called the Faroe Conduit (Fig. 6.1; Stoker *et al.*, 2005). Towards the south to the Rockall Trough region the Faroe-Shetland-Channel ceases at the Wyville-Thomson-Ridge with a present sill depth of ~500 m (Fig. 6.1; Wright and Miller, 1996). Only the distal eastern part of the GSR was subsided enough to allow deep-water exchange in Early Oligocene (Davies *et al.*, 2001). At that time a southward directed NCW flow was documented only in the very eastern part of the North Atlantic in the southeast Faroe Drift north of the GSR (Davies *et al.*, 2001), the Feni Drift (Wold, 1994) and also seabed erosion was observed in the NW Rockall Trough (Fig. 6.1; Howe *et al.*, 2001). With the ongoing subsidence of the GSR and enhanced overflows, a more complex NCW flow pattern in the North Atlantic developed. Stoker *et al.* (2005) stated that with the creation of the Faroe Conduit in early Miocene the first true deep-water connection between the Nordic Seas and the Atlantic was established. At that time strong erosional events were observed at the Bjorn, Gardar, Feni (Fig. 6.1; Miller and Tucholke, 1983) and Eirik Drifts (Müller-Michaelis *et al.*, 2013). In mid Miocene strong NCW fluxes are documented at Snorri, Bjorn, Gardar and Hatton Drifts (Fig. 6.1; Wold, 1994). The first observations of LSW production are documented in the Gloria Drift (Fig. 6.1; Wold, 1994) at ~4.5 Ma following the closure of the Panama Isthmus (Burton *et al.*, 1997). The closure of this important seaway accounted for an increase in northward deflection of warm and saline surface water, which facilitated open ocean convection in the Labrador Sea (Via and Thomas, 2006). It is assumed that global cooling is a necessary condition for NCW formation before the LSW formation established (Via and Thomas, 2006).

6.4 Methods

6.4.1 Contourite drifts

We first want to briefly explain the nature and characteristics of contour currents and their resulting sediment drifts. This is to understand how the high-resolution seismic reflection data document the deep current activity at the Eirik Drift. Contour currents are thermohaline-driven and received their names as they roughly follow the same depth contours, which are congruent with their density level within the stratified ocean (Heezen *et al.*, 1966). These contour currents comprise a current core and tranquil regions surrounding this core (Faugères and Stow, 2008; Faugères *et al.*, 1999; Nielsen *et al.*, 2008; Stow *et al.*, 2002). The concentrated and intensified flow of the current core accounts for non-deposition and/or erosion of sediments at the current core depth (Faugères and Stow, 2008; Faugères *et al.*, 1999; Nielsen *et al.*, 2008; Stow *et al.*, 2002). The eroded and transported sediment within the current is transported to and re-deposited on the tranquil sides. Due to Coriolis force deposition is always to the right for detached elongated mounded drifts like the Eirik Drift on the Northern Hemisphere (Faugères and Stow, 2008; Faugères *et al.*, 1999; Nielsen *et al.*, 2008; Stow *et al.*, 2002). Therefore, contourite drifts, i.e. sediment drifts formed by contour currents, can be detected by the following typical characteristics (Faugères and Stow, 2008; Faugères *et al.*, 1999; Nielsen *et al.*, 2008; Stow *et al.*, 2002). The depocenters are distributed along-slope at certain depth contours and are of lenticular or sigmoidal shape. Their bedding thickens at the drift axis with diverging internal reflections and thins at their drift flanks with converging internal reflections. These thin parts represent the locations of the contour current core. If the current core was particularly strong, also reflector truncation could be observed at the erosional center. Intense initial pulses of deep current flow at the onset of deep current activity form basal unconformities. These are detected as high amplitude reflectors of regional extent with low-angle downlaps (Faugères and Stow, 2008; Faugères *et al.*, 1999; Nielsen *et al.*, 2008; Stow *et al.*, 2002). Within identified contourite deposits the amplitudes of the internal seismic reflections can give additional information about the strength of the deep current regime. As long as the composition of supplied sediment does not change, the

amplitudes of the internal reflections increase with increasing deep current activity. This is due to the changes in grain sizes and the resulting changes in impedance contrast (Stow *et al.*, 2002).

6.4.2 Seismostratigraphy

High-resolution seismic reflection data gathered in 2009 with RV Maria S. Merian, which were correlated with synthetic seismograms of drill sites ODP Leg 105 Site 646 (ODP 646) and IODP Expedition 303 Sites U1305-U1307 (IODP 1305-1307), form the base of this study (Fig. 6.2).
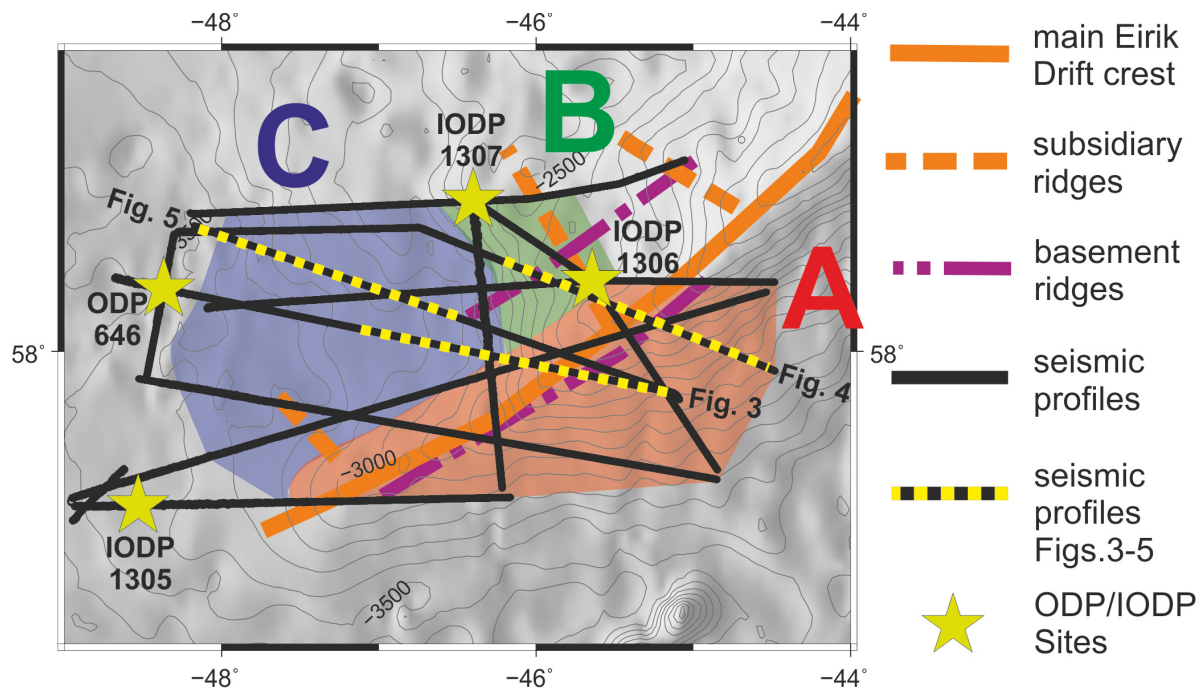
Figure 6.2. Satellite bathymetry map (Smith and Sandwell 1997; red box in Figure 6.1) modified from Müller-Michaelis *et al.* (2013) showing the location of the seismic lines (black lines). The dashed yellow seismic lines are displayed in Figs. 6.3, 6.4, and 6.5. The yellow stars show ODP Leg 105 Site 646 (Shipboard Scientific Party, 1987) and IODP Expedition 303 Sites U1305, U1306 and U1307 (Channell *et al.*, 2010). The orange line shows the NE-SW trending crest of the main Eirik drift. The dashed orange lines indicate the 3 secondary ridges described by Hunter *et al.* (2007b). The dashed purple lines mark the location of the two NE-SW trending basement ridges. Mound A is marked red, mound B green, and mound C blue.

Data processing and methods are described in detail in Müller-Michaelis *et al.* (2013). Müller-Michaelis *et al.* (2013) put forward a seismostratigraphic concept (Fig. 6.3). The characteristics and age of every unit are summarized in Table 6.1 and only briefly described here. Four different units were defined, while prominent internal reflectors subdivide some of these (Table 6.1; Figs. 6.3-6.5).

The irregular seismic basement (60-40 Ma; Figs. 6.3-6.5) is overlain by unit SUIV. Unit SUIV comprises the period 40-8.1 Ma and is subdivided into subunits SUIV-c (40-19 Ma), SUIV-b (17-12 Ma) and SUIV-a (10-8.1 Ma) (Table 6.1; Figs 6.3-6.5). Subunit SUIV-c is almost acoustically transparent and is interpreted to represent an infill and drape of the irregular basement topography in an environment not controlled by deep currents (Figs. 6.3-6.5). Its top horizon A3 (19-17 Ma) is identified as the basal erosional unconformity of the Eirik Drift. The deposition of subunit SUIV-b documents the onset of drift building under the influence of strong NCW fluxes, which were inhibited between 15-12.5 Ma. A renewed onset of strong NCW flow formed horizon R5 (12-10 Ma), which separates subunits SUIV-b and SUIV-a.

Unit SUIII extends from horizon doublet R3/R4 (8.1/7.5 Ma) to the erosional unconformity EU (4.5 Ma) and is subdivided by the internal medium-amplitude horizon R2 (5.6 Ma). Unit SUIII comprises narrowly spaced, parallel to subparallel low amplitude reflections in the lower part (subunit SUIII-b, 7.5-5.6 Ma) and an increase in amplitudes and reflector spacing in the upper part (subunit SUIII-a, 5.6-4.5 Ma). The increase in reflection amplitudes and the reflector truncations observed at the erosional unconformity indicate an increase in NCW flow with time following Stow *et al.* (2002), as no noteworthy changes in lithology were observed until 2.5 Ma (horizon R1) at ODP Site 646 (Cremer *et al.*, 1989).

Unit SUII (4.5-2.5 Ma) is characterized by narrowly-spaced, continuous high-amplitude reflections. Reflector truncations are observed at its top horizon R1 (2.5 Ma). That indicates an intense NCW flow. Furthermore, horizon R1 marks the onset of major ice rafting at the Eirik Drift (Arthur *et al.*, 1989).

The youngest unit SUI (2.5-0 Ma) is subdivided into subunits SUI-c (2.5-1.4 Ma), SUI-b (1.4-0.8 Ma) and SUI-a (0.8-0 Ma) by the internal horizons A2 (1.4 Ma) and A1 (0.8 Ma). Within subunit SUI-c wide-spaced, continuous to discontinuous, parallel to subparallel internal reflections are observed, which increase in amplitude towards its top horizon A2. Subunit SUI-b comprises continuous to discontinuous, narrowly-spaced, parallel medium-amplitude reflections, while SUI-a is characterized by continuous, parallel to subparallel high-amplitude reflections. No reflector truncation is observed at the erosional centers and this implies that the deep current regime weakened after 2.5 Ma. There is a major change in the sediment lithology at 2.5 Ma and a minor change within unit SUI (Cremer *et al.*, 1989). Therefore, the high-amplitude internal reflections cannot be used for the interpretation of the deep current intensity.
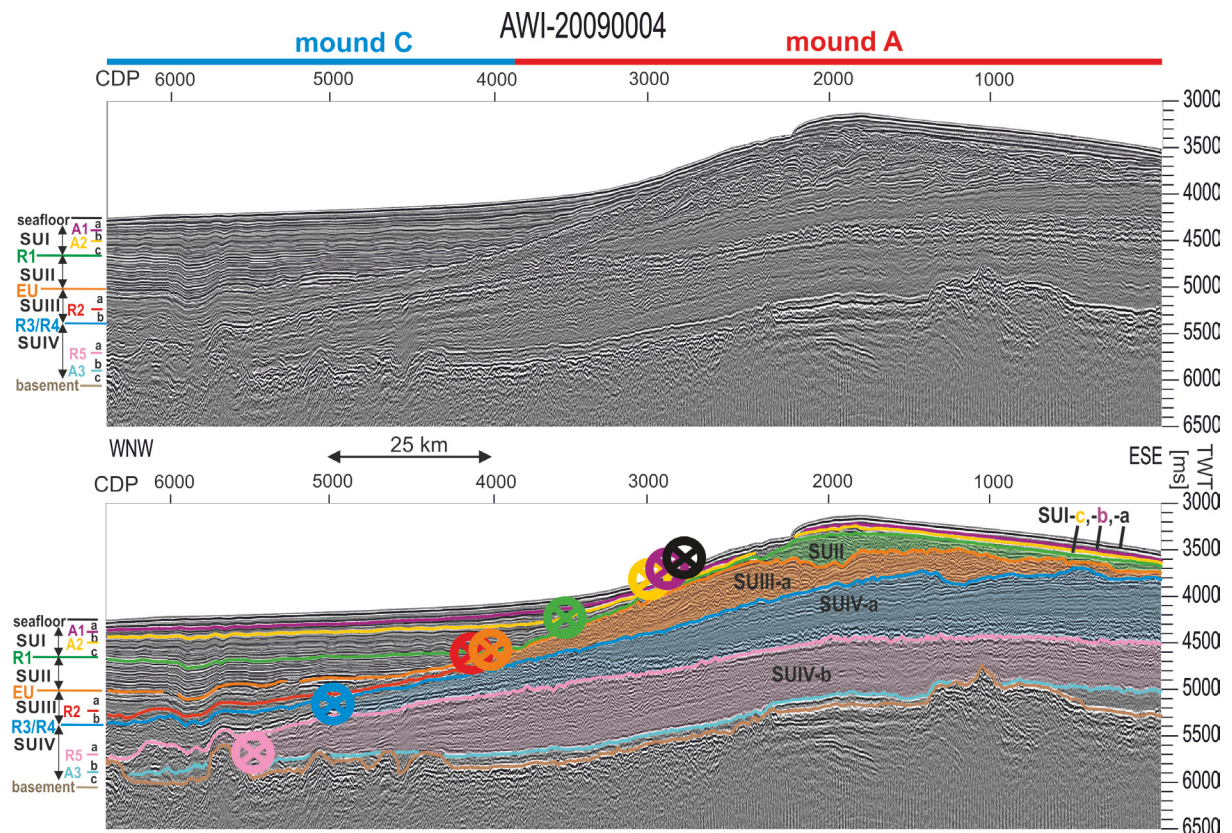
Figure 6.3. Line AWI-20090004. For location see Fig. 6.2. Horizons: A1 (magenta; 0.8 Ma), A2 (yellow; 1.4 Ma), R1 (green; 2.5 Ma), erosional unconformity EU (orange; 4.5 Ma), R2 (red; 5.6 Ma), reflection doublet R3/R4 (blue; 7.5/8.1 Ma), R5 (pink; 10-12 Ma), A3 (cyan; 17-19 Ma) and basement (brown; ~40-60 Ma). Circles in the color of the top-horizon indicate the interpreted location of the current core and its direction for the respective seismic sub-unit.

6.5 Results

Tracking the seismic horizons and mapping the seismic units' thicknesses, we gain a detailed image of interface outlines and depocenter geometries of each seismic unit in the study area (Fig. 6.6). The distribution and relocalisation of topographic highs and lows of the interface outlines as well as of the depocenters of each seismic (sub)unit will be discussed. We define the topographic highs of the interfaces and depocenters as the root mean square (rms) value of the interface depth and unit thickness, respectively. Orientation and location of the depocenters will be interpreted related to the morphology of the underlying horizon. Depocenters parallel to the slope of the basal horizons are interpreted as a result of along-slope sediment transport, i.e. contour current controlled deposition. Stronger flow of a contour current core causes erosion and/or reduced net accumulation, while sediment accumulates in the comparatively tranquil zones to the right (in the Northern Hemisphere) of the current core (Faugères and Stow, 2008; Faugères *et al.*, 1999; Nielsen *et al.*, 2008; Stow *et al.*, 2002). The distribution and relocalisation of the depocenters, the changes in the interface outline morphology as well as the internal reflection characteristics will therefore help to decipher the pathways, directions and strength of the deep current cores in our study area.

First, we will describe the present seafloor morphology of the Eirik Drift for a better overview of our study area. We then describe the (sub)units and their bounding horizons from bottom to top, i.e. from the oldest to the youngest, starting with the seismic basement.

6.5.1 Seafloor

The seafloor is characterized by three mounds (Fig. 6.2). Mound A forms an elongated, ridge-like structure, which extends from the NE to the SW (Fig. 6.2). In the NE mound B extends almost perpendicular to mound A's crest to the NW (Fig. 6.2). Adjacent to mound A and B, mound C slopes to the west (Fig. 6.2).
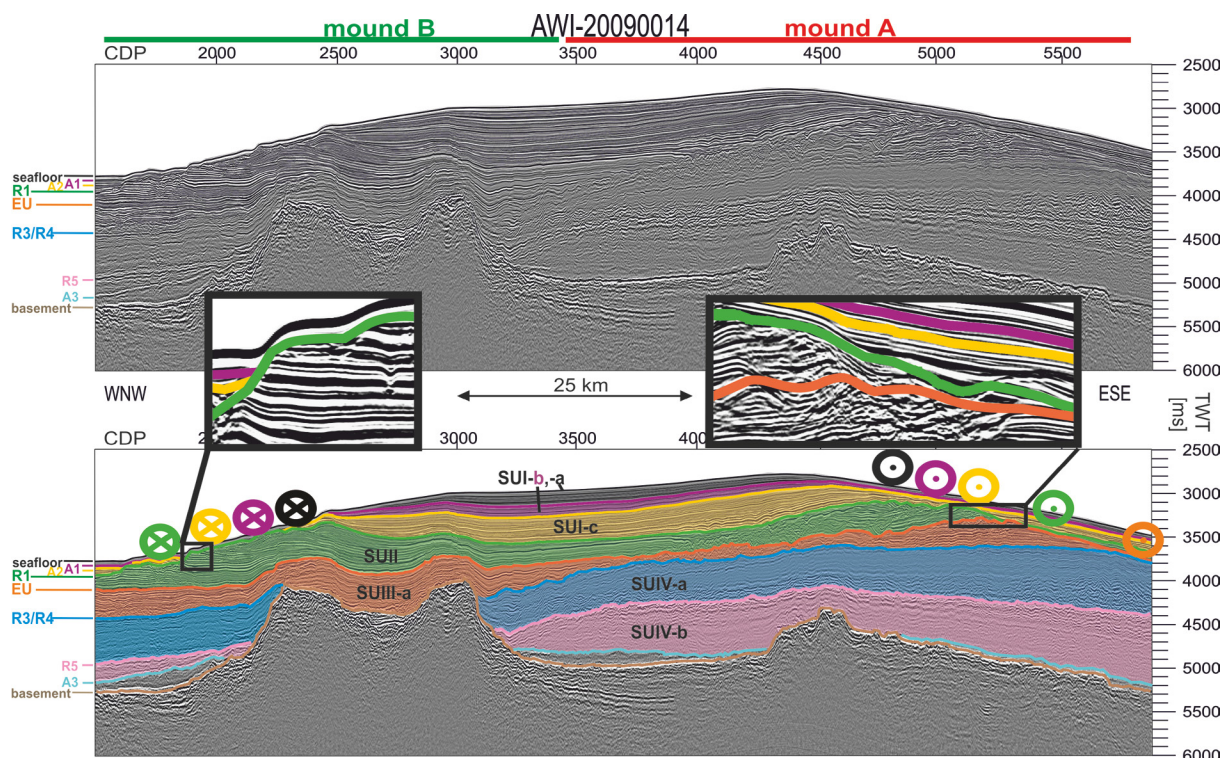
Figure 6.4. Line AWI-20090014. For location see Fig. 6.2. Horizons: A1 (magenta; 0.8 Ma), A2 (yellow; 1.4 Ma), R1 (green; 2.5 Ma), erosional unconformity EU (orange; 4.5 Ma), reflection doublet R3/R4 (blue; 7.5/8.1 Ma), R5 (pink; 10-12 Ma), A3 (cyan; 17-19 Ma) and basement (brown; 40-60 Ma). Circles in the color of the top-horizon indicate the interpreted location of the current core and its direction for the respective seismic sub-unit. Insert shows reflector truncations.
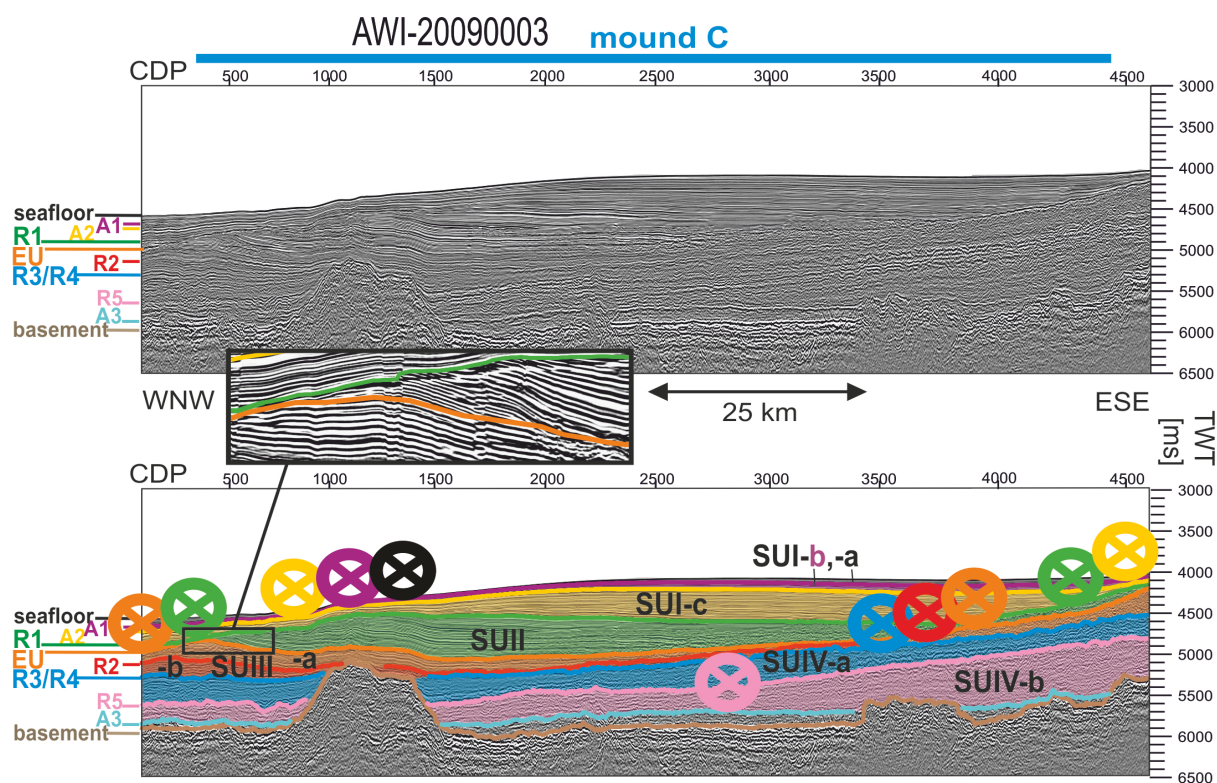
Figure 6.5. Line AWI-20090003. For location see Fig. 6.2. Horizons: A1 (magenta; 0.8 Ma), A2 (yellow; 1.4 Ma), R1 (green; 2.5 Ma), erosional unconformity EU (orange; 4.5 Ma), R2 (red; 5.6 Ma), reflection doublet R3/R4 (blue; 7.5/8.1 Ma), R5 (pink; 10-12 Ma), A3 (cyan; 17-19 Ma) and basement (brown; 40-60 Ma). Circles in the color of the top-horizon indicate interpreted location of the current core and its direction for the respective seismic sub-unit. Insert shows reflector truncations.

6.5.2 Basement

The seismic basement is an irregular, hummocky high amplitude reflector, which marks the top of the oceanic crust (Figs. 6.3-6.5). It shows a high in the NE and the deepest part of the horizon can be observed in the West (Fig. 6.6a). Several basement highs are found at mound A (Figs. 6.3, 6.4 and 6.6a) and form the axes of the southern WSW-trending basement ridge (cf. Figs. 6.2 and 6.6a; Le Pichon *et al.*, 1971; Srivastava and Arthur, 1989). A second WSW-trending basement ridge north of and parallel to the latter (Fig. 6.2; Le Pichon *et al.*, 1971; Srivastava and Arthur, 1989) is found below mound B (Figs. 6.4 and 6.6a). Additional basement elevations are found in the NW at mound C (Figs. 6.5 and 6.6a).

6.5.3 Unit SUIV

The main part of the depocenter of unit SUIV is found in the SE (Fig. 6.6b). It surrounds the NE basement high (Figs. 6.6a and b). In subunit SUIV-c several small depocenters infill the basement topography and thus lead to a smoothed morphology of horizon A3 compared to the underlying basement horizon. In the overlying subunits SUIV-b and SUIV-a a distinct depocenter is observed in the SE. This depocenter encloses the NE topographic high of the basal horizons and shows a meandering western boundary. The depocenter of subunit SUIV-b extends farther to the south than that of subunit SUIV-a. The meanders observed at the western boundary of the depocenter are more pronounced in subunit SUIV-a than in subunit SUIV-b.

6.5.4 Unit SUIII

In contrast to unit SUIV (Fig. 6.6b) the main depocenter of unit SUIII is observed in the SW (Fig. 6.6d). It lies mainly in the topographic low of horizon R3/R4 at mound C (Figs. 6.6c and

d). Smaller depocenters are found aligned along the western flank of the topographic high of horizon R3/R4 (Figs. 6.6c and d), which correspond to the western flanks of mound A and mound B. Subunit SUIII-b thins from 300 ms TWT in the SW to 0 ms TWT in the E where horizon R2 onlaps on horizon R3/R4 (Figs. 6.3 and 6.5). Its depocenter is SW-NNE oriented. In subunit SUIII-a the depocenter shifts towards the E. The smaller depocenters observed along the western flanks of mound A and mound B (Fig. 6.6d) belong to subunit SUIII-a.

6.5.5 Unit SUII

In unit SUII the depocenters shifted to the N (Fig. 6.6f). Two connected main depocenters are observed (Fig. 6.6f). The western part infills the eastern topographic low of horizon EU (Figs. 6.6e and f). The eastern part overlies the topographic high of horizon EU at mound A and mound B (Figs. 6.6e and f). In the south and in the very east unit SUII is characterized by a thin cover (Fig. 6.6f).

6.5.6 Unit SUI

In unit SUI we observe the separation of the two parts of the depocenter (Fig. 6.6h). The western depocenter at mound C fills the eastern topographic low of horizon R1 (Fig. 6.6g and h). This western depocenter has shifted to the south (Figs. 6.6f and h). The eastern depocenter remains in the NE on top of the topographic high of the basal horizon R1 at mound A and mound B (Figs. 6.6g and h). The thinnest part of unit SUI surrounds this NE depocenter. Within the subunits SUI-c, SUI-b and SUI-a the western depocenter at mound C (Fig. 6.6h) is shifted gradually to the south following the changing morphology of the basal horizons.
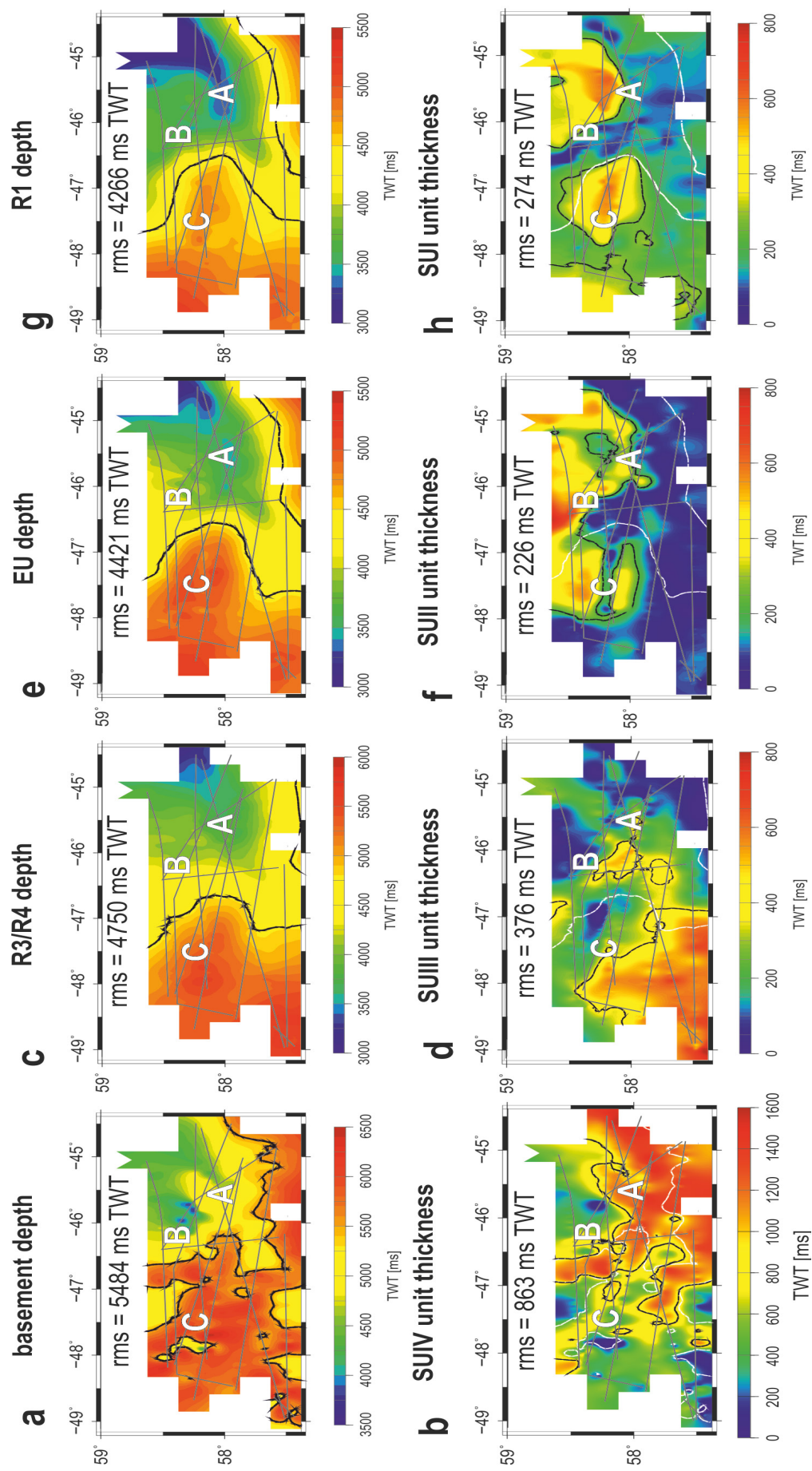
6.6 Discussion

Our grid of seismic reflection data is not uniform (Fig. 6.2). The resulting maps (Fig. 6.6) therefore are afflicted with uncertainties in the uncovered areas, but the overall trend of interface outlines and distribution and re-localization of the depocenters is probably correct. The distinct depocenters observed within each seismic unit after the formation of the basal unconformity A3 (~19-17 Ma; Müller-Michaelis *et al.*, 2013) are found within certain depth contours of the underlying horizons (Figs. 6.6b, d, f and h). This points to current controlled sedimentation (Faugères and Stow, 2008; Faugères *et al.*, 1999; Nielsen *et al.*, 2008; Stow *et al.*, 2002). The shapes and locations of these depocenters shift from one unit to the next (Figs. 6.6b, d, f and h). These shifts along with changes in the internal structure and reflection characteristics reflect changes in the prevailing contour current flow in each time interval. The thinnest parts of each seismic (sub)unit with converging internal reflections or even observed reflector truncations are interpreted as the erosional centers and therefore as the location of the prevailing deep current core within each time frame (Faugères and Stow, 2008; Faugères *et al.*, 1999; Nielsen *et al.*, 2008; Stow *et al.*, 2002). For each seismic subunit this interpretation of the deep current core location was transferred from the seismic lines (Figs. 6.3-6.5) to the contour plots of the basal horizons (Fig. 6.7). Contour currents roughly follow bathymetric contours and therefore, the pathways of the deep current core in between the seismic lines were deduced (Fig. 6.7). Additionally, the locations of their depocenters were marked (Fig. 6.7), which we expect to the right of the erosional centers, and thus we retrieve the deep current direction (Faugères and Stow, 2008; Faugères *et al.*, 1999; Nielsen *et al.*, 2008; Stow *et al.*, 2002). Hence, a model for the development of the deep paleocurrents at the Eirik Drift is assessed (Fig. 6.7). Based on this model (Fig. 6.7) a possible interplay of oceanographic, climatic and tectonic conditions in the northern North Atlantic will be discussed (Fig. 6.8).

Table 6.1.
Seismic stratigraphy and reflector nomenclature at the Eirik Drift after Müller-Michaelis *et al.* (2013). The trend of the intensity of the Western Boundary Undercurrent (WBUC) and of the climate conditions as well as the Time Epoch are indicated on the left.

Epoch	Temp. trend	WBUC intensity	Age [Ma]	Reflector/ unit name	Depth at ODP 646 [ms TWT]	Thickness (min/max) [ms TWT]	Seismic characteristic
late Pleistocene				SUI-a		0/170	continuous high amplitude reflctions, parallel to subparallel to seafloor
			0.8	A1	456		High-amplitude reflector
early Pleistocene				SUI-b		0/150	continuous to discontinuous, narrowly-spaced, parallel medium amplitude reflections
			1.4	A2	470		High-amplitude reflector
				SUI-c		50/440	wide-spaced, continuous to discontinuous, parallel to subparallel reflections, upward increase in amplitudes
	NHG		2.5	R1	490		Medium- to high amplitude reflector
late Pliocene				SUII		50/720	narrowly-spaced, continuous high-amplitude reflections; unit rises from W to E
	3.2 Ma		4.5	EU	500		Erosional unconformity; high-amplitude reflector; reflector truncation
early Pliocene				SUIII-a		50/580	upward increase in amplitudes and reflector spacing; unit thickens from W to E
			5.6	R2	510		Medium-amplitude reflector
	6.0 Ma			SUIII-b		0/430	narrowly-spaced, parallel to subparallel, low-amplitude reflections
late Miocene	NHG		7.5/ 8.1	R3/ R4	540/ 545		Medium- to high-amplitude reflector doublet
				SUIV-a		0/940	parallel to subparallel, low-amplitude reflections
middle Miocene			10-12	R5	570		Band of 3-4 high-amplitude reflections
	15 Ma			SUIV-b		0/900	converging, low- to medium-amplitude reflections; unit thins from W to E
early Miocene			17-19	A3	580		Basal erosional unconformity
				SUIV-c		0/380	almost acoustically transparent
			40-60	basement	590		Irregular basement topography

Figure 6.6. Contour maps of horizon depth (a, c, e, g) and unit thickness (b, d, f, h). The black lines indicate the root mean square (rms) depth (a, c, e, g) and rms thickness (b, d, f, h), respectively. The rms depth outline of the basal horizon is added in the unit thickness plots (b, d, f, h) as white lines. The locations of mounds A, B and C are indicated by the white letters. (a) basement depth; (b) unit SUIV thickness, white line: basement topographic high outline; (c) horizon R3/R4 depth; (d) unit SUIII thickness, white line: R3/R4 topographic high outline; (e) horizon EU depth; (f) unit SUII thickness, white line: EU topographic high outline; (g) horizon R1 depth; (h) unit SUI thickness, white line: R1 topographic high outline.

55

6.6.1 Unit SUIV (> 7.5 Ma)

The various depocenters in the basement topographic lows of subunit SUIV-c (40-19 Ma) are interpreted as an infill and drape in a tranquil environment (Müller-Michaelis *et al.*, 2013). Subunit SUIV-c is overlain by horizon A3 (~19-17 Ma), which shows the characteristics of a basal unconformity, as it is a continuous, high amplitude reflector of regional extent with observed low-angle downlaps (Müller-Michaelis *et al.*, 2013). The formation of horizon A3 (~19-17 Ma) requires strong deep current activity and thus is interpreted to mark the onset of drift building at the Eirik Drift, presumably accompanied by an erosional hiatus (Müller-Michaelis *et al.*, 2013). The depocenters of subunits SUIV-b (~17-15 Ma; Fig. 6.7a) and SUIV-a (~12-8.1 Ma; Fig. 6.7b) are found in the SE of the study area, surrounding the topographic high of their basal horizons in the NE (Figs. 6.7a and b). The erosional centers, i.e. the interpreted locations of the deep current core, follow a certain depth contour in the western part of the study area (Figs. 6.7a and b). The locations of erosional and depositional centers as well as the morphology of the basal horizons suggest a W-E meandering, northward-directed flow in the western part of the study area before it turns to the NE (Figs. 6.7a and b). The depositions and therefore also the suggested NCW flow shallowed and shifted to the E from subunit SUIV-b (Fig. 6.7a) to subunit SUIV-a (Fig. 6.7b) and the undulations at the western flank are more pronounced. The NCW flow and thus deep current controlled sedimentation at the Eirik Drift was interrupted between these two subunits (14-12.5 Ma) (Müller-Michaelis *et al.*, 2013). The high-amplitude reflection band surrounding R5 represents a renewed onset and a change in the deep current system at 12-10 Ma (Müller-Michaelis *et al.*, 2013). The more pronounced NCW flow meandering of the western flank of the depocenter observed within subunit SUIV-a (Fig. 6.7b) might be caused by an intensified NCW flow with enhanced erosion. Our study area does not cover the spatial extent of the depocenters to the S and E (Figs. 6.7a and b). However, the slope of the basal horizons from NE to SW and the orientation of the depocenters along this slope suggest a WSW directed flow at the SE flank of mound A outside of the study area, before it turns to the observed northern direction (Figs. 6.7a and b).

Cooling is a necessary condition for NCW production but the shallow sills of the GSR have been the limiting factor for the overflows of NCW into the north Atlantic before early Oligocene (Via and Thomas, 2006). Sufficient subsidence of the GSR and NCW overflow at the distal eastern part is determined at the early Oligocene (Wright and Miller, 1996). Davies *et al.* (2001) suggested the onset of NCW overflow into the Rockall Trough region at ~35-33 Ma with a continuing southward directed flow (Fig. 6.8a). This southward-directed NCW flow is documented in the Feni Drift (Fig. 6.8a) with a stable drift accumulation since ~34 Ma (Miller *et al.*, 2009; Wold, 1994; Wright and Miller, 1996). This early, southward directed NCW flow during the cold Oligocene climate would not have affected the Eirik Drift, and in concordance we did not observe any deep current activity here (Fig. 6.8a). Presumably due to the cold climate the NCW was denser and therefore flowing at a deeper depth contour towards the south instead of recirculating around the northern North Atlantic. The onset of strong NCW fluxes at ~19-17 Ma (Wright and Miller, 1996) was not only observed at horizon A3 at the Eirik Drift (Müller-Michaelis *et al.*, 2013) but is also documented in a widespread erosional unconformity in the northern North Atlantic (Miller and Tucholke, 1983; van Weering *et al.*, 2008; Wold, 1994). Stoker *et al.* (2005) suggested that the Faroe Conduit developed in early Miocene and formed the first true deep-water connection between the Atlantic Ocean and the Nordic Seas. The early Miocene NCW overflow over the eastern part of the Iceland-Scotland-Ridge and the resulting NCW deep circulation is documented in the onset of drift building within the Iceland Basin at Bjorn and Gardar Drift but not traceable within the Irminger Sea (Fig. 6.8b). We therefore suggest a NCW flow between 19 and 15 Ma as depicted in Figure 6.8b with presumably no overflow at the Denmark Strait and at the Iceland-Faroe-Ridge. These first indications for strong NCW flow at the Eirik Drift (~19-15

Ma) and in the northern North Atlantic are interpreted for the Mid Miocene Climate Optimum (~20-15 Ma).

Low to no NCW flux in the North Atlantic has been observed between 16-12.5 Ma (Woodruff and Savin, 1989; Wright *et al.*, 1992) and also at the Eirik Drift at 15-12.5 Ma (Müller-Michaelis *et al.*, 2013). This coincides with the cooling during the Mid Miocene Climatic Transition (Zachos *et al.*, 2001). Presumably, this cooling accounted for the production of NCW with increased density and additionally, the GSR was still too shallow to allow a significant overflow (Poore *et al.*, 2006; Wright, 1998). The renewed onset of strong deep current activity at the Eirik Drift at ~12 Ma follows the cooling of the mid Miocene Climate Transition along with the ongoing subsidence of the GSR (Poore *et al.*, 2006; Wright, 1998). We suggest that the high amplitude reflection band and horizon R5 (~12-10 Ma; Figs. 6.3-6.5) was created by a renewed onset of strong NCW flux. This renewed onset of strong NCW flux was also observed at Snorri, Bjorn, Gardar and Hatton Drifts between 13-10 Ma (Wold, 1994). We therefore suggest a deep current activity as depicted in Figure 6.8c for the time interval 12-9 Ma. The shallowing of the deep circulation observed at the Eirik Drift is reflected in circulation at shallower water depths of the northern North Atlantic, with drift building at Hatton Drift and the recirculation through the Irminger Sea (Fig. 6.8c). Bohrmann *et al.* (1990) reported of the first significant overflow over the western part of the Iceland-Scotland-Ridge at ~13-11 Ma (Fig. 6.8c). This strengthened the branch recirculating via the outer Labrador Sea. The top of SUIV is defined by horizon doublet R3/R4 (7.5/8.1 Ma). Short-term climate fluctuations with a temperature increase between ~9-8 Ma followed by a decrease between ~8-7.5 Ma (Zachos *et al.*, 2001) might be responsible for reduced NCW production and overflows at 9 and 7 Ma with a high NCW production between 8.5-8 Ma (Poore *et al.*, 2006; Wright, 1998; Wright and Miller, 1996). Bohrmann *et al.* (1990) also observed a weak NCW flow in the northern North Atlantic between 9.3 and 8.7 Ma and an increase in NCW flow at 8.7-8.2 Ma. These fluctuations in NCW flow are interpreted to have formed reflector doublet R3/R4 (~7.5/8.1 Ma).

6.6.2   Unit SUIII (7.5-4.5 Ma)

The main depocenter of unit SUIII (~7.5-4.5 Ma) is found S-N orientated at mound C (Figs. 6.7c and d). It has shifted to the east, and additional smaller depocenters are found aligned along the western flanks of mound A and B for subunit SUIII-a. The internal horizon R2 (~5.6 Ma) is only found in the west and onlaps on the rise of horizon R3/R4 (Figs. 6.3 and 6.5). The alongslope, S-N oriented depocenter in the west with parallel to subparallel internal reflections of low amplitudes is interpreted as a contourite deposit. The shape and orientation of subunit SUIII-b point to a northward directed NCW flow west of our study area for the period 7.5 to 5.6 Ma (Fig. 6.7c). With the shift of this depocenter to the E between 5.6 and 4.5 Ma we evidence this deeper, second branch of northward-directed flow with the observation of erosional centers in the NW of our study area (Fig. 6.7d). The locations of the onlap of the top horizon R2 (~5.6 Ma) onto horizon R3/R4 (7.5/8.1 Ma) can be interpreted as the erosional core of a shallower contour current branch, but no deposits are observed in the east (to the right of the erosional centers; Fig. 6.7c). The onlap of horizon R2 (~5.6 Ma) onto horizon R3/R4 (7.5/8.1 Ma), i.e. the erosional deep current core center, is observed within a distinct depth contour between ~4700 and 5300 ms TWT. The weak internal reflection amplitudes also point to a weak contour current as no lithological changes of the sediments were observed until 2.5 Ma (Cremer *et al.*, 1989). It might have been too weak to transport sediments to the top of mounds A and B. Therefore, we suggest that the onlaps observed within the depth contour ~4700 to 5300 ms TWT mark the erosional center of a shallower, weak contour current core even though no deposition is found to its right. The depositions along the western flanks of mounds A and B of subunit SUIII-a (~5.6-4.5 Ma) evidence this undulating shallow NW directed flow (Figs. 6.7d). The amplitudes of the internal reflections
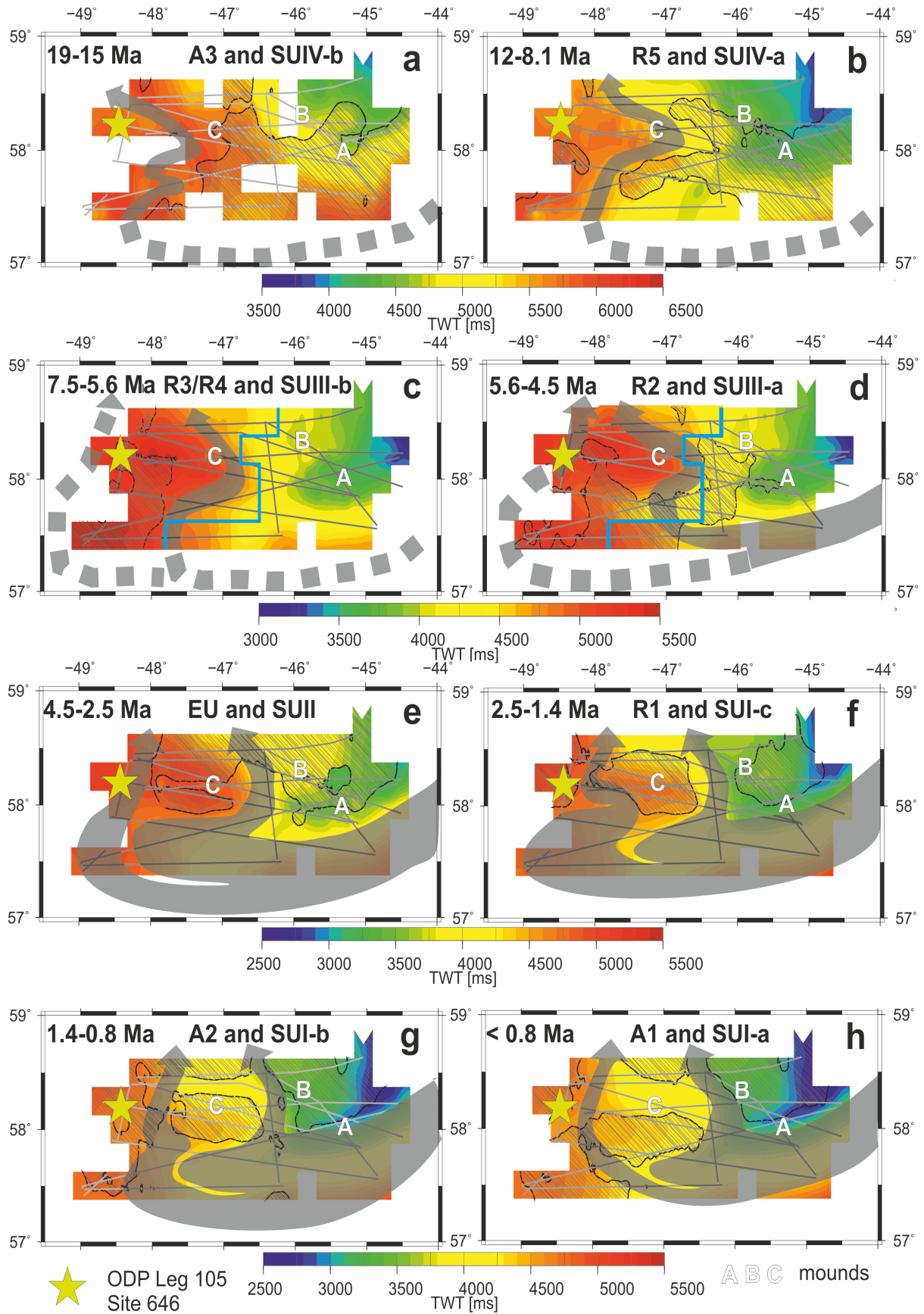
increase from the upper part of subunit SUIII-b towards the top of subunit SUIII-a (Figs. 6.3-6.5), where reflector truncations are observed at the erosional unconformity EU (inserts Figs. 6.4-6.5). The enhanced erosional facies (reflector truncations) along with the increase in reflection amplitudes are interpreted as an increase in deep current intensity towards ~4.5 Ma. The two branches of NCW flow observed after 5.6 Ma additionally flowed within a shallower depth contour (~4400-4800 ms TWT) than observed within subunit SUIII-b (~4700-5300 ms TWT; 7.5-5.6 Ma). Our data for the first time resolve the WSW flowing part at the SE flank of mound A via erosional centers with depocenters to their right (Fig. 6.7d).

The first influence of NCW flow with an increased sedimentation rate at ODP Leg 105 Site 646 is reported at ~7.5 Ma (horizon R3) and was identified as DSOW (Kaminski *et al.*, 1989). The onset of DSOW in the northern North Atlantic was also observed and dated ~7 Ma by Bohrmann *et al.* (1990). Thus, the depocenter overlying ODP Site 646 observed since 7.5 Ma might have been deposited under the influence of DSOW flow. We conclude that after 7.5 Ma the lower branch of the WBUC west of the study area transported (ancient) DSOW. Analogue to the modern deep current system we suggest that the upper observed branch conveyed Pre-ISOW. The observed weak NCW flow between 7.5 and 5.6 Ma have also been observed by Poore *et al.* (2006). Wright and Miller (1996) reported restricted overflows before ~6 Ma, and Arthur *et al.* (1989) also interpreted subunit SUIII-b to have formed under the influence of weak deep currents. Thus, the NCW flow at the Eirik Drift and the northern North Atlantic is suggested to have been weak during the ongoing Miocene cooling (until ~6 Ma; Zachos *et al.*, 2001). A weakening of NCW production and flow during the ongoing Miocene cooling is in conflict with our expectation of strong NCW production and flow during cold climate. We suggest a significant ice cover of the Nordic Seas during this time interval. The ice cover would inhibit the open ocean convection as the ocean would be isolated from the atmosphere and no exchange in heat and freshwater would be possible. Unfortunately, only few details of the exact extent of sea ice are known for this period. A local glaciation at Svalbard is thought to have yielded a general strengthening of NHG at ~6.9 Ma (Winkler *et al.*, 2002) and an enhanced sea-ice extent at the Greenland Sea between ~7.5 and 6.2 Ma (Wolf-Welling *et al.*, 1996). This would easily have resulted in a shift of the NCW formation area south towards the Norwegian Sea (Fig. 6.8d). With this southward shift, the pathways for the intense NCW branches would also have shifted, and therefore the Eirik and maybe also other Northwest Atlantic drifts experienced only a weaker branch of NCW flow. A denser, southward-directed NCW flow following a deeper depth contour is suggested as conveyor of the main deep circulation at that time (Fig. 6.8d). A dense and deep NCW

Figure 6.7. Model for the development of palaeocurrents at the Eirik Drift. The grey arrows indicate location and direction of the interpreted current core for the respective (sub)unit. The background morphology is that of each basal horizon for the sub-unit overlain by the black-hatched depocentres of each sub-unit. The light grey lines show the location of the seismic profiles. The locations of mounds A, B and C are indicated by the white letters. The location of ODP 646 is marked by the yellow star. (a) Horizon A3 with depocentre and resulting palaeocurrent of seismic sub-unit SUIV-b (19-15 Ma); (b) horizon R5 with depocentre and resulting palaeocurrent of seismic sub-unit SUIV-a (12-8.1 Ma); (c) horizon R3/R4 with depocentre and resulting palaeocurrent of seismic sub-unit SUIII-b (7.5-5.6 Ma), the blue line indicates maximum eastern extent of top horizon R2; (d) horizon R2 (west of blue line) and R3/R4 (east of blue line) with depocentre and resulting palaeocurrent of seismic sub-unit SUIII-a (5.6-4.5 Ma), blue line indicates maximum eastern extent of bottom horizon R2; (e) horizon EU with depocentre and resulting palaeocurrent of seismic unit SUII (4.5-2.5 Ma); (f) horizon R1 with depocentre and resulting palaeocurrent of seismic sub-unit SUI-c (2.5-1.4 Ma); (g) horizon A2 with depocentre and resulting palaeocurrent of seismic sub-unit SUI-b (1.4-0.8 Ma); (h) horizon A1 with depocentre and resulting palaeocurrent of seismic sub-unit SUI-a (<0.8 Ma).

flow would be more likely through the supposedly deepest passage, the Faroe Conduit (Stoker *et al.*, 2005), preceding south through the Iceland Basin. As no changes are observed at the Feni Drift (Wold, 1994), a deep southward-directed NCW flow through the Rockall Trough region cannot be excluded either. We cannot clarify the exact pathway based on our data. The intensification of NCW flow at the Eirik Drift started with the climate reversal to the early Pliocene warm period at ~5 Ma. The onset of increasing deep current activity is documented at ODP 646 by an increase in deep ventilation at horizon R2 (5.6 Ma; Kaminski *et al.*, 1989) and here, highest deep current velocity is documented at the EU (4.5 Ma) (Kaminski *et al.*, 1989). Increases in formation of ISOW are observed at ~4.5 Ma (Haug and Tiedemann, 1998; Mikolajewicz and Crowley, 1997) and DSOW at ~4.6 Ma (Haug and Tiedemann, 1998). A distinct increase in drift accumulation at ~5 Ma is also observed at Bjorn and Gardar Drift (Wold, 1994). How can we explain this widespread observed intensification of the deep current system during the early Pliocene warm period? With the climate reversal and the warming, the suggested ice cover in the Greenland Sea was declined. The deep-water formation region would then have shifted back to the Nordic Sea region including the Greenland Sea. With the climate warming a less dense and therefore shallower NCW flow (Fig. 6.7d) is expected. We suggest that the main pathways of the NCW flow would then again have been similar to the present and therefore an intensification of the NCW flow along these pathways was observed (Fig. 6.8e).

6.6.3   Unit SUII (4.5-2.5 Ma)

For the period 4.5-2.5 Ma two connected depocenters are found shifted to the north (Fig. 6.7e), while low to no deposition is found in the south and in the very east (Fig. 6.6f). The western part of the depocenter is found in the topographic low of the erosional unconformity at mound C, and the eastern part of the depocenter is found at the topographic high of the erosional unconformity in the NE. In between these two parts the depocenter thins, and the internal reflection converge. Reflection truncations were found at horizon R1 at the western flanks of mound B (Fig, 7.4) and mound C (Fig. 6.5) with the depocenters located to their right. These erosional centers again indicate an intense NCW flow of two branches in different depths. The locations of erosional and depositional centers as well as the morphology of the basal horizons suggest a WSW directed deep current flowing over the southern part of the study area and having been responsible for the low to non-deposition there. This NCW flow recirculated and split up into two northward-directed branches with the deeper branch accounting for the deposition at mound C (Fig. 6.7e). The upper branch overflowed the thinned indentation of the depocenter and deposits on top of mound A and B (Fig. 6.7e). Enhanced erosion and less sedimentation at the depth interval of the lower deep current branch indicate that the deeper part of NCW flow was more intense than the shallower branch. The pathways of the two deep current branches are similar to before. This might indicate that we again observe a strong NCW flow of DSOW (lower NCW) and ISOW (upper NCW), with a stronger DSOW than ISOW flow. Our interpretation of strong NCW flow from 4.5-2.5 Ma is supported by the findings of Arthur *et al.* (1989) at ODP Site 646. Poore *et al.* (2006) also reported strong NCW production between 5.2 and 2.7 Ma and Bohrmann *et al.* (1990) observed strong NCW flow between 4.8 and 3.2 Ma. Even though we interpret the NCW flow as strong, the two branches of the NCW flow shallowed and thus shifted upslope to the NE (Figs. 6.7d and 7.7e).

We again observe a strong NCW flow at the Eirik Drift accompanied by a warm climate, the Pliocene warm period, which lasted until ~3.5 Ma, (Ravelo, 2010; Zachos *et al.*, 2001). We suggest that the Eirik Drift to still have lain within the main NCW flow produced in the complete Nordic Sea region. A major change to the period of unit SUIII is the observed shallowing of the deep current system (Fig. 6.8f). Following the closure of the Panama Isthmus (Burton *et al.*, 1997) the formation of LSW commenced and was entrained into NCW

(Poore *et al.*, 2006). This is documented by the onset of Drift building at the Gloria Drift at ~4.5 Ma (Wold, 1994). The entrainment of Labrador Sea Water (LSW) to both overflows, DSOW and ISOW, is supposed to have changed the density structure of the NCW and therefore yield a shallowed NCW flow at the Eirik Drift (Fig. 6.8f). The NCW flow remained strong during the transition to Pliocene cooling at ~3.2 Ma until 2.5 Ma.

6.6.4 Unit SUI (2.5-0 Ma)

In the following time intervals (2.5-1.4 Ma; 1.4-0.8 Ma; <0.8 Ma) the depocenter in the north separated into two (Figs 6.7f-h). The western depocenter infilled the eastern topographic low of the basal horizon and shifted southwards (Figs. 6.7f-h). The eastern depocenter remained on top of the topographic high of the basal horizon (Figs. 6.7f-h). Low deposition is observed in the south and surrounding the two depocenters, with less deposition found around the upper, eastern depocenter. Therefore, the suggested path of the deep current appeared to have remained almost unmodified with a gradual shift upslope (Figs. 6.7f-h), but with changes in intensity of the two branches. For 7.5-4.5 Ma we observed a higher intensity of the deeper flow but now the stronger erosion is found at the upper branch, indicating a more intense upper NCW flow branch compared to the deeper. Converging reflectors but no reflector truncations are observed at the NCW core locations (Figs. 6.3-6.5), and therefore the erosion at the current core and thus the NCW flow is interpreted as less intense. This indicates that the NCW flow not only shallowed but also weakened. Our interpretation is supported by Arthur *et al.* (1989), Kaminski *et al.* (1989) and Hunter *et al.* (2007b) who also observed a decrease in current intensity and an upslope migration of the drift crests at the Eirik Drift after 2.5 Ma.
The observed shallowing and weakening of the NCW flow system at the Eirik Drift is accompanied by Pliocene cooling with intensification of Northern Hemisphere Glaciation (NHG). The onset of NHG intensification is documented at ODP 646 via horizon R1 (2.5 Ma) with the onset of ice-rafting (Arthur *et al.*, 1989; Cremer *et al.*, 1989). Pronounced ice-sheet expansion in the Northern Hemisphere is reported for 2.75 Ma (Ravelo, 2010) and 2.6 Ma (Bohrmann *et al.*, 1990; Wolf-Welling *et al.*, 1996).

We propose that the sea ice cover of the Nordic Seas again shifted the NCW formation regions towards the south and that the Eirik Drift only experience the influence of weaker branch of the NCW circulation. The main part of NCW flow is suggested to have been dense and to have flowed at deeper depth contours directly towards the south (Fig. 6.8g). With an enhanced ice extent not only covering the Greenland Sea but also the northern part of the Norwegian Sea, the NCW formation region would have been shifted to the SE Norwegian Sea. In that case, the leakage through the Denmark Strait would have stopped and the two branches observed of NCW flow observed at the Eirik Drift comprised ISOW (lower) and LSW (upper). During cold phases enhanced deep-water formation would have taken place in the Labrador Sea south of the sill. The distinct drift growths at the Gloria and Snorri Drifts during this time interval (Wold, 1994) and also the enhanced erosion of the upper branch compared to the lower branch at the Eirik Drift is suggested to have been forced by an enhanced LSW circulation during this time interval.

6.7 Conclusion

A detailed model for the paleocirculation at the Eirik Drift was developed by analyzing the morphology of prominent horizons and the location and orientation of erosional and depositional centers (Fig. 6.7). The local changes derived for the Eirik Drift were linked to changes in North Atlantic climate (Fig. 6.8).
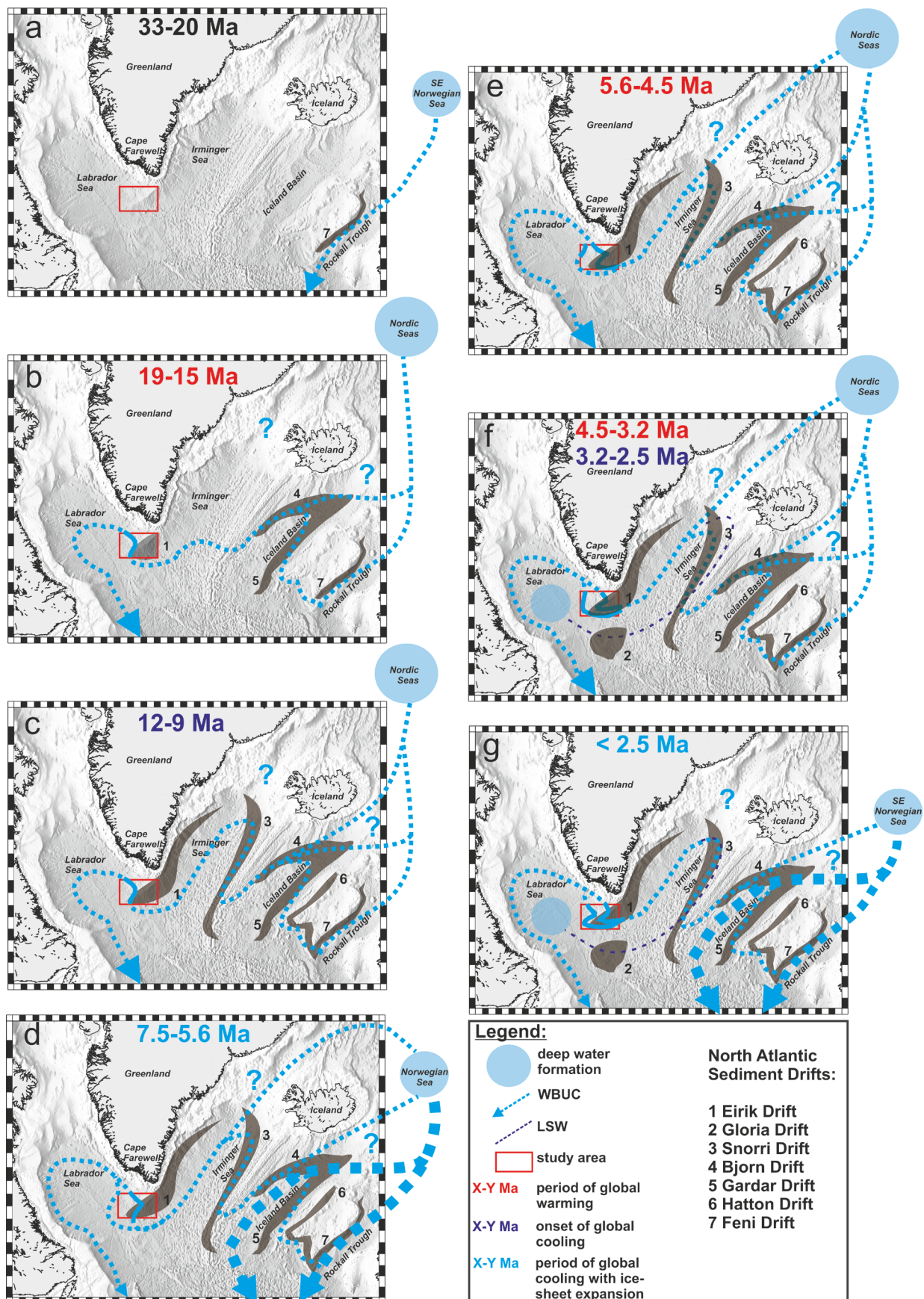
Figure 6.8. Model for the deep paleocirculation and location of NCW formation regions for the North Atlantic invoking our results from the Eirik Drift. Location of the North Atlantic sediment drifts modified after Faugères *et al.* (1999). (a) 33-20 Ma. (b) 19-15 Ma (c) 12-9 Ma. (d) 7.5-5.6 Ma. (e) 5.6-4.5 Ma. (f) 4.5-2.5 Ma (g) < 2.5 Ma.

1. The export of NCW flow was controlled by the subsidence history of the GSR rather than by the climate conditions (Wright and Miller, 1996). For ~35-33 Ma Davies *et al.* (2001) suggested the onset of NCW overflow at the Faroe-Shetland-Channel to the Rockall Trough region. This southward-directed NCW flow is only documented in the Feni Drift and therefore is interpreted to have continued its southward-directed flow in the eastern North Atlantic (Fig. 6.8a). The Eirik Drift was found in a tranquil environment until ~19 Ma.

2. The onset of noteworthy deep circulation at the Eirik Drift took place at ~19 Ma. It followed the formation of the Faroe Conduit (Stoker *et al.*, 2005).

3. Strong NCW flow was observed between 19 and 15 Ma during Miocene warming (Fig. 6.8b).

4. NCW overflow was inhibited between ~15-12.5 Ma following the Mid Miocene Climatic Optimum.

5. A renewed onset of strong NCW flow is observed between 12 and 9 Ma following the Miocene transition to a colder climate and the subsidence of the GSR (Fig. 6.8c).

6. Presumably short-term climate variations and temperature fluctuations with depleted/enhanced NCW production and flow formed reflector doublet R3/R4 at 7.5/8.1 Ma.

7. We observe a weak WBUC for the period 7.5-5.6 Ma during Miocene cooling (~13-6 Ma). The Miocene cooling may have yield an enhanced ice cover of the Nordic Seas between ~7.5 and 6.2 Ma. For the first time the separation of NCW flow into two branches in two different water depths is observed. These are interpreted to represent DSOW (lower NCW) and ISOW (upper NCW) (Fig. 6.8d).

8. An intense NCW flow is observed during the early Pliocene warm period and the beginning of Pliocene cooling between 5.6 and 2.5 Ma (Figs. 6.8e and f). The NCW flow system shallows after 4.5 Ma, presumably due to the influence of LSW on the density structure of the overflows (Fig. 6.8f).

9. With the intensification of Northern Hemisphere Glaciation a weakening of the deep current system is observed after 2.5 Ma (Fig. 6.8g).

All in all we observed strong NCW flow during warm climates and at the beginning of cooling phases and weak NCW flow during enhanced cooling phases accompanied by NHG. This is in conflict with our expectations of strong NCW production and flow during cold climate and weak NCW production and flow during warm phases. We conclude that the NCW formation regions shifted southwards during phases with enhanced ice cover over the Nordic Seas and that the main NCW flow during these cold phases does not affect the Eirik Drift. We suggest a dense, deep southward-directed NCW flow during these cold phases, whilst the residual northern North Atlantic is just affected by weaker branches of the deep circulation system. During warmer phases, when the Nordic Seas showed a significant smaller ice cover, the NCW formation regions shifted back north and the flow pattern is more similar to the modern one with overflows over the GSR and a main NCW flow recirculating via the outer Labrador Sea (Eirik Drift). Therefore, the NCW flow is observed intensified at the Eirik Drift region during warm phases and at the beginning of cooling with no observed ice cover of the Nordic Sea region and weakened during cool climate with enhanced ice extent.

Our investigation helped to shed more light on the complex interplay of changes in ocean currents, climate and tectonics in the northern North Atlantic. Still, further details are needed to decipher the whole complex system. More high-resolution seismic lines covering a larger study area as well as additional deep drilling at mound A to gather ground truth information are needed to advance our knowledge.

6.8 Acknowledgements

6.9 References

Arthur, M.A., Srivastava, S.P., Kaminski, M., Jarrard, R.D., Osler, J., 1989. Seismic Stratigraphy and History of Deep Circulation and Sediment Drift Development in Baffin Bay and the Labrador Sea. In: Srivastava, S.P., Arthur, M., Clement, B., et al. (Eds.), Scientific Results. Ocean Drilling Program, College Station, TX, USA, 957-988.

Bohrmann, G., Henrich, R., Thiede, J., 1990. Miocene to Quaternary Paleoceanography in the Northern North Atlantic: Variability in Carbonate and Biogenic Opal Accumulation. In: Bleil, U., Thiede, J. (Eds.), Geological History of the Polar Oceans: Arctic versus Antarctic. Springer Netherlands, 647-675.

Burton, K.W., Ling, H.-F., O'Nions, R.K., 1997. Closure of the Central American Isthmus and its effect on deep-water formation in the North Atlantic. Nature 386, 382-385.

Chalmers, J.A., Pulvertaft, T.C.R., 2001. Development of the continental margins of the Labrador Sea – a review. In: Wilson, R.C.L., Whitmarsh, R.B., Froitzheim, N. (Eds.), Non-volcanic rifting of the continental margins: a comparison of evidence from land and sea. Geological Society London, UK, 77-105.

Channell, J.E.T., Sato, T., Kanamatsu, T., Stein, R., Alvarez Zarikian, C.A., 2010. Expedition 303/306 synthesis: North Atlantic climate. In: Channell, J.E.T., Kanamatsu, T., Sato, T., Stein, R., Alvarez Zarikian, C.A., Malone, M.J., Scientists, a.t.E. (Eds.), Proceedings of the Integrated Ocean Drilling Program. Integrated Ocean Drilling Program, College Station, TX, USA.

Cremer, M., Maillet, N., Latouche, C., 1989. Analysis of sedimentary facies and clay mineralogy of the Neogene-Quaternary sediments in ODP Site 646, Labrador Sea. In: Srivastava, S.P., Arthur, M., Clement, B. (Eds.), Proceedings of the Ocean Drilling Program, Scientific Results. Ocean Drilling Program, College Station, TX, USA, 71-80.

Davies, R., Cartright, J., Pike, J., Line, C., 2001. Early Oligocene initiation of North Atlantic Deep Water formation. Nature 410, 917-920.

Dickson, R.R., Brown, J., 1994. The production of North Atlantic Deep Water: Sources, rates, and pathways. Journal of Geophysical Research 99 (C6), 12319-12341.

Faugères, J.C., Stow, D.A.V., 2008. Contourite Drifts: Nature, Evolution and Controls. In: Rebesco, M. and Camerlenghi, A. (Eds.), Contourites. Elsevier, Amsterdam, the Netherlands, 259-288.

Faugères, J.C., Stow, D.A.V., Imbert, P., Viana, A.R., 1999. Seismic Features Diagnostic of Contourite Drifts. Marine Geology 162, 1-38.

Haug, G.H., Tiedemann, R., 1998. Effect of the formation of the Isthmus of Panama on Atlantic Ocean thermohaline circulation. Nature 393, 673-676.

Heezen, B.C., Hollister, C.D., Ruddiman, W.F., 1966. Shaping the continental rise by deep geostrophic contour currents. Science 152, 502-508.

Howe, J.A., Stoker, M.S., Woolfe, K.J., 2001. Deep-marine seabed erosion and gravel lags in the northwestern Rockall Trough, North Atlantic Ocean. Geological Society London Journal 158, 427-438.

Hunter, S., Wilkinson, D., Louarn, E., McCave, I.N., Rohling, E., Stow, D.A.V., Bacon, S., 2007a. Deep western boundary current dynamics and associated sedimentation on the Eirik Drift, Southern Greenland Margin. Deep-Sea research I 54, 2036-2066.

Hunter, S., Wilkinson, D., Stanford, J., Stow, D.A.V., Bacon, S., Akhmetzhanov, A.M., Kenyon, N.H., 2007b. The Eirik Drift: A long-term barometer of North Atlantic deepwater flux south of Cape Farewell, Greenland. In: Viana, A.R., Rebesco, M. (Eds.), Economic and Palaeoceanographic Significance of Contourite Deposits. Geological Society, London, UK, 245-263.

Kaminski, M.A., Gradstein, F.M., Scott, D.B., Mackinnon, K.D., 1989. Neogene Benthic Foraminifer Biostratigraphy and Deep-Water History of Sites 645, 646, and 647, Baffin Bay and Labrador Sea. In: Srivastava, S.P., Arthur, M., Clement, B., et al. (Eds.), Scientific Results. Ocean Drilling Program, College Station, TX, USA, 731-756.

Kuhlbrodt, T., Griesel, A., Montoya, M., Levermann, A., Hofmann, M., Rahmstorf, S., 2007. On the driving processes of the Atlantic meridional overturning circulation. Reviews of Geophysics 45 (2), doi:10.1029/2004RG000166.

Le Pichon, X., Hyndman, R.D., Pautot, G., 1971. Geophysical Study of the Opening of the Labrador Sea. Journal of Geophysical Research 76 (20), 4724-4743.

Mikolajewicz, U., Crowley, T.J., 1997. Response of a coupled ocean / energy balance model to restricted flow through the central American isthmus. Paleoceanography 12 (3), 429-441.

Miller, K.G., Tucholke, B.E., 1983. Development of Cenozoic Abyssal Circulation south of the Greenland-Scotland Ridge. In: Bott, M.H.P., Saxov, S., Talwani, M., Thiede, J. (Eds.), Structures and Development of the Greenland-Scotland Ridge - New Methods and Concepts. Plenum Press, New York and London, 549-589.

Miller, K.G., Wright, J.D., Katz, M.E., Wade, B.S., Browning, J.V., Cramer, B.S., Rosenthal, Y., 2009. Climate threshold at the Eocene-Oligocene transition: Antarctic ice sheet influence on ocean circulation. In: Koeberl, C., Montanari, A. (Eds.), The Late Eocene Earth-Hothouse, Icehouse, and Impacts. Geological Society of America Special Paper, USA, 169-178.

Müller-Michaelis, A., Uenzelmann-Neben, G., Stein, R., 2013. A revised Early Miocene age for the instigation of the Eirik Drift, offshore southern Greenland: Evidence from high-resolution seismic reflection data. Marine Geology, doi:10.1016/j.margeo.2013.04.012.

Nielsen, T., Knutz, P.C., Kuijpers, 2008. Seismic Expression of Contourite Depositional Systems. In: Rebesco, M. and Camerlenghi, A. (Eds.), Contourites. Amsterdam, the Netherlands, Elsevier, 301-321.

Pickart, R.S., 1992. Water mass components of the North Atlantic Deep Western boundary current. Deep Sea Research 39, 1553-1572.

Poore, H.R., Samworth, R., White, N.J., Jones, S.M., McCave, I.N., 2006. Neogene overflow of Northern Component Water at the Greenland-Scotland Ridge. Geochemistry, Geophysics, Geosystems 7 (6), Q06010.

Quadfasel, D., Käse, R., 2007. Present-Day Manifestation of the Nordic Seas Overflows. In: Schmittner, A., Chiang, J.C.H., Hemming, S.R. (Eds.), Ocean Circulation - Mechanisms and Impacts. American Geophysical Union, Washington, DC, USA, 75-89.

Ravelo, A.C., 2010. Palaeoclimate: Warmth and glaciation. Nature GeoScience 3 (10), 672-674.

Schmitz, W.J., Jr., 1996. On the World Ocean Circulation: Volume I Some Global Features / North Atlantic Circulation. Technical Report. Woods Hole Oceanographic Institution, Woods Hole, MA, USA.

Shipboard Scientific Party, 1987. Site 646. In: Srivastava, S.P., Arthur, M., Clement, B., et al. (Eds.), Init. Repts. Ocean Drilling Program, College Station, TX, US, 419-674.

Smethie, W.R.J., Fine, R.A., 2001. Rates of North Atlantic Deep Water formation calculated from chlorofluorocarbon inventories. Deep Sea Research I 48, 189-215.

Smith, W. H.S., Sandwell, D.T., 1997. Global Sea Floor Topography from Satellite Altimetry and Ship Depth Soundings. Science 277, 1956-1962.

Srivastava, S.P., Arthur, M.A., 1989. Tectonic Evolution of the Labrador Sea and Baffin Bay: Constraints Imposed by Regional Geophysics and Drilling Results from Leg 105. In: Srivastava, S.P., Arthur, M., Clement, B., et al. (Eds.), Scientific Results. Ocean Drilling Program, College Station, TX, USA, 989-1009.

Srivastava, S.P., Roest, W.R., 1999. Extent of oceanic crust in the Labrador Sea. Marine and Petroleum Geology 16 (1), 65-84.

Stoker, M.S., Hoult, R.J., Nielsen, T., Hjelstuen, B.O., Laberg, J.S., Shannon, P.M., Praeg, D., Mathiesen, A., van Weering, T.C.E., McDonnell, A., 2005. Sedimentary and oceanographic responses to early Neogene compression on the NW European margin. Marine and Petroleum Geology 22 (9–10), 1031-1044.

Stow, D.A.V., Faugères, J.-C., Howe, J.A., Pudsey, C.J., Viana, A.R., 2002. Bottom currents, contourites and deep-sea sediment drifts: current state-of-the-art. In: Stow, D.A.V., Pudsey, C.J., Howe, J.A., Faugères, J.-C., Viana, A.R. (Eds.), Deep-water contourite systems: Modern drifts and ancient series. Geological Society of London, London, UK, 7-20.

Van Aken, H.M., 2007. The Oceanic Thermohaline Circulation. Springer, New York, USA.

van Weering, T., Stoker, M., Rebesco, M., 2008. High-Latitude Contourites. In: Rebesco, M. and Camerlenghi, A. (Eds.), Contourites. Elsevier, Amsterdam, the Netherlands, 457-489.

Via, R.K., Thomas, D.J., 2006. Evolution of Atlantic thermohaline circulation: Early Oligocene onset of deep-water production in the North Atlantic. Geology 34, 441–444.

Winkler, A., Wolf-Welling, T., Stattegger, K., Thiede, J., 2002. Clay mineral sedimentation in high northern latitude deep-sea basins since the Middle Miocene (ODP Leg 151, NAAG). International Journal of Earth Sciences 91 (1), 133-148.

Wold, C.N., 1994. Cenozoic Sediment Accumulation on Drifts in the Northern North Atlantic. Paleoceanography 9 (6), 917-941.

Wolf-Welling, T.C.W., Cremer, M., O'Connell, S., Winkler, A., Thiede, J., 1996. Cenozonic Arctic Gateway Paleoclimate Variability: Indications from changes in coarse-fraction compositions. In: Thiede, J., Myhre, A.M., Firth, J.V., Johnson, G.L., Ruddiman, W.F. (Eds.), Proceedings of the Ocean Drilling Program - Scientific Results. Ocean Drilling Program, College Station, TX, USA, 515-567.

Woodruff, F., Savin, S., 1989. Miocene deepwater oceanography. Palaeogeography 4, 87-140.

Wright, J.D., 1998. Role of the Greenland-Scotland Ridge in Neogene climate changes. In: Crowley, T.J., Burke, K. (Eds.), Tectonic Boundary Conditions for Climate Reconstructions. Oxford University Press, Oxford, UK, 192-211.

Wright, J.D., Miller, K.G., 1996. Control of North Atlantic Deep Water Circulation by the Greenland-Scotland Ridge. Paleoceanography 11 (2), 157-170.

Wright, J.D., Miller, K.G., Fairbanks, R.G., 1992. Early and middle Miocene stable isotopes: implications for deepwater circulation and climate. Paleoceanography 7, 357-389.

Zachos, J.C., Pagani, M., Sloan, L., Thomas, E., Billups, K., 2001. Trends, Rhythms, and Aberrations in Global Climate 65 Ma to Present. Science 292, 686-693.

7 Third paper: Seismic Oceanography at the Eirik Drift

7.1 Abstract

For the first time the method of seismic oceanography was applied to identify fine structure of a water mass in greater depths (> 1500 m). The pathway of the upper high-velocity Western Boundary Undercurrent (WBUC) branch was tracked over the Eirik Drift, 200 km south of Greenland at seafloor depths between ~2200 and 3000 m. It appears as an upward convex structure attached to the slope with a transparent, i.e. well mixed, core surrounded by higher amplitude reflections. These reflect gradients and fine structure. Fine structure is a result of enhanced mixing processes, presumably due to entrainment of surrounding water of less momentum by the intensified deep current core. We show that this new information about structure and pathways of the WBUC could not have been gained by conventional oceanographic measurements alone.

7.2 Introduction

The North Atlantic Western Boundary Undercurrent (WBUC; also referred to as Deep Western Boundary Current (DWBC)) is a deep (~1900-3000 m), equator ward contour current along the western continental slope. It is fed by Labrador Sea Water (LSW) and the overflow waters of the Nordic Seas, Iceland Scotland Overflow Water (ISOW) and Denmark Strait Overflow Water (DSOW), and represents the main component of the deep branch of the North Atlantic Thermohaline Circulation (THC) (e.g., Dickson and Brown, 1994; Schmitz, 1996; Stanford *et al.*, 2011). The THC impacts the world's climate, and therefore, many oceanographic (e.g., Holliday *et al.*, 2009; Rhein, 1994; Stanford *et al.*, 2011) and paleooceanographic (e.g., Hillaire-Marcel *et al.*, 2011; Hunter *et al.*, 2007; Müller-Michaelis and Uenzelmann-Neben, 2013 (in revision)) studies have concentrated on studying structure, dynamics and properties of the WBUC in the vicinity of Cape Farewell (Fig. 7.1). The WBUC (location, intensity) is believed to be an important indicator for climate changes, and since the Eirik Drift is located closely downstream (Fig. 7.1) of the WBUC formation region it appears as a well-suited location to detect changes in the complex WBUC system. We aim for a better understanding of the structure and pathway of the upper WBUC core at the Eirik Drift (Fig. 7.1) and hypothesize that the complex topography of the drift influences both, the pathway as well as the structure of the WBUC core.

Holbrook *et al.* (2003) established the idea of using seismic reflection data for oceanographic research purposes as a new promising method for ocean investigations. The high spatial resolution of the seismic reflection data bears the ability to create detailed images of thermohaline structure in the ocean compared to traditional oceanographic measurements (e.g., Holbrook *et al.*, 2003; Ruddick *et al.*, 2009). Several seismic oceanography studies followed, which focused on studies within the upper ocean (< 1500 m depth) (e.g., Biescas *et al.*, 2008; Buffett *et al.*, 2009; Krahmann *et al.*, 2008; Nandi *et al.*, 2004; Pinheiro *et al.*, 2010). We analyzed high-resolution seismic reflection data along with discrete CTD stations aiming for the first seismic oceanography study of deep-water circulation in water depths > 1500 m. This study will show that tracking the high-velocity core of the WBUC at the Eirik Drift (Fig. 7.1) and imaging its pathway, morphology and structure in a high lateral resolution by using seismic data represents an important supplement for the conventional, discrete oceanographic measurements.

7.3 Data and Methods

The data available was gathered to study the sedimentary structure of the Eirik Drift. In 2009, ~2000 km of high-resolution multichannel seismic reflection data were collected in this region during RV Maria S. Merian cruise MSM12/2 (Fig. 7.1). The seismic sources were four GI-guns© with a volume of about 1.4 l each fired every 10 s and the sample rate was 1 ms resulting in a vertical resolution of 5 m. 240 hydrophone channels mounted to a 3000 m streamer received the data. Eight CTD casts were conducted during MSM12/2 cruise for calibration of the hydro acoustic instruments (Fig 7.1). Additionally, we used a CTD cross-section at the entrance of the Labrador Sea of the following cruise MSM12/3 (CTDs 8-12; by courtesy of Rhein (2011)), which lies east of our study area (Fig. 7.1).
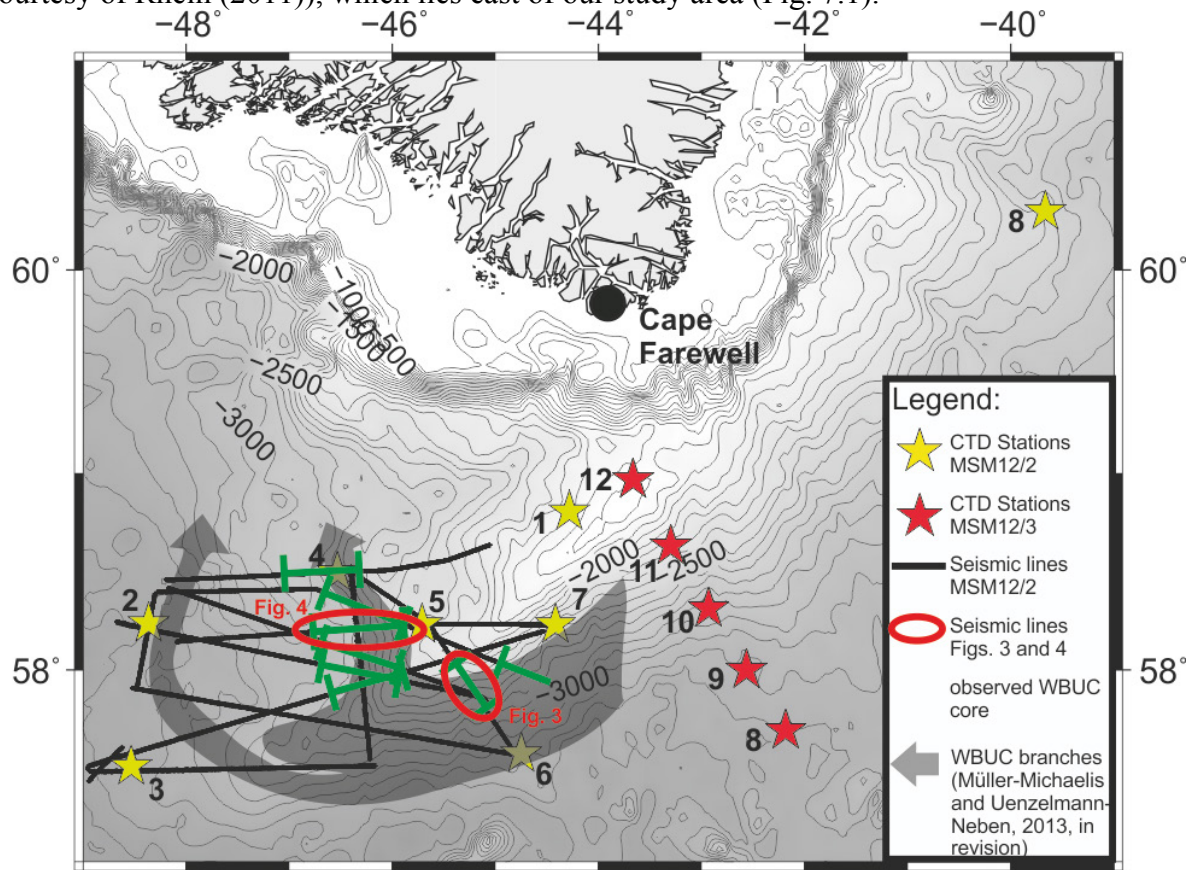
Figure 7.1. Satellite bathymetric map (Smith and Sandwell, 1997) including the locations of the seismic lines and CTD stations. Branches of the Western Boundary Undercurrent (WBUC) at the study area for the period < 800000 years after Müller-Michaelis and Uenzelmann-Neben (2013 (in revision)). The location of the observed WBUC core in the seismic data is indicated by the green lines. The seismic sections shown in Fig. 7.3 and 7.4 are indicated by the red circles.

7.3.1 Seismic data processing

The conventional processing steps of geometry definition, zero-phase filtering and static shift were applied to the shot-sorted seismic reflection data. The low amplitudes of reflections in the water column compared to those of the seafloor and the increasing loss of energy in greater depths are a challenging problem in the seismic oceanography data processing close to the seafloor. To preserve the amplitudes in the water column, the seafloor reflection was picked and the amplitudes below were reduced to approximately the amplitudes of the water column. A median filter was used to suppress the direct wave energy. The seismic data then was CDP sorted, normal move-out (NMO) correction was applied and the data was stacked. A weighted mean of the sound velocity profiles of the MSM12/2 CTD stations was used for

the NMO correction, which is an improvement over using a fixed sound velocity value (Fortin and Holbrook, 2009). A lateral running mix to increase the signal to noise ratio of the data was applied as well as a gain to the profile for display to visualize the thermohaline reflections.

7.3.2 CTD data processing

The CTD data were depth-time converted with the sound velocity calculated after Chen and Millero (1977) and resampled to the seismic sample rate of 1 ms. The reflectivity series for each CTD station was calculated using the acoustic impedance contrast (Yilmaz, 2001). The synthetic seismograms were computed by convolution of the reflectivity series with a 70 Hz Ricker wavelet to match the seismic data. The synthetic seismograms were then converted back to the depth domain to display them matching to the temperature-depth profiles of the CTD casts (Fig. 7.2a).

7.4 Results and Discussion

Based on the analysis of the sedimentary sequences at the Eirik Drift Müller-Michaelis and Uenzelmann-Neben (2013 (in revision)) suggested a pathway for the upper WBUC core in water depths of 2000-2800 m for the past 800000 years. As we aimed to track the upper core of the WBUC, we used the CTD stations along this. These are listed in Table 7.1, where the order of the stations is resorted following their location, i.e. downstream along the pathways of the suggested upper WBUC core (Fig. 7.1).

Acoustic impedance is more sensitive (~2 orders of magnitude) to temperature (T) than to salinity (S), which allows us to interpret seismic oceanography images in terms of T (e.g., Buffett *et al.*, 2009; Nandi *et al.*, 2004; Ruddick *et al.*, 2009). A contour plot of the cross-section of the MSM12/3 CTD stations indicates the T structure of the deep-water entering the Labrador Sea upstream of the Eirik Drift (Figs. 7.1 and 7.2b). In physical oceanography the WBUC and its components are defined by specific density or T levels for the interpretation of hydrographic sections like this. The choice of these parameters can significantly influence the result. Saunders (2001) defined the WBUC with T < 3° C and the boundary between the upper WBUC (ISOW) and the lower WBUC (DSOW) at 2° C. Following this definition (<3° C) the CTD section shows the WBUC attached to the slope at 1500 m depth extending towards the ocean basin in depths > 2500 m (Fig. 7.2b). Its cold, deeper core (DSOW; < 2° C) is found below 2800 m depth concentrated at the slope (Fig. 7.2b). The structure at the slope is unfortunately not well resolved due to the large staircases resulting from the distance (~41-42 km) between the CTD stations (Fig. 7.2b).

The temperature-depth profiles (Fig. 7.2a) of the CTDs MSM12/2 #4, #5 and #7 show a similar pattern: A homogenous bottom layer (T ~2° C) of different thickness is observed (Fig. 7.2a). The gradient above the bottom layer is strongest, i.e. it has the least vertical extent, in the upstream CTD cast and weakens, i.e. vertical extent of the gradient increases, downstream from CTD #7 to #5 to #4 (Fig. 7.2a; Table 7.1). Above the gradient a section of fine structure is observed, which extends up to ~2000 m, where pronounced intrusions mark the top of the section of enhanced T variability (Fig. 7.2a; Table 7.1). The T profiles then continue upward to 1500 m depth with an almost linear increase (Fig. 7.2a).

The bottom layers are homogenous, i.e. these are well mixed. The strong T gradients indicate the difference between the well-mixed bottom layer and above lying water. The fine structures observed above denote mixing processes. As the CTD locations lie approximately along the flow axis of the upper core of the WBUC suggested by Müller-Michaelis and Uenzelmann-Neben (2013 (in revision)) (Fig. 7.1) we interpret the homogenous bottom layers as an intensified, well mixed contour current core of the WBUC at the Eirik Drift. Its T of ~2° C represents the boundary between the upper and the lower WBUC core. The increased T
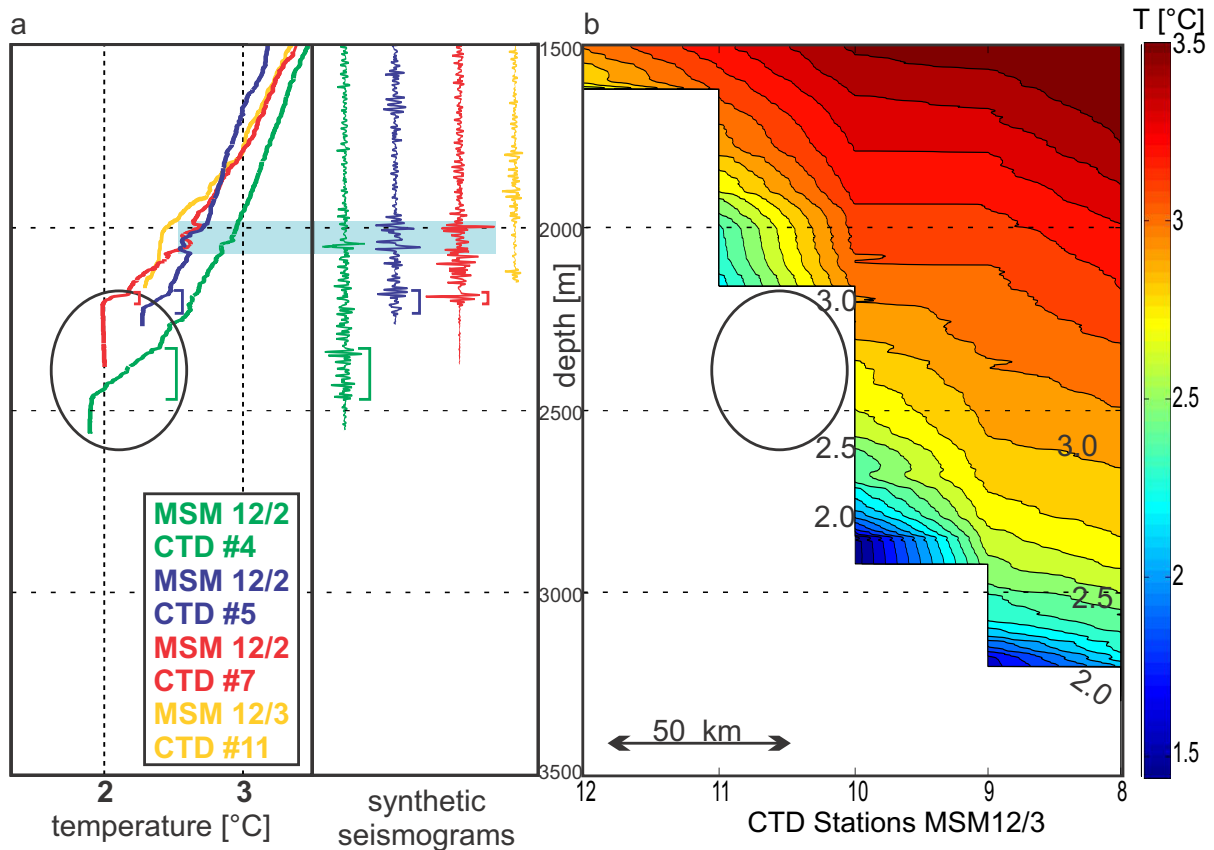
Figure 7.2. (a) Temperature vs. depth (> 1500 m) profiles and synthetic seismograms of the CTD casts as listed in Table 7.1. The brackets indicate the vertical extent of the gradient above the mixed bottom layer, which represents the lower boundary of the increased reflectivity in the synthetic seismograms. The colors are according to each CTD cast. The light blue box indicates intrusions in the temperature profiles at the top of the increased reflectivity in the synthetic seismograms at ~2000 m depth. (b) Contour plot of the temperature of the MSM12/3 CTD stations 8-12. MSM12/3 CTD data by courtesy of Rhein (2011).
The black circle indicates the depth of the boundary mixed layer in the CTD profiles.

Table 7.1.

Analyzed CTD stations along the path downstream of the upper core of the WBUC

Cruise- No.	CTD	Location	Date of cast	Depth [m]	TWT [s]	BL [m]	T[°C]	refl. depth [m]
MSM12/3	#11	Entrance LS	2009/07/18	2160	2.92	-	-	-
MSM12/2	#07	SE flank	2009/07/07	2370	3.20	180	1.98	2190-2000
MSM12/2	#05	Drift crest	2009/07/02	2260	3.05	50	2.30	2210-1950
MSM12/2	#04	NW flank	2009/07/02	2565	3.47	105	1.93	2460-2030

CTD, Conductivity-Temperature-Depth; TWT, two-way-travel time; BL, boundary layer thickness; T, boundary layer temperature; refl. depth, depth of increased reflectivity; MSM, research vessel Maria S. Merian; LS, Labrador Sea.

variability depicted by the fine structure (Fig. 7.2a) reflects enhanced mixing processes at the upper boundary of this core and is suggested to result at least partly from entrainment of ambient waters of less momentum to the intensified WBUC core along its pathway. The observed downstream weakening of the gradient above the bottom mixed layer may result from the persistent entrainment to the core, which erodes the gradient step by step. Nevertheless, fine structures and intrusions can also reflect pure thermohaline driven mixing processes.

The sections of strong T gradients and fine structure of the CTD casts are reflected in the synthetic seismograms as sections of enhanced reflectivity (Fig. 7.2a; Table 7.1). This is in agreement to the findings of Nandi *et al.* (2004) who stated that T differences of ~0.2° C over a vertical extent of 5-10 m can generate high amplitude reflections within seismic oceanography profiles. The vertical resolution corresponds to 1/4 wavelength of the seismic signal and thus depends on the seismic velocity in seawater (~1480 m/s) and the dominant frequency of the seismic signal (70 Hz in our data). From this it follows that layer thicknesses of > 5 m can be resolved by our data. Therefore, we are confident that we can resolve the structure of the upper WBUC core even in depths > 1500 m, especially in the upstream parts at the SE flank of the drift, where the gradients and fine structure are better developed (MSM12/2 CTD #7; Fig. 7.2a) than downstream (MSM12/2 CTD #4).
The described pattern of the T profiles, homogenous bottom layer, gradient and enhanced fine structure, is not found in the data of CTD MSM12/3 #11, which shows no strong T variability (Fig. 7.2a; Table 7.1). We suggest that the differences seen in the T profiles in thicknesses of bottom mixed layer and high variable zone above and non-occurrence of these features are a result of the sampling location, i.e. within the center, the sides or outside of the WBUC core as well as upstream or downstream of the WBUC flow. Based on the CTD location with regard to the suggested WBUC pathway (Fig. 7.1) (Müller-Michaelis and Uenzelmann-Neben, 2013 (in revision)) and the different T trend (Fig. 7.2a) we assume that the CTD station MSM12/3 #11 lies above the seafloor depth of the upper WBUC core.

To prove our assumptions, we will have a look at seismic profile AWI-20090010 (Fig. 7.3; for location see Fig. 7.1), which extends perpendicular to the depth contours of the SE flank of the Eirik Drift (Fig. 7.3). As the WBUC is a contour current, this section is assumed to lie perpendicular to the WBUC flow. This is important as the stationary assumption of seismic reflection data is violated by high current velocities, which we expect in the WBUC core, and this yields a decrease of reflection amplitude (Klaeschen *et al.*, 2009; Papenberg *et al.*, 2010). Cutting the WBUC perpendicularly minimizes this problem and in addition, the horizontal extent of the core will be captured correctly. We displayed the synthetic seismograms to the seismic section according to their TWT depths (Fig. 7.3). Please note that these are not the true CTD locations since the CTDs were not taken along the seismic profile (Fig. 7.1). Even though the synthetic seismograms are projected onto the seismic profile, the reflectivity is in good agreement with the seismic data showing that we are able to resolve the reflectivity of the fine structure within our seismic data even in depths > 1500 m. In our seismic data we observe an upward convex band of higher reflectivity attached to the SE slope of the Eirik Drift at seafloor depths between 3.0 to 3.8 s TWT (Fig. 7.3, CDP 3500-4750). The higher reflectivity band domes up from the seafloor and the reflections diverge at the center of the structure (Fig. 7.3). The area enclosed by this reflections and the seafloor appears rather transparent (Fig. 7.3, CDP 3600-4500). The transparent interior of the structure correlates with the non-reflective mixed layer (Fig. 7.3). The high reflections of the synthetic seismograms resulting from thermohaline fine structure correlate with the high reflection band in the seismic profile (Fig. 7.3). Thus, we assume that this structure is the upper core of the WBUC with its mixed interior surrounded by higher reflections representing fine structure due to mixing processes as suggested by the CTD data. However, depth and the vertical extent of both, bottom mixed layer and reflectivity zone does not match exactly (Fig. 7.3). This may result from the projection of the synthetic seismograms from the CTD locations onto the seismic profile. As mentioned above, the T structure in the CTD casts changes downstream as the gradient erodes due to enhanced mixing processes and therefore it is unlikely that the synthetic seismograms correlate perfectly with the seismic profile depicted as an example. Furthermore, the vertical extent of the bottom mixed layer and the reflectivity zone is also a matter of the location within the core. At the center of the WBUC core the bottom mixed layer as well as the reflectivity above have a larger thickness than at the sides
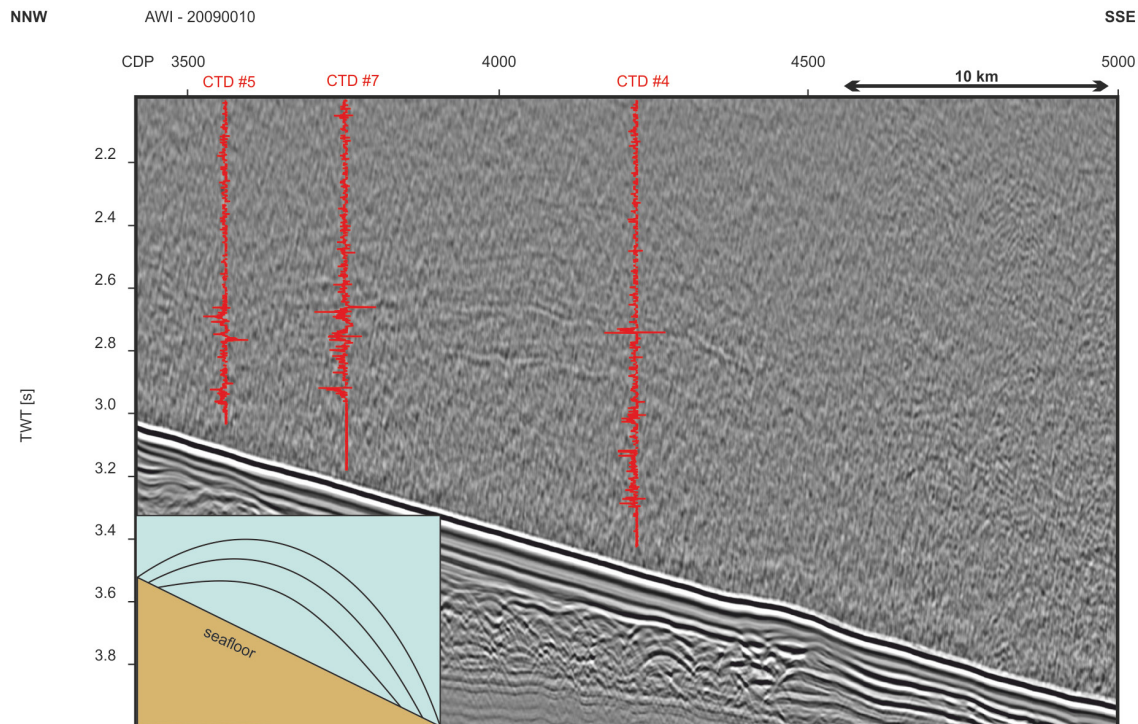
Figure 7.3. Seismic line AWI-20090010 (CDP 3400-5000; for location see Fig. 7.1). The synthetic seismograms calculated out of CTDs MSM12/2 #4, #5, and #7 are inserted according to the water depths of each CTD cast. Please note that these are not the true but projected locations of the MSM12/2 CTD casts. The box in the lower left corner depicts a schematic sketch of the structure observed in the seismic data at the SE flank of the Eirik Drift.

of the core (Fig. 7.3). Figure 7.3 proves not only that we can resolve fine structure in seismic data even in depths > 1500 m but also our assumption that the CTD profiles and hence the synthetic seismograms are biased by their location relative to the WBUC core. MSM12/3 #11 lies above the WBUC core as its seafloor depth is at 2.9 s TWT, which is upslope of our observed feature to the NNW (Fig. 7.3). The next deeper station in the MSM12/3 section is CTD #10 (Figs. 7.1 and 7.2b), which lies at a seafloor depth of 3.93 s TWT, i.e. downslope from our observed structure to the SSE (Fig. 7.3). Interpolation of the data between these two MSM12/3 stations misses out the WBUC core identified in the seismic section (Figs. 7.2b and 7.3) as it is located in the depth range between these two CTD stations and its horizontal extent of ~34 km is smaller than the CTD distance of ~41 km. The drawback of capturing such structures with classical oceanographic measurements is thus clearly demonstrated. Interpolation between discrete CTD stations can miss out certain depth structures or yield distortion of the truth, the horizontal as well as the vertical extent and thus the correct structure may not be resolved.

The WBUC core described above is attached to the slopes of the main Eirik Drift at seafloor depths between 3.0 and 3.8 s TWT (~2200-2800 m; Fig. 7.1 and Fig. 7.3 CDP 3500-4750) at the SE flank of the Eirik Drift and at seafloor depths between 3.1 and 4.15 s TWT at the NW flank (~ 2300-3000 m; Fig. 7.1 and Fig. 7.4 CDP 4200-7200). The change in direction from SW to NNW of the WBUC core is unfortunately not resolved by our seismic data (Fig. 7.1). The observed downslope shift of the WBUC core from the SE to the NW flank of ~200 m may result from an increased sediment load carried by the WBUC core at the NW flank due to enhanced erosion at the SE flank. Also the bathymetric structure may be responsible for this shift. The thickness of the WBUC core is about ~800 m at the SE flank and ~600 m at the NW flank and its domed structure is found flattened at the NW flank (Figs.
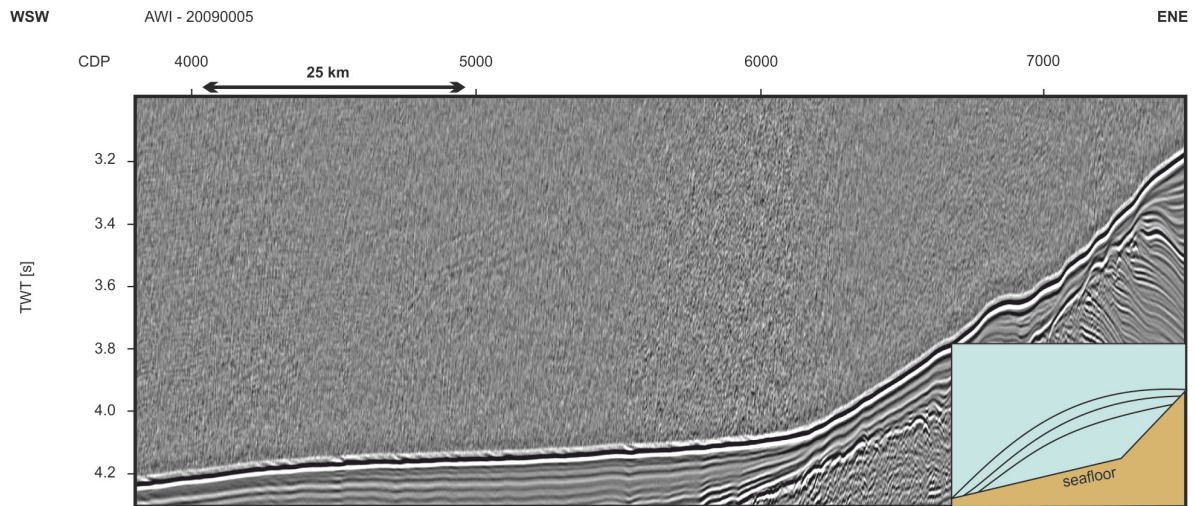
Figure 7.4. Seismic line AWI-20090005 (CDP 3800-7500; for location see Fig. 7.1). The box in the lower right corner depicts a schematic sketch of the structure observed in the seismic data at the NW flank of the Eirik Drift.

7.3 and 7.4). Also the lateral extent of the structure changes from ~35 km at the SE flank of the Eirik Drift to 70-90 km at the NW flank. The observed structural changes at the downstream and upstream flanks of the drift go along with a strong change in the slope of the flanks. The SE flank of the Eirik Drift shows an almost homogenous dip of ~1.3° from 2000 to 3500 m depth (Figs. 7.1 and 7.3). The NE flank, however, has a steep upper part (slope ~1.3-1.5°) and continues almost horizontally to the west (slope < 0.3°; Figs. 7.1 and 7.4). We can therefore conclude that the change in topography over the drift influences the shape of the WBUC core. It appears concentrated and domed at the homogenous, steep slope at the SE flank and broadens, flattens and maybe also deepens at the NW flank due to the influence of an almost horizontal part of the slope (Figs. 7.3 and 7.4).

The observed horizontal (35-90 km) and vertical (600-800 m) extent matches the mean values of 50-150 km horizontal extent and 300-800 m vertical extent of the WBUC modeled by Rhein (1994) for the area 65° N to 10° S, which supports our assumption that we image a core of the WBUC with our seismic data. The observed pathway of the upper WBUC core over the drift is in good agreement with that suggested by Müller-Michaelis and Uenzelmann-Neben (2013 (in revision)) (Fig. 7.1) for the time period < 800000 years based on a subsurface seismic study. Our interpretation of the seismic oceanography data thus concurs with the interpretation of the distribution of sedimentary strata and we can state that the observed WBUC core is guided by the topography. The structure of a concentrated WBUC core attached to the slope of the flank as observed in the seismic data (Figs. 7.3 and 7.4) cannot be observed in the MSM12/3 CTD section at the entrance of the Labrador Sea (Fig. 7.2b). Again, we can state that discrete CTD stations alone are not sufficient to resolve the structure of the WBUC core. Holliday *et al.* (2009) identified solely a colder, deeper WBUC core in depth > 2800 m in their hydrographic sections which is comparable to our observation in the MSM12/3 section for T < 2° C (Fig. 7.2b). Their additional velocity measurements, however, revealed the upper high velocity core at 2000 - 2700 m (Holliday *et al.,* 2009). This is in good agreement with our observation of the upper WBUC core at 2200 - 3000 m. Holliday *et al.* (2009) ascribed this upper high velocity core to consist of modified ISOW, which has also been suggested for the upper WBUC core during warm climate conditions by Müller-Michaelis and Uenzelmann-Neben (2013 (in revision)).

Indications for the deeper core of the WBUC were found in the CTD stations MSM12/3 #9, #10 and MSM12/2 #6 with a core depth of ~3250 m but not in CTDs MSM12/2 #2 and #3 (Fig. 7.1). The agreement in T and S indicates that the CTD stations

MSM12/2 #6 and MSM12/3 #9 and #10 captured the same, deep WBUC core with T ~1.5° C and S ~34.89 PSU. This is interpreted to represent the DSOW component of the WBUC, as DSOW is typically found at depths between 3000 and 3500 m with T < 1.5° C and S ~34.89 PSU (Dickson and Brown, 1994; Quadfasel and Käse, 2007). However, we cannot clearly image this deeper WBUC core in our seismic data. The reflectivity of the amplitudes for the expected deep WBUC core location is found to be weak, the amplitudes are hard to distinguish from the noisy surrounding and the deep WBUC core is not identifiable on all seismic lines. We assume, that the greater signal loss due to the increased depth of the deep WBUC core (> 3200 m) restricts the use of the seismic oceanography method here.

7.5 Conclusion

We were able to identify and track the upper core of the WBUC via the combination of CTD and seismic reflection data. It appears as a concentrated transparent seismic feature with a high reflectivity surrounding attached to the slope of the Eirik Drift at seafloor depths between 2200 and 3000 m. Its lateral and vertical extent changes with the dip of the seafloor slope from a concentrated domed core (35 km broad and 800 m thick) at the steep, homogenous SE drift flank to the flattened, broader core (70-90 km broad and 600 m thick) at the NW drift flank, where the slope changed significantly and provides an almost horizontal part (< 3° steep). The pathway of the upper WBUC core suggested by Müller-Michaelis and Uenzelmann-Neben (2013 (in revision)) for the period < 800000 years was confirmed by our observations. For the first time the seismic oceanography method was successfully applied to depths > 1500 m, but seems restricted in depths > 3000 m. This study revealed that seismic oceanography provides an important supplement to conventional oceanographic measurements as the small-scale structures of the deep-water masses cannot always be resolved properly by discrete CTD measurements due to their large distance.

7.6 Acknowledgements

7.7 References

Biescas, B., Sallarès, V., Pelegrí, J.L., Machín, F., Carbonell, R., Buffett, G., Dañobeitia, J.J., Calahorrano, A., 2008. Imaging meddy finestructure using multichannel seismic reflection data. Geophysical Research Letters 35.

Buffett, G.G., Biescas, B., Pelegrí, J.L., Machín, F., Sallarès, V., Carbonell, R., Klaeschen, D., Hobbs, R., 2009. Seismic reflection along the path of the Mediterranean Undercurrent. Continental Shelf Research 29 (15), 1848-1860.

Chen, C.-T., Millero, F.J., 1977. Speed of sound in seawater at high pressures. Journal of the Acoustic Society of America 62 (5), 1129-1135.

Dickson, R.R., Brown, J., 1994. The production of North Atlantic Deep Water: Sources, rates, and pathways. Journal of Geophysical Research 99 (C6), 12319-12341.

Fortin, W.F.J., Holbrook, W.S., 2009. Sound speed requirements for optimal imaging of seismic oceanographic data. Geophysical Research Letters 36.

Hillaire-Marcel, C., de Vernal, A., McKay, J., 2011. Foraminifer isotope study of the Pleistocene Labrador Sea, northwest North Atlantic (IODP Sites 1302/03 and 1305),

with emphasis on paleoceanographical differences between its "inner" and "outer" basins. Marine Geology 279 (1–4), 188-198.

Holbrook, W. S., Paramo, P., Pearse, S., Schmitt, R.W., 2003. Thermohaline Fine Structure in an Oceanographic Front from Seismic Reflection Profiling. Science, 301, 821-824.

Holliday, N.P., Bacon, S., Allen, J., McDonagh, E.L., 2009. Circulation and Transport in the Western Boundary Currents at Cape Farewell, Greenland, Journal of Physical Oceanography 39 (8), 1854-1870.

Hunter, S., Wilkinson, D., Louarn, E., McCave, I.N., Rohling, E., Stow, D.A.V., Bacon, S., 2007. Deep western boundary current dynamics and associated sedimentation on the Eirik Drift, Southern Greenland Margin. Deep-Sea research I 54, 2036-2066.

Klaeschen, D., R. W. Hobbs, G. Krahmann, C. Papenberg, and E. Vsemirnova (2009), Estimating movement of reflectors in the water column using seismic oceanography, Geophysical Research Letters 36.

Krahmann, G., Brandt, P., Klaeschen, D., Reston, T., 2008. Mid-depth internal wave energy off the Iberian Peninsula estimated from seismic reflection data, Journal of Geophysical Research C113.

Müller-Michaelis, A., Uenzelmann-Neben, G., 2013 (in revision). Development of the Western Boundary Undercurrent at the Eirik Drift related to changing climate since the early Miocene. Deep-Sea research I.

Nandi, P., Holbrook, W.S., Pearse, S., Paramo, P., Schmitt, R.W., 2004. Seismic reflection imaging of water mass boundaries in the Norwegian Sea. Geophysical Research Letters 31.

Papenberg, C., Klaeschen, D., Krahmann, G., Hobbs, R.W., 2010. Ocean temperature and salinity inverted from combined hydrographic and seismic data. Geophysical Research Letters 37.

Pinheiro, L.M., Song, H., Ruddick, B., Dubert, J., Ambar, I., Mustafa, K., Bezerra, R., 2010. Detailed 2-D imaging of the Mediterranean outflow and meddies off W Iberia from multichannel seismic data. Journal of Marine Systems 79, 89-100.

Quadfasel, D., Käse, R., 2007. Present-Day Manifestation of the Nordic Seas Overflows. In: Schmittner, A., Chiang, J.C.H., Hemming, S.R. (Eds.), Ocean Circulation - Mechanisms and Impacts, American Geophysical Union, Washington, DC, USA, 75-89.

Rhein, M., 1994. The Deep Western Boundary Current: tracers and velocities. Deep-Sea research I 41(2), 263-281.

Rhein, M., 2011. Strength of the Subpolar Gyre and the Formation of Deep Water. Rep., Institut für Meereskunde, Hamburg, Germany.

Ruddick, B., Song, H., Dong, C., Pinheiro, L., 2009. Water Column Seismic Images as Maps of Temperature Gradient. Oceanography 22 (1), 193-205.

Saunders, P. M., 2001. The dense northern overflows. In: Siedler, G., Church, J., Gould, W.J. (Eds.), Ocean Circulation and Climate: Observing and Modelling the Global Ocean, Academic Press, San Francisco CA, USA, 401-418.

Schmitz, W. J. Jr., 1996. On the World Ocean Circulation: Volume I Some Global Features / North Atlantic Circulation. Technical Report, Woods Hole Oceanographic Institution, Woods Hole, MA, USA.

Smith, W.H.S., Sandwell, D.T., 1997. Global Sea Floor Topography from Satellite Altimetry and Ship Depth Soundings. Science 277, 1956-1962.

Stanford, J.D., Rohling, E.J., Bacon, S., Holliday, N.P., 2011. A review of the deep and surface currents around Eirik Drift, south of Greenland: Comparison of the past with the present. Global and Planetary Change 79 (3–4), 244-254.

Tsuji, T., Noguchi, T., Niino, H., Matsuoka, T., Nakamura, Y., Tokuyama, H., Kuramoto, S., Bangs, N., 2005. Two-dimensional mapping of fine structures in the Kuroshio Current using seismic reflection data. Geophysical Research Letters 32, L14609.

Yilmaz, Ö., 2001. Acoustic Impedance Estimation. In: Doherty, S.M. (Ed.), Seismic Data Analysis Volume II, Investigations in Geophysics, Vol. 10. Society of Exploration Geophysicists, Tulsa, USA, 1863-1896.

8 Conclusion and Outlook

A new set of high-resolution seismic reflection data has been analyzed to decipher the WBUC at the Eirik Drift in the past and at present. Here, the conclusions of this thesis are described, following the major questions of the survey.

- What is the detailed structure of the Eirik Drift?
- For which period can the first impact of deep-water circulation recorded at the Eirik Drift be identified?

The correlation of the new seismic reflection data with synthetic seismograms based on scientific drill site information provided the basis for a revised seismostratigraphic concept at the Eirik Drift (see Ch. 5). The revised seismostratigraphic concept at the Eirik Drift comprises five major seismic units and eight internal reflectors, which confine the major changes in reflection characteristics. The seismostratigraphic concept for the Eirik Drift of Arthur *et al.* (1989) was refined by three additional horizons, A1 (0.8 Ma), A2 (1.4 Ma) and A3 (17-19 Ma), and the age of horizon R5 was estimated as 12-10 Ma.

In my first paper, I concentrated on a detailed structural analysis of the oldest seismic unit SUIV (40-19 Ma) based on the revised seismostratigraphic concept. It revealed that the sedimentation at the Eirik Drift was not deep current controlled until the early Miocene. The newly introduced reflector A3 was identified as a basal unconformity, which marks the onset of drift building at 19-17 Ma under the influence of a strong deep-water flow (see Ch. 5). This timing correlates with the onset of deep-water exchange at the Fram Strait (Ehlers and Jokat, 2013) and the firstly observed overflows at the Faroe Conduit in early Miocene (Stoker *et al.*, 2005) but contrasts with the hypotheses of Arthur *et al.* (1989) and Wold (1994), who dated the drift build-up after ~4.5 Ma and after ~7-8 Ma, respectively.

The dating of reflector R5 and the basal unconformity A3 could not be confirmed by the drill sites, as the oldest geological record from ODP Leg 105 Site 646 reaches back only to ~8 Ma. The dating of the reflectors below was conducted by using the sedimentation rate of the lowest part of that drill site in combination with interpretations from observations at other sediment drifts in the northern North Atlantic. To gather ground truth of the suggested ages of reflector R5 (12-10 Ma) and the basal unconformity A3 (19-17 Ma) an additional deep drilling down to the basement reflector is needed. Even though the exact age of reflector A3 could not be confirmed by drilling results, it has clearly been demonstrated that the onset of drift building took place much earlier than thought previously. This is an important finding as it improves the knowledge of the paleo deep current development in the northern North Atlantic.

- Can the development of the WBUC be reconstructed for this region?
- Have modifications in the WBUC been documented in the sediment transport? In what way did oceanographic modifications affect the sedimentary sequences?
- Can oceanographic modifications observed locally be linked to major changes in the North Atlantic climate?

The revised seismiostratigraphic concept was used for a detailed structural analysis of all seismic sequences at the Eirik Drift. Analysis of the morphology of the bounding horizons and the location and orientation of the depocenters observed in each seismic (sub)unit put forward a detailed model of paleocirculation at the Erik Drift. The changes in the deep current system at the Eirik Drift were linked to changes in the North Atlantic climate (see Ch. 6).

The structural analysis of each seismic (sub)unit revealed the influence of the WBUC responsible for shaping the drift. At the Eirik Drift an intense WBUC is observed during warm climates and at the beginning of cooling phases, while there is weak WBUC influence during enhanced cooling phases accompanied by increased ice extent in the Nordic Seas. A southward shift of the deep-water formation regions along with a shift in the main pathways of the northern sourced deep-water during phases of enhanced ice-cover is suggested.

Therefore, the main WBUC route did not affect the Eirik Drift during Northern Hemisphere Glaciation. Based on our interpretation at the Eirik Drift and observations at other North Atlantic drifts, a model of the deep-water pathways for the Nordic Seas and northern North Atlantic during the different climatic stages is suggested.

Two separated WBUC branches of different core depth are observed at the Eirik Drift after 7.5 Ma. At roughly the same time the first overflows at the Denmark Strait were observed (~7 Ma) (Bohrmann *et al.*, 1990). Therefore, and in accordance to the present WBUC, it is suggested that the upper core transports ISOW and the deeper core DSOW.

The development of the WBUC at the Eirik Drift was reconstructed in detail. The changes in pathways and intensity of the WBUC were documented in the sedimentary sequences and interpreted with regard to major tectonic events and climate changes. The suggested model for the Nordic Seas and northern North Atlantic constitutes an important supplement to the understanding of the complex interplay of changes in THC, climate and tectonics in the northern North Atlantic. Still, further investigations are needed to improve our knowledge and decipher the complex system. More seismic data from a survey, which covers the connection to the Greenland shelf and the SE flank of the drift, are needed. Besides, a deeper drill core could reach the oldest sediments and would shed light on the timing history prior to 8 Ma.

- Can deep currents of depth > 1500 m be studied with the seismic oceanography method?
- Does the observation of the WBUC in seismic reflection data improve the knowledge gained by classical physical oceanography methods?
- Can we identify and track the present WBUC at the Eirik Drift? Does our observation from the present WBUC support our interpretation from the past?

The seismic data data were re-processed in combination with CTD data to analyse the structure of the deeper water column above the Erik Drift and provided the first seismic oceanography study in depths > 1500 m (see Ch. 7). It was possible to identify the upper WBUC core in the seismic lines at depths between 2200 and 3150 m, but it was not possible to clearly identify the deeper core. The seismic oceanography method seems restricted by greater depths (> 3000 m) due to the increased signal loss, at least with the frequencies used for this data aquisition.

The identified upper core of the present WBUC at the Eirik Drift was tracked in the seismic lines. It is found in good agreement with -and thus supports- the suggested pathway for the time span < 800000 years (Müller-Michaelis and Uenzelmann-Neben, 2013 (in revision); Ch. 6). The detailed structure observed in the seismic data revealed that the lateral extent of the WBUC core broadens when the slope of the drift flank flattens. A more concentrated and intensified deep current core at steeper slopes was also suggested by the analysis of the seismic reflection data (Müller-Michaelis and Uenzelmann-Neben, 2013 (in revision); Ch. 6)

It was shown that discrete CTD measurements cannot always properly resolve -or even fail to detect- such structures depending on sampling location and -interval. Therefore, the seismic oceanography method can be used as an important supplement for oceanographic studies, especially for resolving structures in a high lateral and temporal resolution.

The seismic oceanography method was successfully applied to an analysis of seismic data in depths between 1500 m and 3000 m. The present upper WBUC core was identified and tracked and the findings supported the observations from the past. Also the possibility to improve oceanographic research by use of seismic oceanography was clarified. However, this method bears some disadvantages. The data processing was quite time consuming as the main processing steps of seafloor amplitude reduction and direct wave removal had to be applied to single shots (or shot gathers). These had to be manually checked and corrected, as required. Moreover, the seismic oceanography method allows just a relative interpretation of oceanographic features and not an interpretation in absolute terms of water mass characteristics, so long as no inverse methods can be applied due to the lack of

contemporaneously conducted CTD/XBT measurements. The development of an automated data processing tool would be helpful to avoid long processing times in the future. Future campaigns aiming to use seismic reflection data (also) for the seismic oceanography method, should contemplate contemporaneous CTD/XBT measurements and consider the data acquisition parameters carefully.

The major task of the analysis of the seismic reflection data, a detailed reconstruction of the WBUC at the Eirik Drift in the past and at present, has been carried out. The findings have improved the knowledge about the deep palaeocirculation in the North Atlantic during climate modifications and a structual analysis of the present WBUC supported our interpretation. These new insights can now be used to improve future climate models.

More high-resolution seismic reflection data covering a larger area will be helpful to enlarge the knowledge gained and will close the gaps in the interpretation. A deeper drill core down to the oldest sediments will gather ground truth to the dating of the interpretation prior to 8 Ma. It is advised that the suitability of the seismic data in terms of seismic oceanography should be probably considered when defining the data aquisition parameters.

9 Complete Bibliography

Arthur, M.A., Srivastava, S.P., Kaminski, M., Jarrard, R.D., Osler, J., 1989. Seismic Stratigraphy and History of Deep Circulation and Sediment Drift Development in Baffin Bay and the Labrador Sea. In: Srivastava, S.P., Arthur, M., Clement, B., et al. (Eds.), Scientific Results. Ocean Drilling Program, College Station, TX, USA, 957-988.

Biescas, B., Sallarès, V., Pelegrí, J.L., Machín, F., Carbonell, R., Buffett, G., Dañobeitia, J.J., Calahorrano, A., 2008. Imaging meddy finestructure using multichannel seismic reflection data. Geophysical Research Letters 35, doi:10.1029/2008GL033971.

Blum, P., 1997. Physical Properties Handbook: A guide to the shipboard measurement of physical properties of deep-sea cores. ODP Technical Note 26, doi:10.2973/odp.tn.26.1997.

Bohrmann, G., Henrich, R., Thiede, J., 1990. Miocene to Quaternary Paleoceanography in the Northern North Atlantic: Variability in Carbonate and Biogenic Opal Accumulation. In: Bleil, U., Thiede, J. (Eds), Geological History of the Polar Oceans: Arctic versus Antarctic. Springer Netherlands, 308, 647-675.

Buffett, G.G., Biescas, B., Pelegrí, J.L., Machín, F., Sallarès, V., Carbonell, R., Klaeschen, D., Hobbs, R., 2009. Seismic reflection along the path of the Mediterranean Undercurrent. Continental Shelf Research 29 (15), 1848-1860.

Burton, K.W., Ling, H.-F., O'Nions, R.K., 1997. Closure of the Central American Isthmus and its effect on deep-water formation in the North Atlantic. Nature 386, 382-385.

Cartwright, J., 2011. Diagenetically induced shear failure of fine-grained sediments and the development of polygonal fault systems. Marine and Petroleum Geology 28, 1593-1610.

Chalmers, J.A., Pulvertaft, T.C.R., 2001. Development of the continental margins of the Labrador Sea – a review. In: Wilson, R.C.L., Whitmarsh, R.B., Froitzheim, N. (Eds.), Non-volcanic rifting of the continental margins: a comparison of evidence from land and sea. Geological Society London, UK, 77-105.

Channell, J.E.T., Kanamatsu, T., Sato, T., Stein, R., Alvarez Zarikian, C.A., Malone, M.J., and the Expedition 303/306 Scientists, 2006. Proceedings of the Intergrated Ocean Drilling Program. Vol 303/306 Expeditions Report North Atlantic Climate. Integrated Ocean Drilling Program, College Station, TX, USA, doi:10.2204/iodp.proc.303306.2006.

Channell, J.E.T., Sato, T., Kanamatsu, T., Stein, R., Alvarez Zarikian, C.A., 2010. Expedition 303/306 synthesis: North Atlantic climate. In: Channell, J.E.T., Kanamatsu, T., Sato, T., Stein, R., Alvarez Zarikian, C.A., Malone, M.J., and the Expedition 303/306 Scientists (Eds.), Proceedings of the Integrated Ocean Drilling Program. Integrated Ocean Drilling Program, College Station, TX, USA, doi:10.2204/iodp.proc.303306.214.2010.

Chen, C.-T., Millero, F.J., 1977. Speed of sound in seawater at high pressures. Journal of the Acoustic Society of America 62 (5), 1129-1135.

Cramer, B.S., Toggweiler, J.R., Wright, J.D., Katz, M.E., Miller, K.G., 2009. Ocean overturning since the Late Cretaceous: Inferences from a new benthic foraminiferal isotope compilation. Paleoceanography 24, PA 4216, doi:10.1029/2008PA001683.

Cremer, M., 1989. Texture and Microstructure of Neogene-Quaternary Sediments, ODP Sites 645 and 646, Baffin Bay and Labrador Sea. In: Srivastava, S.P., Arthur, M., Clement, B., et al. (Eds.), Proceedings of the Ocean Drilling Program, Scientific Results. Ocean Drilling Program, College Station, TX, USA, 7-20.

Cremer, M., Maillet, N., Latouche, C., 1989. Analysis of sedimentary facies and clay mineralogy of the Neogene-Quaternary sediments in ODP Site 646, Labrador Sea. In: Srivastava, S.P., Arthur, M., Clement, B. (Eds.), Proceedings of the Ocean Drilling Program, Scientific Results. Ocean Drilling Program, College Station, TX, USA, 71-80.

Davies, R., Cartright, J., Pike, J., Line, C., 2001. Early Oligocene initiation of North Atlantic Deep Water formation. Nature 410, 917-920.

Dickson, R.R., Brown, J., 1994. The production of North Atlantic Deep Water: Sources, rates, and pathways. Journal of Geophysical Research 99, 12319-12341.

Dingle, R.V., Megson, J.B., Scrutton, R.A., 1982. Acoustic Stratigraphy of the sedimentary succession west of Porcupine Bank, N.E. Atlantic Ocean: A preliminary account. Marine Geology 47, 17-35.

Ehlers, B.-M., Jokat, W., 2013. Paleo-bathymetry of the northern North Atlantic and consequences for the opening of the Fram Strait. Marine Geophysical Research, doi:10.1007/s11001-013-9165-9.

Expedition 303 Scientists, 2006. Expedition 303 summary. In: Channell, J.E.T., Kanamatsu, T., Sato, T., Stein, R., Alvarez Zarikian, C.A., Malone, M.J., Expedition Scientists (Eds.), Proceedings of the Integrated Ocean Drilling Program. Integrated Ocean Drilling Program, College Station, TX, USA, doi:10.2204/iodp.proc.303306.101.2006.

Faugères, J.C., Stow, D.A.V., 2008. Contourite Drifts: Nature, Evolution and Controls. In: Rebesco, M. and Camerlenghi, A. (Eds.), Contourites. Elsevier, Amsterdam, the Netherlands, 259-288.

Faugères, J.C., Stow, D.A.V., Imbert, P., Viana, A.R., 1999. Seismic Features Diagnostic of Contourite Drifts. Marine Geology 162, 1-38.

Fortin, W.F.J., Holbrook, W.S., 2009. Sound speed requirements for optimal imaging of seismic oceanographic data. Geophysical Research Letters 36, doi:10.1029/2009GL038991.

Gibbard, P.L., Head, M.J., Walker, M.J.C., 2010. Formal ratification of the Quaternary System/Period and the Pleistocene Series/Epoch with a base at 2.58 Ma. Journal of Quaternary Science 25, 96-102.

Hansen, B., Østerhus, S., 2000. North Atlantic–Nordic Seas exchanges. Progress in Oceanography 45, 109-208.

Haq, B.U., Hardenbol, J., Vail, P.R., 1987. Chronology of fluctuating sea levels since Tirassic. Science 235, 1156-1167.

Haug, G.H., Tiedemann, R., 1998. Effect of the formation of the Isthmus of Panama on Atlantic Ocean thermohaline circulation. Nature 393, 673-676.

Heezen, B.C., Hollister, C.D., Ruddiman, W.F., 1966. Shaping the continental rise by deep geostrophic contour currents. Science 152, 502-508.

Hillaire-Marcel, C., Vernal, A.d., Bilodeau, G., Wu, G., 1994. Isotope stratigraphy, sedimentation rates, deep circulation, and carbonate events in the Labrador Sea during the last ~ 200 ka. Canadian Journal of Earth Sciences 31 (1), 63-89.

Hillaire-Marcel, C., de Vernal, A., McKay, J., 2011. Foraminifer isotope study of the Pleistocene Labrador Sea, northwest North Atlantic (IODP Sites 1302/03 and 1305), with emphasis on paleoceanographical differences between its "inner" and "outer" basins. Marine Geology, 279 (1–4), 188-198.

Holbrook, W.S., Paramo, P., Pearse, S., Schmitt, R.W., 2003. Thermohaline Fine Structure in an Oceanographic Front from Seismic Reflection Profiling. Science 301, 821-824.

Holliday, N. P., S. Bacon, J. Allen, and E. L. McDonagh, 2009. Circulation and Transport in the Western Boundary Currents at Cape Farewell, Greenland, Journal of Physical Oceanography, 39 (8), 1854-1870.

Howe, J.A., Stoker, M.S., Woolfe, K.J., 2001. Deep-marine seabed erosion and gravel lags in the northwestern Rockall Trough, North Atlantic Ocean. Geological Society London Journal 158, 427-438.

Hunter, S., Wilkinson, D., Louarn, E., McCave, I.N., Rohling, E., Stow, D.A.V., Bacon, S., 2007a. Deep western boundary current dynamics and associated sedimentation on the Eirik Drift, Southern Greenland Margin. Deep-Sea research I 54, 2036-2066.

Hunter, S., Wilkinson, D., Stanford, J., Stow, D.A.V., Bacon, S., Akhmetzhanov, A.M., Kenyon, N.H., 2007b. The Eirik Drift: A long-term barometer of North Atlantic deepwater flux south of Cape Farewell, Greenland. In: Viana, A.R., Rebesco, M. (Eds.), Economic and Palaeoceanographic Significance of Contourite Deposits. Geological Society, London, UK, 245-263.

Kaminski, M.A., Gradstein, F.M., Scott, D.B., Mackinnon, K.D., 1989. Neogene benthic foraminifer biostratigraphy and deep-water history of Sites 645, 646, and 647, Baffin Bay and Labrador Sea. In: Srivastava, S.P., Arthur, M., Clement, B., et al. (Eds.), Proceedings of the Ocean Drilling Program, Scientific Results. Ocean Drilling Program, College Station, TX, USA, 731-756.

Klaeschen, D., Hobbs, R.W. Krahmann, G., Papenberg, C., Vsemirnova, E, 2009. Estimating movement of reflectors in the water column using seismic oceanography. Geophysical Research Letters, 36., doi:10.1029/2009GL038973.

Krahmann, G., Brandt, P., Klaeschen, D., Reston, T., 2008. Mid-depth internal wave energy off the Iberian Peninsula estimated from seismic reflection data. Journal of Geophysical Research 113, doi:10.1029/2007JC004678.

Kuhlbrodt, T., Griesel, A., Montoya, M., Levermann, A., Hofmann, M., Rahmstorf, S., 2007. On the driving processes of the Atlantic meridional overturning circulation. Reviews of Geophysics 45 (2), doi:10.1029/2004RG000166.

Le Pichon, X., Hyndman, R.D., Pautot, G., 1971. Geophysical Study of the Opening of the Labrador Sea. Journal of Geophysical Research 76, 4724-4743.

Locker, S.D., Laine, E.D., 1992. Paleogene-Neogene depositional history of the middle U.S. Atlantic continental rise: mixed turbidite and contourite depositional systems. Marine Geology 103, 137-164.

Masson, D.G., Kidd, R.B., 1986. Revised Tertiary seismic Stratigraphy of the southern Rockall Trough. In: Ruddimann, W.F., Kidd, R.B., Thomas, E., et al. (Eds.), Initial Reports Deep Sea Drilling Project 94, 1117-1126.

McCave, I.N., Lonsdale, P.F., Hollister, C.D., Gardner, W.D., 1980. Sediment transport over the Hatton and Gardar contourite drifts. Journal of Sedimentary Research 50, 1049-1062.

McCave, I.N., Tucholke, B.E., 1986. Deep Current-Controlled Sedimentation in the Western North Atlantic. In: Vogt, P.R., Tucholke, B.E. (Eds.), The Geology of North America - The Western North Atlantic Region. Geological Society of America, Boulder, USA, 451-468.

McMaster, R.L., Locker, S.D., Laine, E.D., 1989. The early Neogene continental rise off the eastern United States. Marine Geology 87, 137-163.

Mikolajewicz, U., Crowley, T.J., 1997. Response of a coupled ocean / energy balance model to restricted flow through the central American isthmus. Paleoceanography 12 (3), 429-441.

Miller, K.G., Tucholke, B.E., 1983. Development of Cenozoic Abyssal Circulation south of the Greenland-Scotland Ridge. In: Bott, M.H.P., Saxov, S., Talwani, M., Thiede, J. (Eds.), Structures and Development of the Greenland-Scotland Ridge - New Methods and Concepts. Plenum Press, New York and London, 549-589.

Miller, K.G., Wright, J.D., Katz, M.E., Wade, B.S., Browning, J.V., Cramer, B.S., Rosenthal, Y., 2009. Climate threshold at the Eocene-Oligocene transition: Antarctic ice sheet influence on ocean circulation. In: Koeberl, C., Montanari, A. (Eds.), The Late Eocene Earth-Hothouse, Icehouse, and Impacts. Geological Society of America Special Paper, USA, 169-178.

Mountain, G.S., Tucholke, B.E., 1985. Mesozoic and Cenozoic Geology of the U.S. Atlantic continental slope and rise. In: Poag, C.W. (Ed.), Geologic Evolution of the United States Atlantic Margin. Van Nostrand Reinhold Company, New York, USA, 293-341.

Mueller, R.D., Sdrolias, M., Gaina, C., Roest, W.R., 2008. Age, spreading rates, and spreading asymmetry of the world's ocean crust. Geochemistry Geophysics Geosystems 9, doi:10.1029/2007GC001743.

Müller-Michaelis, A., Uenzelmann-Neben, G., Stein, R., 2013 A revised Early Miocene age for the instigation of the Eirik Drift, offshore southern Greenland: Evidence from high-resolution seismic reflection data. Marine Geology. doi:10.1016/j.margeo.2013.04.012.

Müller-Michaelis, A., Uenzelmann-Neben, G., 2013 (in revision). Development of the Western Boundary Undercurrent at the Eirik Drift related to changing climate since the early Miocene. Deep-Sea research I, in revision.

Müller-Michaelis, A., Uenzelmann-Neben, G., 2013 (submitted). Using seismic reflection data to reveal high-resolution structure and pathway of the upper Western Boundary Undercurrent core at the Eirik Drift. Geophysical Research Letters, submitted.

Muza, J.P., Covington, J.M., 1987. Neogene calcareous nannofossils from Deep Sea Drilling Project Site 603, lower continental rise, western North Atlantic: Biostratigraphy and correlations with magnetic and seismic stratigraphy. In: van Hinte, J.E., Wise Jr, S.W., et al. (Eds.), Initial Reports Deep-Sea Drilling Project 93, 593-616.

Nandi, P., Holbrook, W.S., Pearse, S., Paramo, P., Schmitt, R.W., 2004. Seismic reflection imaging of water mass boundaries in the Norwegian Sea. Geophysical Research Letters 31, doi:10.1029/2004GL021325.

Nielsen, T., Knutz, P.C., Kuijpers, 2008. Seismic Expression of Contourite Depositional Systems. In: Rebesco, M. and Camerlenghi, A. (Eds.), Contourites. Elsevier, Amsterdam, the Netherlands, 301-321.

Papenberg, C., Klaeschen, D., Krahmann, G., Hobbs, R.W., 2010. Ocean temperature and salinity inverted from combined hydrographic and seismic data. Geophysical Research Letters 37, doi:10.1029/2009GL042115.

Pickart, R.S., 1992. Water mass components of the North Atlantic Deep Western boundary current. Deep Sea Research 39, 1553-1572.

Pinheiro, L.M., Song, H., Ruddick, B., Dubert, J., Ambar, I., Mustafa, K., Bezerra, R., 2010. Detailed 2-D imaging of the Mediterranean outflow and meddies off W Iberia from multichannel seismic data. Journal of Marine Systems 79, 89-100.

Poore, H.R., Samworth, R., White, N.J., Jones, S.M., McCave, I.N., 2006. Neogene overflow of Northern Component Water at the Greenland-Scotland Ridge. Geochemistry Geophysics Geosystems 7, No. 6, Q06010, doi:10.1029/2005GC001085.

Quadfasel, D., Käse, R., 2007. Present-Day Manifestation of the Nordic Seas Overflows. In: Schmittner, A., Chiang, J.C.H., Hemming, S.R. (Eds.), Ocean Circulation-Mechanisms and Impacts. American Geophysical Union, Washington, DC, USA, 75-89.

Ravelo, A.C., 2010. Palaeoclimate: Warmth and glaciation. Nature GeoScience 3 (10), 672-674.

Rebesco, M., Stow, D.A.V., 2001. Seismic expression of contourites and related deposits: a preface. Marine Geophysical Research 22, 303-308.

Rhein, M., 1994. The Deep Western Boundary Current: tracers and velocities. Deep-Sea research I, 41 (2), 263-281.

Rhein, M., 2011. Strength of the Subpolar Gyre and the Formation of Deep Water. In: Forschungsschiffe, L.D. (Ed.), Cruise Report RV MARIA S. MERIAN. Institut für Meereskunde, Hamburg, Germany.

Ricker, N., 1953. The form and laws of propagation of seismic wavelets. Geophysics 18, 10-40.

Ruddick, B., 2003. Sounding Out Ocean Fine Structure. Science 301, 772-773.

Ruddick, B., Song, H., Dong, C., Pinheiro, L., 2009. Water Column Seismic Images as Maps of Temperature Gradient. Oceanography 22 (1), 193-205.

Saunders, P.M., 2001. The dense northern overflows. In: Siedler, G., Church, J., Gould, J. (Eds.), Ocean Circulation and Climate: Observing and Modelling the Global Ocean. Academic Press, San Francisco CA, USA, 401-418.

Schmitz, W.J., Jr., 1996. On the World Ocean Circulation: Volume I - Some Global Features / North Atlantic Circulation, Technical Report. Woods Hole Oceanographic Institution, Woods Hole, MA, USA, doi:10.1575/1912/355.

Shipboard Scientific Party, 1987a. Site 646. In: Srivastava, S.P., Arthur, M., Clement, B., et al. (Eds.), Initial Reptorts, Ocean Drilling Program, College Station, TX, USA, 419-674.

Shipboard Scientific Party, 1987b. Explanatory Notes: ODP Leg 105, Baffin Bay and Labrador Sea. In: Srivastava, S.P., Arthur, M., Clement, B., et al. (Eds.), Initial Reptorts, Ocean Drilling Program, College Station, TX, USA, 21-41.

Shipboard Scientific Party, 2005. Ice sheet-ocean atmosphere interactions on millenial timescales during the late Neogene-Quaternary using a paleointensity-assisted chronology for the North Atlantic. In Expedition Scientists (Eds.), North Atlantic climate 2, IODP Preliminary Report, 306. doi:10.2204/iodp.pr.306.2005.

Smethie, W.R.J., Fine, R.A., 2001. Rates of North Atlantic Deep Water formation calculated from chlorofluorcarbon inventories. Deep Sea Research I 48, 189-215.

Smith, W.H.S., Sandwell, D.T., 1997. Global Sea Floor Topography from Satellite Altimetry and Ship Depth Soundings. Science 277, 1956-1962.

Srivastava, S.P., Arthur, M.A., 1989. Tectonic Evolution of the Labrador Sea and Baffin Bay: Constraints Imposed by Regional Geophysics and Drilling Results from Leg 105. In: Srivastava, S.P., Arthur, M., Clement, B., et al. (Eds.), Proceedings of the Ocean

Drilling Program, Scientific Results. Ocean Drilling Program, College Station, TX, USA, 989-1009.

Srivastava, S.P., Arthur, M.A., Clement, B., et al (Eds.), 1989. Proceedings of the Ocean Drilling Program, Scientific Results, 105. Ocean Drilling Program, College Station, TX, USA, doi:10.2973/odp.proc.sr.105.1989.

Srivastava, S.P., Roest, W.R., 1999. Extent of oceanic crust in the Labrador Sea. Marine and Petroleum Geology 16, 65-84.

Stanford, J.D., Rohling, E.J., Bacon, S. and Holliday, N.P., 2011. A review of the deep and surface currents around Eirik Drift, south of Greenland: Comparison of the past with the present. Global and Planetary Change, 79 (3–4), 244-254.

Stoker, M.S., van Weering, T.C.E., Svaerdborg, T., 2001. A mid- to late Cenozoic tectostratigraphic framework for the Rockall Trough. In: Shannon, P.M., Haughton, P., Corcoran, D. (Eds), The Petroleum Exploration of Ireland's Offshore Basins- Geological Society, London, UK, Special Publication 188, 411-438.

Stoker, M.S., Hoult, R.J., Nielsen, T., Hjelstuen, B.O., Laberg, J.S., Shannon, P.M., Praeg, D., Mathiesen, A., van Weering, T.C.E., McDonnell, A., 2005. Sedimentary and oceanographic responses to early Neogene compression on the NW European margin. Marine and Petroleum Geology 22, 1031-1044.

Stow, D.A.V., Faugères, J.-C., Howe, J.A., Pudsey, C.J., Viana, A.R., 2002. Bottom currents, contourites and deep-sea sediment drifts: current state-of-the-art. In: Stow, D.A.V., Pudsey, C.J., Howe, J.A., Faugères, J.-C., Viana, A.R. (Eds.), Deep-water contourite systems: Modern drifts and ancient series. Geological Society of London, London, UK, 7- 20.

Stow, D.A.V., Faugères, J.-C., Viana, A., Gonthier, E., 1998. Fossil contourites: a critical review. Sedimentary Geology 115, 3-31.

Tsuji, T., Noguchi, T., Niino, H., Matsuoka, T., Nakamura, Y., Tokuyama, H., Kuramoto, S., Bangs, N., 2005. Two-dimensional mappimg of fine structures in the Kuroshio Current using seismic reflection data. Geophysical Research Letters 32, L14609, doi:10.1029/2005GL023095.

Van Aken, H.M., 2007. The Oceanic Thermohaline Circulation. Springer, New York, USA.

van Weering, T., Stoker, M., Rebesco, M., 2008. High-Latitude Contourites. In: Rebesco, M. and Camerlenghi, A. (Eds.), Contourites. Elsevier, Amsterdam, the Netherlands, 457- 489.

Uenzelmann-Neben, G., 2009. Cruise Report RV MARIA S. MERIAN Cruise MSM12-2. In: Bornemann, H. (Ed.), Berichte zur Polar- und Meeresforschung. Alfred Wegener Institut, Bremerhaven, Germany.

Via, R.K., Thomas, D.J., 2006. Evolution of Atlantic thermohaline circulation: Early Oligocene onset of deep-water production in the North Atlantic. Geology 34, 441– 444.

Wildeboer Schut, E., Uenzelmann-Neben, G., 2006. Tying seismic data to geologic information from core data: An example from ODP Leg 177. Geo-Marine Letters 26, 235-248.

Winkler, A., Wolf-Welling, T., Stattegger, K., Thiede, J., 2002. Clay mineral sedimentation in high northern latitude deep-sea basins since the Middle Miocene (ODP Leg 151, NAAG). International Journal of Earth Sciences 91 (1), 133-148.

Wold, C.N., 1994. Cenozoic Sediment Accumulation on Drifts in the Northern North Atlantic. Paleoceanography 9, 917-941.

Wolf-Welling, T.C.W., Cremer, M., O'Connell, S., Winkler, A., Thiede, J., 1996. Cenozonic Arctic Gateway Paleoclimate Variability: Indications from changes in coarse-fraction compositions. In: Thiede, J., Myhre, A.M., Firth, J.V., Johnson, G.L., Ruddiman, W.F. (Eds.), Proceedings of the Ocean Drilling Program, Scientific Results. Ocean Drilling Program, College Station, TX, USA, 515-567.

Woodruff, F., Savin, S., 1989. Miocene deepwater oceanography. Palaeogeography 4, 87-140.

Wright, J.D., 1998. Role of the Greenland-Scotland Ridge in Neogene climate changes. In: Crowley, T.J., Burke, K. (Eds.), Tectonic Boundary Conditions for Climate Reconstructions. Oxford University Press, Oxford, 192-211.

Wright, J.D., Miller, K.G., 1996. Control of North Atlantic Deep Water Circulation by the Greenland-Scotland Ridge. Paleoceanography 11, 157-170.

Wright, J.D., Miller, K.G., Fairbanks, R.G., 1992. Early and middle Miocene stable isotopes: implications for deepwater circulation and climate. Paleoceanography 7, 357-389.

Yilmaz, Ö., 2001. Seismic Data Analysis. Society of Exploration Geophysicists, Tulsa, OK, USA.

Zachos, J.C., Pagani, M., Sloan, L., Thomas, E., Billups, K., 2001. Trends, Rhythms, and Aberrations in Global Climate 65 Ma to Present. Science 292, 686-693.

10 List of Figures

11 List of Tables

12 List of Abbreviations

A1, A2, A3	Reflection Horizons A1-A3
AABW	Antarctic Bottom Water
AGC	Automatic Gain Control
BL	Boundary Layer
CDP	Common Depth Point
CF	Cape Farewell
CGFZ	Charlie Gibbs Fracture Zone
CLSW	Classical Labrador Sea Water
CTD	Conductivity-Temperature-Depth Probe
DFG	Deutsche Forschungsgemeinschaft
DS	Davis Strait
DSOW	Denmark Strait Overflow Water
DWBC	Deep Western Boundary Current
ED	Eirik Drift
EU	Erosional Unconformity
GMT	General Mapping Tool
GPS	Global Positioning System
GRA	Gamma Ray Attenuation Measurement
GS	Greenland Sea
GSR	Greenland-Scotland Ridge
IODP	Integrated Ocean Drilling Program
IODP 1305	Integrated Ocean Drilling Program Expedition 303 Site U1305
IODP 1306	Integrated Ocean Drilling Program Expedition 303 Site U1306
IODP 1307	Integrated Ocean Drilling Program Expedition 303 Site U1307
ISOW	Iceland Scotland Overflow Water
LDW	Lower Deep Water
LFZ	Leif Fracture Zone
LS	Labrador Sea
LSW	Labrador Sea Water
mbsf	Meters Below Seafloor
MSM	Research Vessel Maria S. Merian
MST	Multi-Sensing Track Tool
NADW	North Atlantic Deep Water
NCW	Northern Component Water
NMO	Normal Moveout
NS	Norwegian Sea
ODP	Ocean Drilling Program
ODP 646	Ocean Drilling Program Leg 105 Site 646
R1-R5	Reflection Horizons R1-R5
rms	Root Mean Square
SUI-IV	Seismic Units I-IV
THC	Thermohaline Circulation
TWT	Two-Way-Traveltime
ULSW	Upper Labrador Sea Water
w.d.	Water Depth
WBUC	Western Boundary Undercurrent
WTR	Wyville-Thomson Ridge
XBT	Expendable Bathythermograph

13 Acknowledgements

Many people supported me during my PhD time which will always be an unforgettable part of my life. In the following, I want to say thank you to:

Curriculum Vitae

Antje Müller-Michaelis

Am Leher Tor 13
D-27568 Bremerhaven
E-mail: mueller-michaelis@web.de
Tel: +49 1578 7114219

Date of Birth: 24th of June 1976
Place of Birth: Hamburg, Germany
Citizenship: German

Academic education:

- Oct 2010 - ongoing   Ph.D. Geophysics

  Alfred-Wegener-Institut, Helmholtz-Zentrum für Polar- und Meeresforschung, Bremerhaven c/o University of Bremen, Department of Geoscience, Germany
  'From early Miocene to present: Reconstruction of the deep Thermohaline Circulation at the Eirik Drift'

- Apr 2004 - Jan 2009   Diploma Physical Oceanography

  Intitute of Oceanography, University of Hamburg, Hamburg, Germany
  'Regional Heat and Freshwater Balances of the Oceanic Surface Mixed Layer derived from Argo Float and Air-Sea Flux Data'

  Diploma Certification "very good" ("sehr gut")
  Secondary subjects:
  Marine Geophysics and Biogeochemistry of Marine Sediments

- General qualification for University entrance: June1995

Scientific work experience:

- Jan 2010 – Jun 2010   Processing and Interpretation of ARGO Float Data as Scientific Staff Member of Prof. Dr. Detlef Quadfasel, University of Hamburg, Germany
- Jan 2009 – Feb 2009   Processing and Interpretation of ARGO Float Data as Scientific Staff Member of Prof. Dr. Detlef Quadfasel, University of Hamburg, Germany
- Mar 2006 – Dec 2008   Student-Job: Processing ARGO Float Data with Prof. Dr. Detlef Quadfasel and Katrin Latarius, University of Hamburg, Germany

Participation in Expeditions:
- Sep - Oct 2006   University of Hamburg: R.R.S. DISCOVERY
  Cruise D311: Physical Oceanography
- Oct - Nov 2006   University of Hamburg: FS HEINCKE
  Cruise HE264: Marine Geophysics
- Nov - Dec 2007   University of Hamburg: FS METEOR
  Cruise M74/4 - NEOMA: Marine Seismic and Geology
- Feb 2008   University of Hamburg: FS MARIA S. MERIAN
  Cruise MSM07/1a: Training ATLAS Parasound System
- May - Jun 2009   University of Hamburg: FS MARIA S. MERIAN
  Cruise MSM 12/1: Physical Oceanography
- Jun - Jul 2009   AWI Bremerhaven: FS MARIA S. MERIAN
  Cruise MSM12/2: Marine Seismic and Geology
- May 2010   University of Hamburg: FS POSEIDON
  Cruise P399/1: Physical Oceanography
- Oct - Nov 2011   AWI Bremerhaven: FS MARIA S. MERIAN
  Cruise MSM19/2: Marine Seismic
- Oct - Nov 2012   AWI Bremerhaven: FS SONNE
  Cruise SO224: Marine Seismic

Publications:
Müller-Michaelis, A., Uenzelmann-Neben, G., Stein, R., 2013. A revised Early Miocene age for the instigation of the Eirik Drift, offshore southern Greenland: Evidence from high-resolution seismic reflection data. Marine Geology. doi:10.1016/j.margeo.2013.04.012.

Under Review:
Müller-Michaelis, A. and Uenzelmann-Neben, G., 2013 (in revision). Development of the Western Boundary Undercurrent at the Eirik Drift related to changing climate since the early Miocene. Deep-Sea Research Part I (submitted 04/2013; in revision 11/2013, moderate revisions advised).

Job experience prior to University entrance (prior to April 2004):
- Dec 2002 – Dec 2003   Sales and Marketing Assistant
  VESEG GmbH, Rehlingen-Siersburg, Germany
- Jan 2000 – Aug 2002   Sales and Marketing Assistant
  WEA Records, Warner Music Germany GmbH & Co. OHG, Hamburg, Germany
- Jan 1999 – Dec 1999   Internship Marketing Department
  Ernst Dello GmbH & Co., Hamburg, Germany
- Aug 1995 – Dec 1998   Bank assistant (training followed by employment)
  Vereins- und Westbank AG, Hamburg, Germany

The following persons can give an assessment of my performance:
- Dr. Gabriele Uenzelmann-Neben: Alfred-Wegener-Institut, Helmholtz-Zentrum für Polar- und Meeresforschung; gabriele.uenzelmann-neben@awi.de
- Prof. Dr. Detlef Quadfasel: Institute of Oceanography, University of Hamburg; detlef.quadfasel@zmaw.de
- Prof. Dr. Christian Hübscher: Institute of Geophysics, University of Hamburg; christian.huebscher@zmaw.de